Astronomy 602. Galactic Astronomy

1. Historical Landmarks

The proper study of the Milky Way galaxy probably begins in 1610, when Galileo first discovered that the Milky Way consists of "innumerable" faint stars. Halley provided a significant contribution in 1718 when he discovered the proper motions of Arcturus, Sirius, and Aldebaran by comparing their positions with those given by Hipparchos in the Almagest. By 1760 Mayer had published proper motions for some 80 stars based upon comparisons of their recorded positions. These results established that the sun and stars were not at rest relative to one another in the Galaxy. In 1785 William Herschel derived the first schematic picture of the Galaxy from optical "star gauging" in 700 separate regions of the sky. He did this by making star counts to the visual limit of his 20 ft. (72-inch diameter) telescope. He assumed that $r \sim N^{1/3}$ (i.e. $N \sim r^3$), and obtained relative thicknesses for the galactic disk in the various directions sampled. No absolute dimensions were established. By 1817 Hershel had adopted a new picture of the Galaxy as a flattened disk of nearly infinite extension (similar to the modern picture). In 1837 Argelander of the Bonn Observatory, and the orginator of the BD catalogue, was able to derive an apex for the solar motion from studying stellar proper motions. His result is very similar to that recognized today. Also in 1837, Frederick Struve found evidence for interstellar extinction in star count data, which was considered necessary at that time to resolve Herschel's "infinite universe" with Olber's paradox (which had been published in 1823).

By the turn of the century many astronomers felt that a concerted, detailed effort should be made to establish reliable dimensions for the Milky Way. The task was initiated by Kapteyn in 1905 with his plan to study in a systematic fashion 206 special areas, each 1° square, covering most of the sky — the well known "Selected Areas" for galactic research. By this time, separately-pursued research programs into the nature of the Milky Way system often produced distinctly different results. In 1918, for example, Shapley noted the asymmetric location of the centre of the globular cluster system with respect to the sun, and suggested that it coincided with the centre of the Galaxy. The 1920 publication of Kapteyn and van Rhijn's initial results from star counts in their selected areas yielded a distinctly different Galaxy model which had a radius of ~4.5 kpc along its major plane and a radius of ~0.8 kpc at the poles. It was not until 1922 that Kapteyn published an alternate model of the Galaxy in which the sun was displaced slightly from the centre, although still by an amount far less than the distance to the centre of the globular cluster system established by Shapley.

The issue reached a turning point, of sorts, in 1920 with the well known Shapley-Curtis debate on the extent of the galactic system. The merits of the arguments presented on both sides of this debate have been the subject of considerable study over the years, but it was years later before the true extragalactic nature of the spiral nebulae was recognized. A big step was Hubble's 1924 derivation of the distance to the Andromeda Nebula using Cepheid variables. Somewhat less well-known is Lindblad's 1926 development of a mathematical model for galactic rotation. Lindblad's model underwent further development in 1927-28 by Oort, who was able to demonstrate its applicability to the radial velocity data for stars. Finally, in 1930 Trumpler was able to provide sound evidence for the existence of interstellar extinction from an extremely detailed study of the distances and diameters of open clusters.

The modern era orginated in 1944 when Baade published his ideas on different stellar populations. In 1940 during World War II, Grote Reber had discovered the radio radiation from the galactic centre, but it was not until after the end of the war that this discovery was pursued by research groups in The Netherlands (Müller and Oort), the U.S. (Ewen and Purcell), and Australia (Christiansen), often making use of radio dishes left behind by German occupation forces. The prediction and confirmation of the 21-cm transition of neutral hydrogen in the galactic disk intiated the new specialty of radio astronomy, and led to a boom era in the study of our Galaxy. Although less popular now than it was 30 years ago, galactic astronomy is still an important area of study.

arrived at the University of Patras on the morni of August 20th, the IAU flags were flying at half-mast. We soon learned that M. K. Vainu Bappu, president of the union, had passed away at age 55 the previous day in Munich, West Germany. Dr. Bappu had been the driving force be-

Appreciations of both these important figures in 20th-c ury astronomy are planned for a future issue.

POLITICS

I suppose at any international gathering these days, it's impossible to avoid interna-

1960's and 1970's. Nowadays many countries share the forefront, and many others, such as Greece, Spain, and Mex , are rapidly increasing their astronomical involvement. This is a very healthy situation; the future of astronomy looks bright indeed!

LEIF J. ROBINSON

Alert for Astronomers: 1984 Is Coming

A number of resolutions adopted by the International Astronomical Union in 1976, 1979, and 1982 will apply to the mathematical reduction of observations after January 1, 1984, and to the preparation of ephemerides for 1984 and thereafter. These resolutions embody decisions that will affect all astronomers to some extent; they will also necessitate sweeping revisions by those who apply reference data and algorithms in fundamental astronomy, astrometry, timekeeping, celestial mechanics, and geodesy.

The changes are as follows:

• There will be a new fundamental epoch, designated J2000.0 and corresponding to January 1.5, 2000, or Julian Day number 2,451,545.0. A Julian century of 36,525 days will be used as the time unit for precession and for proper-motion calculations.

• The new constant of precession will differ from S. Newcomb's 1897 value by 1.1 arc seconds per century. This will cause changes in the stellar proper-motion system.

• The equinox of the Fifth Fundamental Catalogue will replace the FK4 equinox as the origin of right ascension. This means a shift of about 0.06 second of time at 1984 and a correction that is time dependent. The correction to the right ascensions of the FK4 is given by the expression

$$E(T) = 0.035\text{s} + 0.085\text{s}\ (y - 1950)/100,$$

where y is the year.

• The expression for Greenwich mean sidereal time is amended so there will not be a step change at the epoch or in rate due to the FK5 equinox correction.

• The IAU (1976) system of astronomical constants includes corrections to the values of the speed of light, radius of the Earth, Earth-Moon mass ratio, planetary masses, aberration constant, and other quantities.

• The 1980 IAU theory of nutation is based on a flexible mantle and liquid-core model of the Earth and includes forced diurnal polar motion and a change in the definition of the celestial pole.

• Dynamical time scales have been defined to replace Ephemeris time with Terrestrial Dynamic time (TDT), which equals International Atomic time (TAI) plus 32.184s, and Barycentric Dynamical time (TDB), which equals TDT plus relativistic terms.

• New planetary and lunar ephemerides will be based on the new astronomical constants, modified as necessary to fit the available observational data.

• The "E-terms" of aberration will be removed from catalogue mean places of stars. The gravitational deflection of light will be included in apparent-place computations.

A number of efforts are currently in progress to facilitate the implementation of the IAU resolutions. The 1984 edition of the *Astronomical Almanac* will be based on these resolutions and will include a supplement providing the details of the changes. The FK5 catalogue is being prepared at the Astronomisches Rechen-Institut in Heidelberg. Computer subroutines for reducing mean to apparent places for stars are currently being tested at the U. S. Naval Observatory and the Royal Greenwich Observatory.

U. S. Naval Observatory *Circular* 163, edited by G. H. Kaplan, summarizes and explains the resolutions further, and also provides a bibliography and a list of the changes. This circular is available upon request from the director, Nautical Almanac Office, U. S. Naval Observatory, Washington, D. C. 20390.

P. K. SEIDELMANN and
G. H. KAPLAN

2. Current Model of the Galaxy

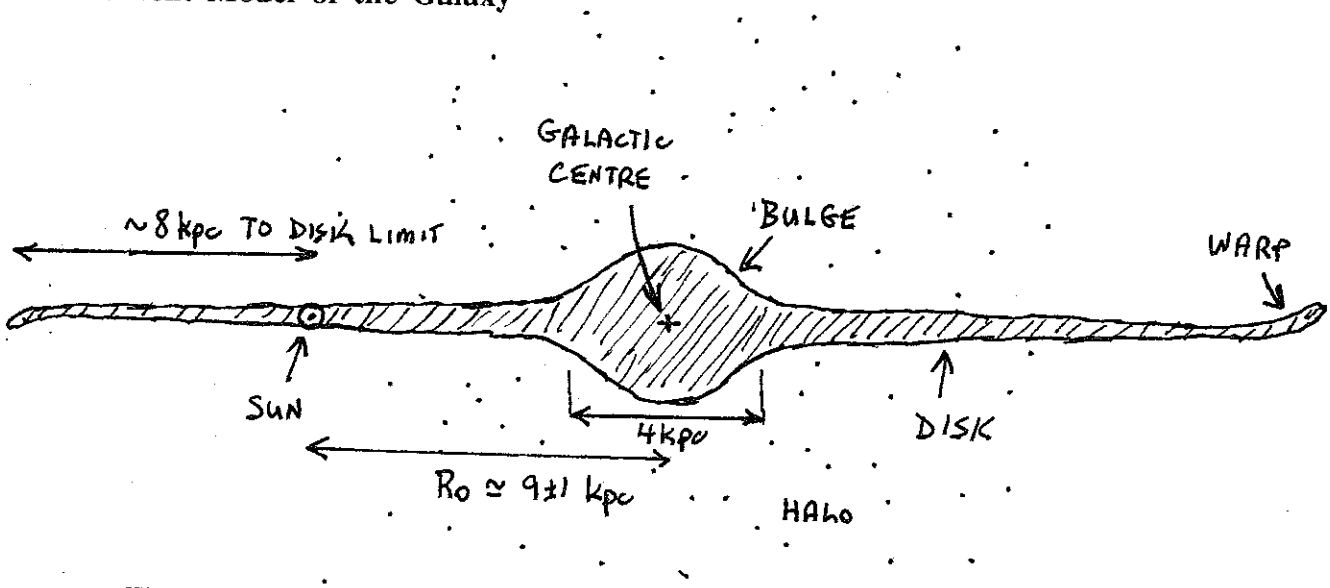

The best current estimates for the distance of the sun from the galactic centre give values which tend to cluster around ~9 ±1 kpc = R_0, although this is not well-established. Estimates as low as ~7 kpc and as high as ~10.5 kpc have been published. The main components of the Galaxy are the bulge, the disk (which contains the spiral arms), and the halo, with some debate about the exact number of subgroups of these. There is considerable evidence for a metallicity gradient in the disk with stars of higher metallicity lying towards the galactic centre. The metal enrichment of the disk is attributed to evolutionary processes in stars, which end their lives by adding a rich supply of heavy elements to the interstellar medium. When the mean metallicity of disk stars is studied as a function of the ages of these stars, there appears to be a net metallicity growth with age amounting to:

Δ<[Fe/H]> $\approx$ 0.5–0.7/10^{10} years, i.e. an increase of Fe/H by 4 ±1 every 10^{10} years.
This relation is not zeroed to the sun, since solar metallicity is calculated to have been reached at an age of ~2.5 × 10^9 years. The parameter [Fe/H] = log[(Fe/H)/(F/H)$_\odot$], i.e. 2 × the solar metallicity is equivalent to [Fe/H] = +0.30.

A suggested division of the main components of the Galaxy is given on a class handout, although this should not be considered definitive. There are at least two components of the halo currently recognized, as well as some argument about the number of disk components which can be identified (thin disk, thick disk, etc.). The components of spiral arms appear to differ only slightly in age, and many astronomers would identify these as a single young Population I component.

3. Stellar Reference Frames and Proper Motions

If we define the equatorial coordinates of a star to be α_1 and δ_1 at epoch T_1, and α_2 and δ_2 at epoch T_2, then:

$\alpha_2 - \alpha_1 = (\mathbf{m + n \sin \alpha \tan \delta} + \mu_\alpha) \times (T_2 - T_1)$

and $\delta_2 - \delta_1 = (\mathbf{n \cos \alpha} + \mu_\delta) \times (T_2 - T_1)$, where m and n are the terms for general precession.

As determined by Newcomb with respect to observations of planets and asteroids, with known (or estimated) masses of solar system objects used to establish a dynamical rest frame, the "constant" of luni-solar precession is given by:

p = 50".2910 + 0".0222 T per year (where T is the number of elapsed centuries since J2000.0), i.e. p = 50".2688 per year for the year J1900.0.

Thus, p(1985.0) = 50".2910 – 0".0222 (85.0/100) per year = 50".27213 per year.

General precession consists of two terms — p_1 = luni-solar precession, and λ = planetary precession (a function of α only).
Thus, $\mathbf{m = p_1 \cos \varepsilon - \lambda = 3^s.07496 + 0^s.00186T}$ **/year**,
and $\mathbf{n = p_1 \sin \varepsilon = 1^s.33621 - 0^s.00057T}$ **/year** $\mathbf{= 20".0431 - 0".0085T}$ **/year**,
where ε is the obliquity of the ecliptic.
The parameters μ_α and μ_δ are the proper motions in right ascension and declination, respectively.

i.e. $\mu_\alpha = \dfrac{d\alpha}{dT} - (\mathbf{m + n \sin \alpha \tan \delta})$, $\mu_\delta = \dfrac{d\delta}{dT} - (\mathbf{n \cos \alpha})$, and the net proper motion of an object is given by $\mu = [(\mu_\alpha \cos \delta)^2 + \mu_\delta^2]^{1/2}$. Accurate proper motions for stars therefore require small internal errors of observation as well as a detailed knowledge of the inertial reference frame and the resulting precession constants (which are not well determined).

The steps usually taken to determine reliable proper motions for stars are:
(i) Meridian telescopes and accurate clocks are used to establish reliable position measurements for bright stars, with stellar observations also being used (if possible) to establish the location of the celestial pole for the epoch of the observations.
(ii) The current right ascensions and declinations for all program stars are obtained from repeated measurements of each star's meridian crossing times as well as its culmination points measured on the telescope's large altitude circle.
(iii) Published precession and nutation constants are used to reduce the observations to a common nearby epoch in time, and the results are published as a Catalogue of Stellar Positions.
(iv) Several such catalogues are reduced to a common epoch to establish the proper motions, systematic observatory errors, systematic precession constant errors, etc. for a common set of stars. The resulting collection of positions and proper motions is a Compilation Catalogue.
(v) When several such catalogues are combined with a new set of planetary observations used to redefine the inertial reference frame for the precessional corrections, the resulting compilation of positions and motions tied to the inertial reference frame is known as a Fundamental Catalogue, e.g. the FK4 and FK5.
(vi) Proper motion data for stars in Position Catalogues but not in a Fundamental Catalogue are obtained by establishing Catalogue corrections tied to the Fundamental Catalogue reference frame. Several such "non-fundamental" catalogues exist, of which the SAO Catalogue and AGK3 are two examples.

A simple way of assessing the problem of deriving reliable proper motions for stars is to consider the various sources of error involved:
The proper motion of a star in a fundamental catalogue, μ_F, is given by:

$$\mu_F = \mathbf{P + S + G} + (\mu + \sigma_F + \varepsilon_F) \text{ , where:}$$

P = the effect due to an error in precession,
S = the effect due to the solar motion,
G = the effect due to galactic rotation,
μ = the residual motion of the star after removal of P, S & G (i.e. the star's space motion),
σ_F = the systematic error of the fundamental system (always a possibility!), and
ε_F = the accidental error for a particular star.

Usually, catalogued μ_F values are used for as many stars as possible, distributed at random in position and magnitude, to remove μ, σ_F, and ε_F from discussion. Any subsequent analyses of μ_F values to derive S and G may therefore contain an error caused by P. In fact, evidence for a residual error in precession for the FK4 system (i.e. $P > 0$) was the primary motivation behind the studies leading to the production of the FK5 Catalogue.

A possible alternate route is to use galaxies as reference objects for the positions of stars, which is possible for images measured on photographic plates. In this case, the proper motion of a star, μ_G, measured in this fashion relative to galaxies, is given by:

$$\mu_G = \mathbf{S + G} + (\mu + \sigma_G + \varepsilon_G), \text{ with the symbols as above.}$$

Proper motions obtained in this fashion do not involve uncertainties in the precession corrections.

The resulting differences in proper motion are: $\mu_F - \mu_G = P + (\sigma_F - \sigma_G + \varepsilon_F - \varepsilon_G)$. Thus, analyses of large numbers of stars measured by both techniques can be used to establish P, provided that the terms in brackets are completely randomized.

The potential advantages of measuring stars relative to galaxies was realized in the 1950s and 1960s, and led to the development of two observatory programs to carry these through. The **Lick Observatory** program (Vasilevskis) used the 0.5-m astrograph with 6° × 6° plates, and typically ~60 (faint) galaxies per field (to ~19th magnitude). The galaxies (which were usually faint and fuzzy) were used to establish the plate constants, their correct orientations, etc., with limited success. The **Pulkovo Observatory** program (Fatchikin) used the normal astrograph with 2° × 2° plates, and typically only 1 or 2 bright (nearby) galaxies (to ~9th magnitude) per field. These galaxies were used to standardize the plates, with stars on the plates used to establish the reference system, plate constants, etc. The Pulkovo program results are clearly based on a different standardization from that used in the Lick program. The **Yale-Columbia** program was a southern replication of the Lick program using an 0.5-m astrograph with 6° × 6° plates, but also with superior optics to the Lick and Carnegie astrographs.

Hanson (AJ, 80, 379, 1975; IAU Symp., 85, 71, 1980) used some of the Lick program plates for the central (and later outer) regions of the Hyades cluster field for his Ph.D. thesis study of the Hyades cluster distance based upon proper motions. This study has been heavily criticized by Luyten (Publ.Univ.Minnesota, XLI, 1975), who has argued that the technique suffers from the non-stellar nature of the galaxy images — which assures that the stars and galaxies in these fields are measured in completely different ways. He has suggested an alternative method of tying the measurements to quasar images, although this may not be practical for fields like the Hyades.

Uncertainties in proper motion measurements are typically on the order of ±0".005 /year to ±0".010 /year, although this will change with the results from the HIPPARCOS satellite. Proper motion studies are also made for open clusters, where they are used to study membership probabilities for cluster stars. In this case, membership discrimination is based upon the analysis of proper motions relative to some inferred field star distribution.

i.e. $P_\alpha = \left(\frac{a}{a+b}\right) \times 100\%,$

$P_\delta = \left(\frac{c}{c+d}\right) \times 100\%,$

and $P = (P_\alpha^2 + P_\delta^2)^{1/2}.$

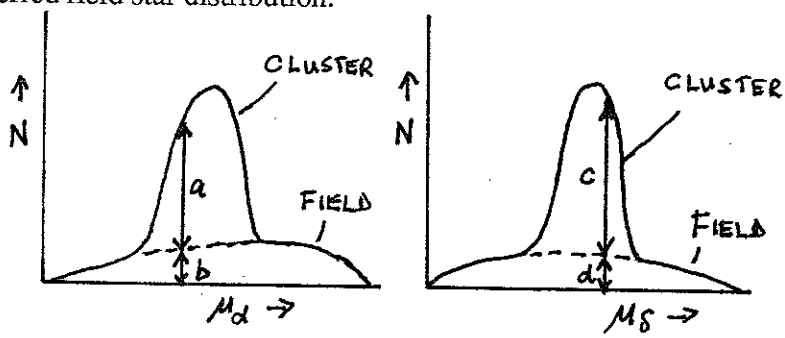

Recent variations of the general method sometimes make use of each star's position in the cluster, in addition to its proper motion, to specify membership probability.

4. Stellar Parallaxes

Stellar parallax is the displacement in a star's position in the sky with respect to the stellar background arising from the orbital motion of the Earth about the sun. Denoted by the angle π, it is defined to be the angle subtended by 1 A.U. (the semi-major axis of the Earth's orbit) at the distance of the star. In the skinny triangle approximation, 1 A.U. is the chord length subtended at the star by the angle π, measured in radians. In this case, the chord length ≈ the arc length subtended at the star = d × π, where d is the distance to the star. Since $\pi < 1"$ for all stars, the equation can be written as an equality, i.e. 1 A.U. = d π.

$\therefore \quad d = \frac{1 \text{ A.U.}}{\pi}$, once the parallax of the star is known.

In order to take advantage of trigonometric stellar parallaxes, which are measured in units of arcseconds, it is useful to define a unit of distance which corresponds to this angle. Thus, the **parsec** is defined to be the distance of an object at which 1 astronomical unit (A.U.) subtends an angle of 1 arcsecond,

i.e. $\mathbf{d\ (parsecs)} = \dfrac{1}{\pi\ \mathbf{(arcseconds)}}$ [$\mathbf{d} = \dfrac{1}{\pi}$ **for short**].

Since 1 radian = 206264".80625 ≈ 206265", it should be clear that:

$$1 \text{ parsec} = \frac{1 \text{ A.U.}}{1/206265} = 206265 \text{ A.U.}$$

Since 1 A.U. $= 1.496 \times 10^8$ km,

$\therefore$ 1 parsec $= 206265 \times 1.496 \times 10^8$ km $= 3.086 \times 10^{13}$ km (= 3.26 light years).

In general practice, parallax images at an observatory are taken ~6 months apart during evening and morning twilight when the program stars lie close to the meridian. This assures that the parallax factor has been maximized (the star lies closest to the extremes of the parallactic ellipse) while the effects of atmospheric refraction are kept to a minimum. Image series (mainly plate series) are continued for several years to allow removal of proper motion from the observed displacements. Other effects, aberration, refraction, etc., are common to all stars in the same field, and are usually negligible. However, all stars in the same field will show the effects of parallax, depending upon how distant they are from the Earth. Since the effects of parallax for the star of interest will also be mimicked to a certain extent by the other stars in the field, it is necessary to take this into account when measuring the parallax of the program star. All parallactic displacements for program stars are therefore measured with respect to the grid of suitably faint (and, hence, distant) field stars in their vicinity. This measured parallax is referred to as the **relative parallax**, π_{rel}. The true, or **absolute, parallax** of the star, π_{abs}, must be obtained by adding a correction for the mean parallax of the reference stars.

i.e. $\pi_{\mathbf{abs}} = \pi_{\mathbf{rel}} + \Delta\pi$.

Typical corrections depend upon the apparent brightness of the reference stars, as well as their luminosities, and are generally of order 0".003. Such corrections are typical of the older plate series made with refracting telescopes, where typical short exposures reached only stars of about 10th or 11th magnitude. Newer plate and imaging series use longer exposures, and reach fainter reference stars, in some cases of 15th and 16th magnitude. The HIPPARCOS satellite is measuring absolute parallaxes directly using twin skewed telescopes to measure angular displacements relative to an absolute reference frame. It has yet to be determined how successful this program will be.

The large proportion of measured trigonometric parallaxes for stars were obtained photographically using long focal length refractors. Modern photographic parallax programs originated with Schlesinger in 1903 with the Yerkes 40-inch refractor. Schlesinger later started the parallax programs at the Allegheny Observatory (1914) and at the Yale Southern Station in Johannesburg, South Africa (1925). Colleagues of Schlesinger were responsible for continuing the program at Yerkes, and for developing the programs at the Van Vleck and Leander McCormick Observatories. Programs at the Greenwich Observatory, Cape Observatory, and Sproul Observatory were intiated in the same mode as Schlesinger's precepts. Van Maanen's parallax program on the 60-inch reflector at Mount Wilson Observatory used different techniques. Since the era of the 1960's, the U.S. Naval Observatory (USNO) has used a 60-inch reflector at Flagstaff to take parallax plates for relatively faint stars. All of the plates in this series have been measured automatically using the Strand Semi-Automatic Measuring Machine (SAMM) in Washington, D.C. A new series makes use of a CCD detector to record even fainter stars.

The standard sources of older trigonometric parallax data are Jenkins' **General Catalogue of Trigonometric Parallaxes** (1952) and its **Supplement** (1963), published by the Yale Observatory. These catalogues contain ~7000 stars with older measured parallaxes, all reduced to a common system using a detailed intercomparison of internal and external Observatory errors known as the Yale precepts. A new, updated, version of this catalogue which incorporates newer results has been promised by Art Upgren of the Yale Observatory since ~1983, but has not yet appeared.

Errors in trigonometric parallaxes arise from several different sources, including optical instabilities in the telescopes (particularly severe for the old refractors), errors in measurement, and the problems of establishing a proper reference frame of field stars. The main sources of error are: (i) **internal errors** (hopefully random) due to all of the above problems, and (ii) **external errors** (systematic) arising from various sources, such as the use of variable-width sectors at Allegheny for measuring bright stars, and corrections from relative to absolute parallax. According to recent studies into such problems: (i) the USNO parallaxes appear to be free of external errors, so that their internal error estimates represent the true parallax errors, and (ii) the old Allegheny parallaxes for bright stars contain a magnitude dependent error. Thus, π_{rel} (Allegheny) = π_{rel} (published) + 0".003 (7 – B), for blue magnitude B such that $3 < B < 7$.

The systematic error in the Allegheny parallaxes is unfortunate, since all other tests indicate that the Allegheny parallaxes have the smallest internal and external errors of all published refractor parallaxes. The McCormick parallaxes have the largest errors, and their internal error estimates appear to be unrelated to the true parallax errors for their stars. Currently, the USNO parallaxes are the most accurate available. The total parallax errors, $\Delta\pi$, for trigonometric parallaxes measured at various observatories (old and new) have been estimated to be:

Allegheny	±0".009	Cambridge	±0".023
McCormick	±0".018	Van Vleck	±0".010
Yale	±0".015	Herstmonceux	±0".008
Cape	±0".017	Lick	±0".008
Greenwich	±0".018	USNO (average)	±0".004
Mt. Wilson	±0".020	USNO (fine-grained emulsions)	±0".002
HIPPARCOS	±0".001	USNO (CCD detector)	±0".001

Since $d = \frac{1}{\pi}$, it follows that $\frac{\Delta d}{d} = \frac{\Delta\pi}{\pi}$, where Δd is the uncertainty in distance, and $\Delta\pi$ is the uncertainty in the measured parallax. Weights are assigned to measured parallaxes from different sources based upon their estimated errors. Thus,

$$(\Delta\pi)^2 = (\Delta\pi_{internal})^2 + (\Delta\pi_{external})^2 \text{ , and Weight, } W_i = \frac{1}{(\Delta\pi)^2} .$$

The mean trigonometric parallax resulting from the combination of several estimates is found using:

$$<\pi> = \frac{\Sigma\, \pi_i W_i}{\Sigma\, W_i} \quad \text{and} \quad <\Delta\pi> = \left(\frac{1}{\Sigma\, W_i}\right)^{1/2} .$$

It has long been recognized that there are problems with the older parallaxes collected in the GCTSP, since its π values are all π_{rel} reduced to the system of the Allegheny Observatory with a correction of +0."003 added to bring them to absolute. The complicated Yale precepts end up making all Observatory corrections negative except those for the Allegheny Observatory. Some of the published π_{rel} values depend on the order of publication for various imaging series. For example, remeasured McCormick parallaxes at one period were in better agreement with Allegheny parallaxes published after the publication of their preliminary value than with their own original estimate! This appears to be a case of trying to match the results from a recognized higher quality institution. Also complicating the issue is the impossibility of retaining a refractor's imaging characteristics after it has been disassembled for cleaning. The advent of computers has allowed new parallax series to be reduced using much larger reference frames (12-16 stars or so) than the original 3-4 star reference frame used in Schlesinger's era. This has reduced the random errors in parallax measurements considerably, although uncertain external Observatory errors remain. The parallaxes generated using the U.S. Naval Observatory reflector are currently the best available, since tests indicate that they seem to be free of any external error. Since they also make use of fairly faint stars for their reference frames, their estimated internal errors of ±0".002 to ±0".004 are actually smaller than the corrections to absolute. Their recent initiation of parallax measurements using CCD detectors has already (1990) generated parallaxes with quoted uncertainties of only ±0".001, which is probably comparable to those being produced by the HIPPARCOS satellite.

Calibration of Luminosities Using Parallax Data.

A variety of problems are encountered when using parallax measurements to calibrate the luminosities of different objects. One of these is the tendency for any survey to sample preferentially the most luminous objects of its type when it is limited by apparent magnitude, for example, the determination of M_V for B5 V stars. This is known as **Malmquist bias**, for which suitable corrections exist. The presence of measuring errors in trigonometric parallaxes also makes their use in luminosity calibrations susceptible to bias. Lutz and Kelker (PASP, 85, 573, 1973) first drew attention to this problem by noting the difference between the observed absolute parallax for a star, π_o, and its true absolute parallax, π_{abs}. The observed parallax has an associated uncertainty, $\pm\sigma$, such that $\pi_o-\sigma < \pi_{abs} < \pi_o+\sigma$. This means that the true distance to the star, d_*, lies somewhere in the spherical-volume shell defined by $d\pm\Delta d$, where $d = 1/\pi_o$. For a uniform distribution of stars in space, there will be more stars lying outside this volume which are scattered into the volume than there are stars lying inside of the volume which are scattered into it. In other words, the distance to the observed star is statistically likely to be larger than d given by the value of $1/\pi_o$. Corrections can be estimated for the amount of this bias based upon the known values for π_o and $\pm\sigma$. A significant improvement upon the general **Lutz/Kelker corrections** has been made by Hanson (MNRAS, 186, 875, 1979). This technique makes use of proper motion data for the sample of parallax stars in order to estimate their actual space distribution. Typical samples of parallax stars lack the degree of completeness necessary to consider them to be drawn from a uniformly distributed spatial selection of stars. As demonstrated by Hanson, different bias corrections are required for non-uniform statistical samples than is the case for the uniform-density samples considered by Lutz and Kelker. Further studies of this type of bias have been published by Lutz (MNRAS, 189, 273, 1979; IAU Colloq., 76, 41, 1983) and Smith (A&A, 188, 233, 1987).

5. Stellar Radial Velocities

Radial velocities of stars are determined from a comparison of the observed wavelengths, λ, for their identified spectral lines with the corresponding rest wavelengths, λ_o, expected for them, i.e. $V_R = \left(\frac{\lambda - \lambda_o}{\lambda_o}\right)c$, where c = the velocity of light.

Note that there is no need for relativistic corrections for most stellar velocities, although observed velocities do need to be corrected for the rotation (0.47 km/s at the equator) and orbital motion (29.8 km/s) of the Earth in order that they are **heliocentric** (or, more properly, **barycentric**).

In photographic stellar spectroscopy, the stellar spectrum is exposed on a photographic emulsion along with a suitable bracketing emission spectrum from a comparison source, normally an Fe arc, hollow cathode Fe comparison source, He Ar lamp, or Ne lamp, depending upon the wavelength region of interest (Fe lines are most plentiful in the blue-green spectral region). The rest wavelengths of these comparison lines are well known from laboratory measurements. The velocity of the star is determined by first establishing a relationship between plate position and wavelength from measurements of the comparison arc lines on a measuring engine, and then comparing the similarly-measured positions of the stellar lines (converted to wavelengths) with their rest positions using the above equation. Each spectral line measured gives an estimate of V_R for the star, and the individual values for the "best" lines are normally averaged to obtain a more accurate mean value. It should be obvious that the procedure is subject to some uncertainties. Early-type stars, for example, have very few spectral lines, and those that are found in their spectra are often quite broad and therefore difficult to measure accurately. The prominent lines are frequently also blends of several separate lines, and their "effective wavelengths" may need to be calibrated using observations of stars of known velocity. The typical uncertainties in radial velocity measurements for these stars are about ±2 to ±3 km/s. Late-type stars exhibit many more spectral lines, most of which are quite sharp and easy to measure. In this case, the effects of line blending are usually better understood. The typical uncertainties in radial velocity measurements

for these stars are about ±1 km/s or less. In general, the uncertainties in radial velocity measurements vary as the inverse of the spectrograph dispersion, i.e. $\sigma \sim$ 1/dispersion.

Currently, most measurements of radial velocities for late-type stars are being done using radial velocity spectrometers (or speedometers) which use a comparison star mask (typically a spectrum of Arcturus or an artificially-generated spectrum) to scan repeatedly across the spectrum of the program star. The stellar spectrum signal transmitted through the mask is recorded as a function of scanning x-position of the mask using a photomultiplier tube, and the position of minimum throughput is used to specify the star's velocity. The spectrometer is calibrated in various ways using a reference source, the sky spectrum (during twilight hours), and the solar spectrum reflected from planetary satellites. These devices are somewhat limited in their spectral coverage by the mask employed (usually they are restricted to spectral types F or later), but are nevertheless easier to use and faster than photographic plates, reach fainter stars, and have high internal accuracy. Typical uncertainties in single radial velocity measurements with these devices (Griffin-type Radial Velocity Scanners, CORAVEL, etc.) are about ±0.5 km/s. The measurements for early-type stars can often be obtained using CCD detectors, with cross-correlation techniques and synthetically-generated comparison spectra used to optimize the results.

The major difficulties encountered in determining reliable radial velocities for stars are:
(i) Variability. Stellar pulsation and orbital motion about an unseen companion produce temporal variations in the observed radial velocities for some types of stars.
(ii) Blending. Double-lined spectroscopic binaries can have blended spectral lines at some or all phases which make it difficult to derive accurate radial velocities for the systems.
(iii) Rapid Rotation. Rapidly-rotating stars viewed nearly equator-on have very broad and diffuse spectral lines which are extremely difficult to measure for radial velocities. Line profile fitting software is extremely valuable in such instances.
(iv) Emission Lines. Emission components of spectral lines usually distort the line profiles in such a manner as to make it impossible to obtain the true radial velocities of the stars. The emission produced by a diffuse shell surrounding a star typically produces a P Cygni–type of profile consisting of a sharp blue absorption feature on an broad emission line. The determination of realistic systemic velocities for such stars is an ongoing problem in astronomy.

In general, the accuracy of radial velocity measurements depends mainly upon the spectroscopic dispersion used to obatin the stellar spectra. The greater the dispersion (10 Å/mm rather than 50 Å/mm), the more accurate the resulting V_R. Spectrographs mounted on telescopes are also susceptible to problems due to flexure, bad optics, and thermal effects, which can produce systematic effects on the derived radial velocities. Radial velocity spectrometers are therefore normally mounted at the Coudé focus of telescopes, where such problems do not arise. This is why they are recognized to produce more reliable results than those obtained from Cassegrain-mounted spectrographs.

6. Spectral Classification

Stellar spectra were observed and recorded long before the field of spectroscopy had fully developed. Prior to the laboratory identification of spectral lines at specific wavelengths with certain elements, some method of classifying stellar spectra was desirable. The hydrogen Balmer line sequence was recognized from the earliest such studies, and so the earliest classification scheme of any duration was a Harvard scheme based upon photographically-recorded blue-green spectra in the λ3900–5000Å region which designated stars according to a letter sequence A, B, C, D,... based upon the increasing degree of complexity of the spectrum relative to the simple Balmer line spectrum (type A being the least complicated). Pickering, at the Harvard Observatory, was able to revise the scheme in 1890 based upon the growing knowledge of atomic physics, which indicated both the element identification and degree of excitation or ionization for specific spectral lines. From this knowledge it became clear that the original scheme needed revision in order to eliminate certain redundant types as well as to order the types in a logical sequence. The revised sequence of types O, B, A, F, G, K, and M was a sequence in order of decreasing surface temperature, and has remained in use ever since.

The arrangement of spectral types in the Harvard scheme was subdivided numerically into finer temperature subtypes, such as B0, B2, B3, B5....A0, A2, A3, A5...etc. Note that not all spectral subtypes were used in this scheme; types B1 and B4, among others, simply did not exist. The O-type stars were subdivided differently, i.e. Oa, Ob, Oc, Od, and Oe, in order to avoid confusion with an alternate classification scheme of that era. Special designations were also developed for stars having peculiar spectral properties, namely:

c = narrow lines (typical of supergiant stars)
g = giant spectrum
d = dwarf (main-sequence) spectrum
pec = peculiar spectrum (also abbreviated to p)
k = interstellar (sharp) Ca II K-line present
pq = nova-like spectrum (broad emission blends) .
e = emission lines present (the letter "f" was used to designate emission for O stars)
ev = variable emission
v = variable spectrum (as, for example, in a pulsating star)
n = wide and diffuse (nebulous) spectral lines (now recognized as due to rapid rotation)
nn = very diffuse spectral lines (for very rapid rotation)
s = sharp lines (generally due to a very low projected rotational velocity)

The MK classification scheme is a refinement to the original Harvard system of stellar classification which includes a designation for the star's luminosity as well as its temperature. This scheme went through an initial stage with a paper by Morgan, Keenan, and Kellerman (called the MKK scheme), but was later revised by Morgan and Keenan to the present MK scheme. Later modifications include more recent MK dagger typers, denoted MK†, and spectral subtypes and designations added by Nolan Walborn, a student of Morgan's (his last!).

The MK scheme includes the basic temperature subtypes of the Harvard scheme, with additions to fill out the temperature subclasses that can be distinguished at the dispersion (~100 Å/mm) used for MK classification, e.g. B0, B0.5, B1,... B9, B9.5, A0, A1,...etc. The O-type stars were reclassified numerically, and the original temperature ordering went O6, O7, O8, O9, O9.5, B0. Luminosity classes were added on the basis of the Saha ionization law, although the scheme was originally established as an empirical system based upon the observable spectral features of similar-temperature stars having known absolute magnitudes (stars with measurable parallaxes and stars in clusters and associations). In all cases, temperature subtypes and luminosity classes are established on the basis of specific line ratios which can be determined from stellar spectra. The luminosity types used are:

Ia = luminous supergiants (class 0 is used for supersupergiants = hypergiants)
Ib = less luminous supergiants
II = bright giants
III = giants
IV = subgiants
V = dwarfs (main-sequence stars)

Interpolated luminosity classes are also possible, such as IV-V, II-III, etc. Provisions were also made in the original scheme for subdwarfs (= VI) and white dwarfs (= VIII), but these classes never became popular.

Subdwarfs are now recognized as metal-poor stars which are difficult to classify in any case, and white dwarfs are degenerate stars (D) which have since been given their own claasification scheme for two recognized sequences — the hydrogen sequence (DO = He II strong, He I or H present, DA = only Balmer lines, no He I or metals present, and DA–F) and the helium-carbon (He-C) sequence (DC = continuous spectrum, no lines deeper than 5%, DB = He I lines, no H or metals present, DZ = metal lines only, no H or He, and DQ = carbon features, molecular or atomic). No luminosity classification is possible for white dwarfs which all have similar surface gravities ($\log g \approx 8$), but their surface temperatures vary from ~5000°K to ~100,000°K, which is specified in a temperature index = $10 \times \theta_{eff} = 50{,}400/T_{eff}$ [e.g. T_{eff} = 15,000°K, index = 3, $T_{eff} \leq$ 5500°K, index = 9 (can be increased if lots of cool degenerates are found), T_{eff} = 50,000 °K, index = 1, and T_{eff} > 100,000°K, index = 0]. Additional designations are used for: P = polarized

magnetic stars, H = magnetic stars with no polarization, Z = peculiar or unclassifiable spectra, and V = optional for VV Ceti variables (pulsating DA's). In this new scheme (Sion et al. 1983, ApJ, 269, 253), D = degenerate star, A,B,C,O,Z & Q = dominant spectroscopic type, A,B,C,O,Z & Q = secondary spectroscopic type (if needed), and 0,1,2,3,...9 = number designating T_{eff} (from colour). The complete designations for white dwarfs can therefore be relatively simple or moderately complex, e.g. DA1, DB3, DBZ4, DXH3, DOZ1.

The original MK scheme has been improved upon by the work of Morgan's students, such as Nolan Walborn, and by students of their students (e.g. Richard Gray). The result has been the extension of the temperature sequence for O stars to subtypes O3, O4, and O5, and a luminosity classification for O-type stars which is based upon their degree of "Of-ness", i.e. type f are class I, type (f) are class III, and type ((f)) are classes IV and V. Abt has done a lot of work classifying the Ap stars (A stars showing anomalous intensities of Mg, Si, Eu, and the rare earths Sr, Cr, etc.) and Am stars (metallic line strong for the strength of Ca K), and these stars are now recognized as being representative of the need for a third parameter in the system, such as chemical composition.

Spectral classification has always been recognized as an essential means of identifying important properties of stars such as: (i) temperature, (ii) luminosity, (iii) chemical composition, (iv) rotation rate, (v) companions, etc. Spectral classification itself is typically performed with the aid of photographic spectrograms (originally prism plates were used, but now grating plates are used exclusively) of stars. Classical MK dispersion is around 100-120 Å/mm, although some classifications are done at dispersions near ~60 Å/mm. The classification of hot (early-type) stars is done exclusively using blue spectra covering the interval 3900-4900 Å, but redder spectral regions are often used in the classification of red M-type stars and other cool (late-type) objects. Standard practice is to widen the spectra by ~1/3 of the separation of Hγ and Hδ. Since this corresponds to 4340Å – 4101Å = 239Å, at a dispersion of ~100 Å/mm the required widening is ~1/3 × (239/100) mm ≈ 0.8 mm.

The characteristics of stars of different temperature and luminosity classes can be explained with atomic physics using the Boltzmann and Saha equations. These specify the energy level populations for atoms and ions, as well as the population of different ionization states for different species of the same element. The principal temperature sensitive criteria are:

O stars: the He II/He I ratio is extremely sensitive to T.

B stars: the ratios of Si III/Si IV and Si II/He I are quite sensitive to T. He I lines peak in strength at B2–B3, the H lines strengthen towards A0, as do Mg II λ4481 and Ca II K λ3933 later than B5.

A stars: all metal lines increase in strength and H lines decrease in strength as T decreases. Balmer lines reach maximum strength at A0–A2.

F stars: the G band (of CH) increases in strength, the H lines decrease in strength, and Ca II H&K increase in strength as T decreases.

G stars: Ca II H&K, the G band, Ca I λ4226, etc. all increase in strength as T decreases.

K stars: Ca I increases in strength with decreasing T, and the lines of Fe I reach maximum strength.

M stars: molecular bands (such as TiO) overwhelm the blue part of the spectrum.

The anomalies are of different types. The most important represent stars in which the products of nuclear energy generation at the stellar core are seen at the stellar surface. These include the **Wolf-Rayet stars** (WR), which were first discovered by Wolf and Rayet in 1867. In these stars the products of H–burning in the CNO cycle (excess N and He — the WN stars), He–burning (excess C and He — the WC stars), and C–burning (excess O — the WO stars) are seen at the surface of OB stars (of ~20 $M_\odot$) which apparently have very high mass loss rates, or to a minor degree in the spectra of the central stars of some planetary nebulae, which are evolved Population II or old disk stars (of ~1 $M_\odot$) in which the outer layers have been stripped away by envelope helium flash events prior to the planetary nebula stage (all such objects are WC or WO types).

Also exhibiting compositional anomalies are **carbon stars**, which are late-type stars exhibiting excessive amounts of C in their spectra. The older types R, N, the carbon star equivalents of types K and M have now been replaced by the newer designation C#,#, where the

first number is the temperature type and the second is the abundance excess e.g. C1,0; C7,4; etc. (see Keenan's chapter in Basic Astronomical Data). These stars are all giants which have lost their outer layers, or stars in which deep convective eddies have dredged up nuclear-processed material from their cores. The **S stars** are equivalent to M-type stars, but the monoxides Ti0, V0, Sc0, Al0, etc. of light metals have been replaced by oxides of heavy metals, e.g. ZrO, La0, YO, etc. Comparable objects are the barium stars. The S stars represent objects in which nuclear-processed material by the S (slow) process has been brought to the stellar surface. They therefore represent advanced evolutionary stages of low mass stars.

The **peculiar A stars**, designated Ap, are stars which have anomalously intense lines of rare earth elements (La, Ce, Sm, Eu, Yb, etc.) and Mn, Si, Cr, and Sr, of differing intensity. They are subdivided into different subtypes (Mn, Si, Cr-Eu, Sr groups) on the basis of which spectral lines dominate. These represent different temperature subclasses in the B5 to F0 spectral interval. They appear to be slowly-rotating stars in which gravitational settling and magnetic effects have stratified and enhanced the surface compositions of some elements in the outer layers. The **metallic-lined stars**, designated Am, are otherwise normal A dwarfs in which the metallic lines appear anomalously strong in comparison with the lines of Ca II H&K. Generally of spectral types A1–A6 on the basis of their H&K lines, their metallic line strengths are typically those of cooler objects. The present notation is to estimate their temperature class using the strength of Ca II H&K, with a separate designation preceded by "m" to denote their temperature class based on the metal line strengths, e.g. AlmA6.

Low metallicity can make normal spectral classification particularly difficult, as is the case for Population II stars of all metallicities (see Keenan's chapter in Basic Astronomical Data). The need for a third dimension (metallicity) in the classification of these stars has made reliAble classification of such stars a daunting task.

Luminosity Effects.

Since $L \sim R^2T^4$, then $L \sim R^2$ for T constant. The surface gravity, $g = \frac{GM}{R^2}$.

$$\therefore \quad L \sim \frac{GMT^4}{g} \sim \frac{M}{g} \text{ for T constant.}$$

Even in the extreme case of M-type stars, g changes are greater than mass differences for stars of similar spectral type, and act to strengthen the L ratio between stars of different luminosity classes. A typical M supergiant has a mass of ~10–25 $M_\odot$ and $g \approx 1$–10, while a typical M dwarf as a mass of ~0.1 $M_\odot$ and $g \approx 10^4$–10^5.

$$\therefore \quad \frac{L(\text{supergiant})}{L(\text{dwarf})} \approx \frac{(10\text{–}25)}{(0.1)} \times \frac{(10^4\text{–}10^5)}{(1\text{–}10)} \approx 10^6 \text{ or so.}$$

Typically, log g ≈ 0–1 for extreme supergiants, ≈ 4–5 for dwarfs (it is 4.44 for the sun), and ≈ 8 for white dwarfs.

Hydrogen Lines.

The strength of the hydrogen lines in stellar spectra is governed by the abundance of hydrogen, by the effects of Stark broadening on the H spectral lines (caused by the charge effects of passing electrons), and by the continuous opacity source in the stellar atmosphere. The normal method of expressing line strength is to write it as:

$$\eta = \frac{l_\lambda}{\kappa_\lambda},$$

where l_λ is the line opacity function, and κ_λ is the continuous opacity function. For hydrogen, one can express the line opacity function in fairly simple terms:

$l_\lambda(H) = f(\lambda,T)\, N_H\, N_e$, where N_H is the number of hydrogen atoms, N_e is the number of electrons, and $f(\lambda,T)$ is the function governing the profile of the hydrogen line.

For hot O-type stars, the dominant continuous opacity source in stellar atmospheres is electron scattering, for which $\kappa_\lambda \sim N_e$. In this situation,

$\eta = \frac{j_\lambda}{\kappa_\lambda} = \frac{f(\lambda,T)\, N_H\, N_e}{N_e} \sim N_H$, which is a dependence independent of gravity (which governs N_e). Hot O-type stars are therefore not expected to exhibit much gravity (or luminosity) dependence in their hydrogen lines, a prediction well substantiated by observations of stellar spectra.

For B and A-type stars, the dominant continuous opacity source in stellar atmospheres is atomic hydrogen, for which $\kappa_\lambda \sim N_H$. In this situation,

$\eta = \frac{j_\lambda}{\kappa_\lambda} = \frac{f(\lambda,T)\, N_H\, N_e}{N_H} \sim N_e$, which is a dependence very dependent on gravity (which governs N_e). The B and A-type stars are therefore expected to exhibit quite dramatic variations in the strengths of their hydrogen lines as a function of surface gravity, or luminosity class, which is also a prediction well substantiated by observation.

For cool F, G, and K-type stars, the dominant continuous opacity source in stellar atmospheres is the negative hydrogen ion (H^-), for which $\kappa_\lambda \sim N_H N_e$. In this situation,

$\eta = \frac{j_\lambda}{\kappa_\lambda} = \frac{f(\lambda,T)\, N_H\, N_e}{N_H\, N_e} \sim f(\lambda,T)$, which is a dependence independent of gravity, similar to what was predicted for the hot O-type stars. Cool F, G, and K-type stars are therefore not expected to exhibit much gravity (or luminosity) dependence in their hydrogen lines, and this prediction is likewise well substantiated by observation.

The Balmer lines of hydrogen so prominent in stellar spectra are produced by hydrogen atoms in the n = 2 level (the ground state is n = 1), and this abundance is governed by the temperature T. As T increases, the population of the n = 2 level also increases, according to the predictions of the Boltzmann equation. However, as T increases, increasing ionization predicted by the Saha equation leads to a gradual depletion in the number of neutral atoms capable of producing Balmer lines. For hydrogen, $N_H = N_n + N_i$ [there are no other states for the singly charged H nucleus], where N_H is the total number of hydrogen atoms, N_n is the total number of neutral hydrogen atoms, and N_i is the total number of hydrogen ions. The strength of the hydrogen Balmer lines can be determined from the ratio of the number of atoms N_2 in the n = 2 level to the total number of hydrogen atoms, i.e. by:

$$\frac{N_2}{N_H} = \frac{N_2}{N_n + N_i} = \frac{\frac{N_2}{N_n}}{1 + \frac{N_i}{N_n}} .$$

The top term of this relation can be calculated from the Boltzmann equation, and the bottom term from the Saha equation, and both combined lead to a function which reaches a maximum at $T \approx 10{,}000°K$. The hydrogen Balmer lines in stellar spectra are observed to reach their greatest strength for dwarf stars of spectral type A0. This implies that the effective temperature T_{eff} of a typical A0 V class star must be very close to 10,000°K, which is one of many conclusions used to establish a correspondence between spectral type and T_{eff} for normal stars.

Gravity Dependence of Metal Line Ratios.

In standard MK spectral classification, it is line ratios, rather than just line strengths, which are important. The method of examining this type of dependence is to consider the following different cases:

Case 1. The lines of an element in one ionization state, where most of the atoms of that element are in the next higher ionization state,

Case 2. The lines of an element in one ionization state, where most of the atoms of that element are in the same ionization state, and

Case 3. The lines of an element in one ionization state, where most of the atoms of that element are in the next lower ionization state.

Ionic broadening plays only a minor role in the strength of metal lines; the strength of most is governed primarily by the abundance of the species responsible for the lines. Recall the simple form of the Saha equation:

$$\left[\frac{N^{n+1}}{N^n}\right] P_e = \Phi(T) .$$

For Case 1, the line opacity coefficient is $l_\lambda \sim N^n$, while the abundance of the element can be approximated by $N \approx N^{n+1}$.

$$\therefore \quad l_\lambda \sim N^n = \frac{N^{n+1} P_e}{\Phi(T)} \approx \frac{N P_e}{\Phi(T)} \sim P_e .$$

For Case 2, the line opacity coefficient is $l_\lambda \sim N^n \approx N$ (the abundance of the element).

For Case 3, the line opacity coefficient is $l_\lambda \sim N^{n+1}$, while the abundance of the element can be approximated by $N \approx N^n$.

$$\therefore \quad l_\lambda \sim N^{n+1} = \frac{N^n \Phi(T)}{P_e} \approx \frac{N \Phi(T)}{P_e} \sim \frac{1}{P_e} .$$

Recall that, for early-type stars, $\kappa_\lambda \sim N_H$ (the abundance of hydrogen).

$$\therefore \quad \eta = \frac{l_\lambda}{\kappa_\lambda} \sim P_e \text{ (for Case 1)},$$

$$\sim \text{constant terms (for Case 2), and}$$

$$\sim \frac{1}{P_e} \text{ (for Case 3)} .$$

The obvious conclusion from this analysis is that luminosity-sensitive (P_e–dependent) metal lines for early-type stars are those arising from elements in ionization states other than those where the element is most abundant. Good examples are the O II lines and N II (e.g. λ3995)lines in early B stars, where most of the species are O III and N III, respectively.

For late-type stars, $\kappa_\lambda \sim N_H N_e \approx N_H P_e$ (the abundance of H^- ions depends upon both N_H and N_e).

$$\therefore \quad \eta = \frac{l_\lambda}{\kappa_\lambda} \sim \text{constant terms (for Case 1)},$$

$$\sim \frac{1}{P_e} \text{ (for Case 2), and}$$

$$\sim \frac{1}{P_e^2} \text{ (for Case 3)} .$$

In this case, it appears that highly-ionized species are very sensitive luminosity indicators in late-type stars, where most of the species is either neutral or in a lower ionization state. Some specific examples can be found in the spectra of late-type stars. In F, G, and K-type stars, for instance, the lines of Fe I (neutral iron, e.g. λ4045) <u>are not</u> gravity dependent, whereas the lines of Fe II (singly ionized iron, e.g. λ4233) <u>are</u> gravity dependent. In G and K-type stars, the lines of Sr II (singly ionized strontium, e.g. λ4215) <u>are</u> also gravity dependent. Actually, the specific luminosity indicators in MK classification are <u>line ratios</u>. Thus, for late-type stars, the ratio of line strengths for $\frac{\text{Sr II } (\lambda 4215)}{\text{Fe I } (\lambda 4260)}$ is an excellent indicator of luminosity class for these stars (most Sr and Fe is neutral), and is relatively independent of any variations in the abundance of strontium or iron.

The main problems with spectral classification are inexperience and the use of observational data of questionable quality. Novices invariably attempt to match the overall appearance of stellar spectra with those of established spectroscopic standards, and it takes some practice to develop the techniques of using observable line ratios to classify stellar spectra. The best spectral classifiers were invariably taught by Morgan or his students. Automated techniques are somewhat poorly designed for the examination of spectral line ratios in comparison with eye estimates, although these techniques are gradually being introduced successfully. High signal-to-noise ratio spectra (as obtained, for example, using CCD detectors) are also highly desirable.

7. Photometric Systems

The primary purpose of photometry is to obtain information equivalent to spectroscopic data in a smaller amount of observing time. It is also a highly efficient method of studying variable stars. Stellar continua vary with spectral type, and different photometric systems are designed to sample selected portions of these continua which are of use either for the equivalent of spectral classification or for estimating third dimensions for stars, e.g. metallicity, etc. Basically any photometric system must be capable of determining a star's spectral class, corrected for interstellar extinction, without serious problems due to luminosity differences, or population effects. Systems are classified on the basis of the widths of the wavelength–bands used to define them. Broad band systems make use of passbands which are anywhere from 300 to 1000Å wide (e.g. the UBV system), intermediate band systems make use of passbands which are anywhere from 100 to 300Å wide (e.g. the Strömgren uvby system), and narrow band systems make use of passbands which are less than 100Å wide (e.g. Hβ photometry). Systems are usually classified on the basis of the narrowest passband used, although this convention varies, e.g. Strömgren photometry (uvby) is still intermediate band photometry, even though it is normally done in conjunction with Hβ photometry.

For early-type stars, the Balmer jump (λ3647) and Paschen jump (λ8206) result from the opacity due to neutral H, and these features are modified by electron scattering in hot O-type stars and H^- (negative hydrogen ion) opacity in cool G and K–type stars. The Balmer jump is very sensitive to both temperature and gravity, and so many photometric systems employ filter sets which attempt to isolate the stellar continuum on either side of the discontinuity.

Johnson's UBV System.

The UBV system is designed to give magnitudes which are similar to those on the old International photographic and photovisual system, with a magnitude added on the short wavelength side of the Balmer discontinuity in order to give luminosity discrimination.

Filter	**λeff**	**Δλ (half-width)**
U	3500Å	700Å (faintest magnitude)
B	4350Å	970Å (brightest magnitude)
V	5550Å	850Å

The UBV system was defined by Johnson using: (i) an RCA 1P21 photomultiplier with U (Corning no. 9863 filter), B (Corning no. 5030 filter + 2 mm Schott GG13 filter), and V (Corning no. 3384 filter) standard filter sets, (ii) a reflecting telescope with aluminized mirrors, (iii) standard reduction procedures (later), and (iv) an altitude for observations of ~7000 feet. The standard colour indices in this system were defined to be U–B = B–V = 0.00 for unreddened AO V stars in the North Polar Sequence. The major problem with UBV photometry has always been that there is a small red leak in the U filter which can result in contamination by red light from stars for later production runs of the RCA 1P21. Also, transformation difficulties are notorious for other photometer types e.g. EMI tubes with their greater red-light sensitivity. The system is therefore not easily adapted to other photometers or filter sets, particularly since the rule of reducing (U–B) colours by ignoring second order terms is often misunderstood. The effective wavelengths of the filters are determined both by the shape of the incident stellar continuum and the amount of interstellar and atmospheric reddening, which theorists find difficult to model. The redward shift in λ_{eff} caused by atmospheric extinction or large reddening is less of a problem for interference filters with their square wavelength sensitivity patterns, so other systems are often preferred by many astronomers. UBV observations can also be difficult to reduce (and interpret) when they are made at non-standard altitudes, such as sea level or the high altitudes of Mauna Kea. It should also be kept in mind that UBV photometry is not defined for refracting telescopes, or for reflectors with deteriorated aluminized mirrors. Transformation problems often appear most significantly in U–B colours, which are sensitive to how the Balmer discontinuity is sampled. Finally, corrections for dead-time are always a problem for bright stars with photon-counting techniques.

Extinction Corrections.

In order to properly understand an important source of random and systematic error in stellar photometry, it is informative to review how astronomers correct their observations for atmospheric extinction. In the simple case where observations are made at small zenith distances, z, one can approximate the atmosphere using a flat slab model. In this case, the air mass, X, along the line-of-sight to a star at zenith distance z is given by (see figure):

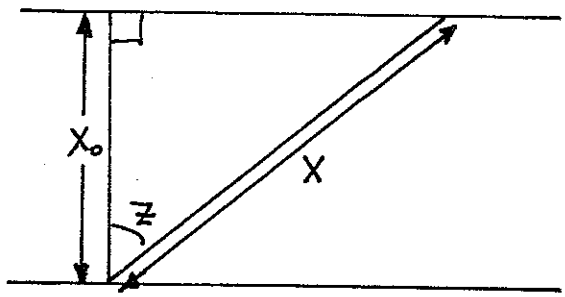

$$X = \frac{X_o}{\cos z} = X_o \sec z = X_o [\sin \phi \sin \delta + \cos \phi \cos \delta \cos H]^{-1},$$

where ϕ is the observer's latitude, δ is the declination of the star, and H is the hour angle of the star = sidereal time – α (the right ascension of the star). This simple formula breaks down for large air masses,X, due to the Earth's curvature and the initial approximations.

e.g.

z	sec z	X
0°	1.000	1.000
30°	1.155	1.154
60°	2.000	1.995
70°	2.924	2.904
79°	5.241	5.120

Hardie, in **Astronomical Techniques**, p.178, gives a complicated general formula for air mass:

$X = \sec z - 0.0018167 (\sec z - 1)$ – etc., with terms in $(\sec z - 1)^2$ and $(\sec z - 1)^3$.

Young, in **Methods in Experimental Physics**, 12A, 123, 1974, gives a simpler and more accurate formula, namely:

$X = \sec z (1 - 0.0012 \tan^2 z)$.

Air molecules decrease the light intensity of a star by the amount $dI = -I\tau_\lambda dx$, where $\tau_\lambda dx$ is the fraction of light lost through extinction over the distance dx, and τ_λ is the absorption coefficient per unit distance at wavelength λ.

$$\therefore \quad \frac{dI}{I} = -\tau_\lambda dx ,$$

and $$\int_{I_o}^{I} \frac{dI}{I} = -\int_0^X \tau_\lambda dx .$$

$$\therefore \quad \log I - \log I_o = -k_\lambda X ,$$

or $$\log I = \log I_o - k_\lambda X .$$

Magnitudes vary as $-2.5 \log I$.

$$\therefore \quad m = m_o + 2.5 \tau_\lambda X = m_o + k_\lambda X .$$

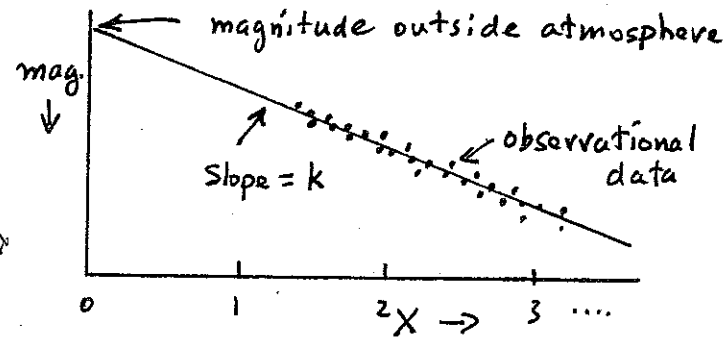

The extinction coefficient k varies nightly due to changes in moisture, air pressure, dust content of the air, etc. Extinction is largest in the ultraviolet region and smallest in the infrared. Therefore, k-values increase exponentially with decreasing wavelength.

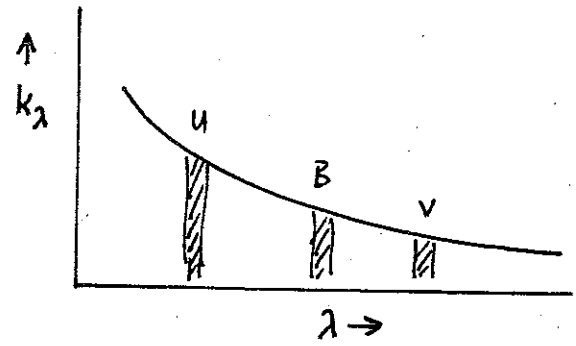

Mean values for the extinction coefficients will generally apply to a particular observing run at a good site. However, the best determinations of k require a range of 2 or 3 in X, which means that standard stars must be observed to within only ~15° of the horizon. Photometer drift (due to changing sensitivity of the photocathode) is a moderately common problem in actual observations, and results in extinction coefficients which change during the course of a night's observations.

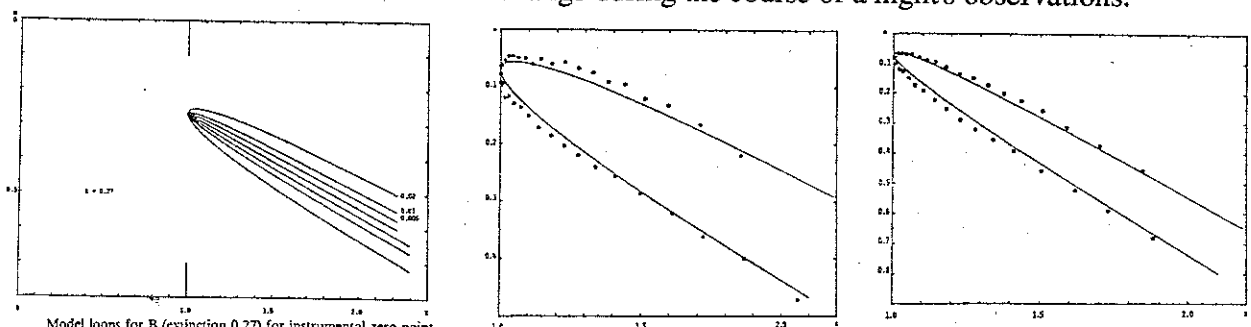

Model loops for B (extinction 0.27) for instrumental zero-point drifts 0.005, 0.01, 0.02. The centre line is for constant extinction with no drift.

One must be careful following extinction stars since they can give anamalously different k-values on different sides of the meridian due to changing phototube sensitivity.

There are also problems with the reduction of UBV photometry according to the outline provided by Johnson. Since the U-filter includes the Balmer discontinuity, the derived value of $k_{U-B} = k'_{U-B} + k''_{U-B}$ will depend upon the spectral types of the standard stars (see diagram). Thus, a combination of O and M standards will yield a negative second order term for k_{U-B} (i.e. $k''_{U-B} < 0$) while a combination of A and K standards will yield a positive second order term for k_{U-B} (i.e. $k''_{U-B} > 0$). Johnson decided that the best solution was simply to ignore the second order extinction coefficient for k_{U-B} (i.e. $k''_{U-B} \equiv 0$, by definition) and to put up with larger-than-usual errors in photoelectric U–B values. The result is that typical uncertainties in U–B are of order ±0.02, while those in V and B–V are usually better than ± 0.01. Popper (PASP, 94, 204, 1982) provides a very readable article on the many overlooked problems of UBV photometry.

Results for the UBV System:

The system was calibrated and the colours normalized relative to stars in the North Polar Sequence, so that U–B = B–V ≡ 0.00 for A0 V stars. The nature of the system is such that the B and V filters are located on the Paschen continuum of stellar spectra, while the U filter straddles the Balmer discontinuity at λ3647Å. The slope of the Paschen continuum in stars is reasonably similar to the slope of a black body continuum, and is therefore temperature sensitive, making B–V very useful for measuring stellar temperatures. The Balmer discontinuity, particularly for stars hotter than the sun, is gravity (or luminosity) sensitive, so that U–B is useful as a luminosity indicator. For cool stars, both B–V and U–B are sensitive to chemical composition differences, since the U and B bands, in particular, are susceptible to the effects of line blocking and line blanketing on stellar continua (see diagram below). Photometric ultraviolet excesses measured relative to standard metallicity colours are therefore useful for segregating stars according to their metallicity.

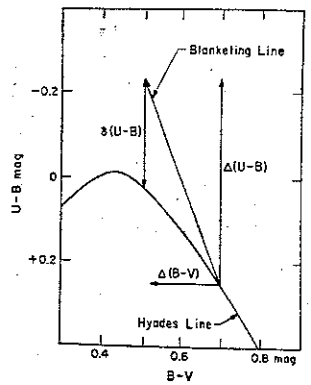

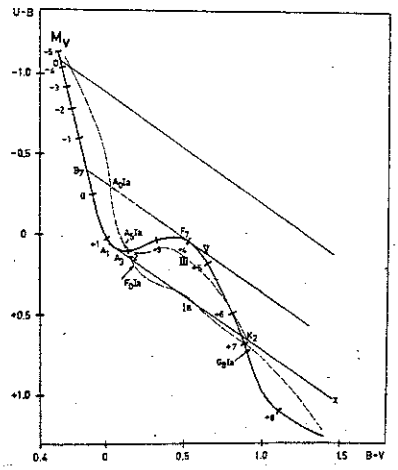

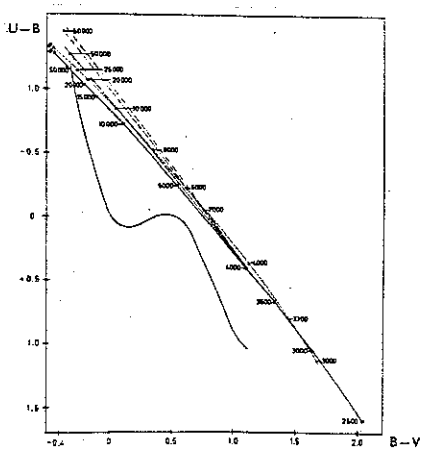

The diagram on the previous page is the standard two-colour (or colour-colour) diagram for the UBV system. Plotted here are the observed intrinsic relation for main-sequence stars of the indicated spectral types, the intrinsic locus for black bodies radiating at temperatures of 4000°K, 5000°K, 6000°K, 8000°K, etc., and the general direction imposed upon star colours due to the effects of interstellar reddening. The primary opacity source in the atmospheres of B and A-type stars is atomic hydrogen, which makes its presence obvious in the flux distributions of such stars with discrete discontinuities in the stellar continua at λ912Å (the Lyman discontinuity, due to ionization from the n = 1 level of hydrogen), λ3647Å (the Balmer discontinuity, due to ionization of hydrogen atoms from the n = 2 level), and λ8206Å (the Paschen discontinuity, due to ionization from the n = 3 level of hydrogen). The primary opacity source in the atmospheres of F, G, and K-type stars is the negative hydrogen ion (H^-), which does not produce any discrete breaks in the flux output as a function of wavelength. For the very hottest O-type stars, the primary opacity source is scattering by free electrons, which also does not produce any breaks in the stellar continua. The intrinsic relation for main-sequence stars in the two-colour diagram therefore falls close to the black body curve for very hot stars and stars of solar temperature. It deviates noticeably from the black body curve for B and A-type stars due to the atomic hydrogen opacity source, and for K and M-type stars mainly due to the effects that the many spectral lines in the blue region of their spectra have on blocking the stellar flux in the B and U photometric bands. In the very cool M-type stars, in particular, molecular bands appear in the spectra which can make the UBV photometric indices virtually useless as temperature indicators for these stars.

Other Broad Band Systems:

Several other broad band systems have been established over the years, generally with some specific purpose in mind. Some of these are listed below, and many others exist:

UBVRI. This extension of standard UBV photometry to red wavelengths has different effective wavelength filters for either Johnson system or Kron-Cousins system RI photometry.

UBVRIJKLMNO. This system was designed for the study of interstellar reddening, and makes use of a lead sulfide photocell with special filters to take advantage of spectral windows in the infrared. The particulars of this system are:

Band	$\lambda_{eff}(\mu m)$	$1/\lambda_{eff}$
U	0.36	2.78
B	0.44	2.27
V	0.55	1.82
R	0.70	1.43
I	0.88	1.14
J	1.25	0.80
K	2.2	0.45
L	3.4	0.29
M	5.0	0.20
N	10.2	0.10
O	~11.5	0.09

UVBGRI. This is the Lick six-colour system of Kron and Stebbins, which has found considerable use in the study of Cepheid reddenings.

Washington System. The broad band Washington system was established at the University of Washington for detailed studies of G and K giants (Canterna, AJ, 81, 228, 1976), and has found considerable use in the study of Cepheid reddenings (Harris, AJ, 86, 707 & 719, 1981). The filters were chosen to sample both the stellar continuum (a T index once corrected for reddening) and to provide both metallicity (G-band sensitive) and luminosity (CN sensitive) indices.

Filter	λ_{eff}	$\Delta\lambda$ (half-width)	
C	3910Å	1100Å	(Corning CS-7-59 + $CuSO_4$)
M	5085Å	1050Å	(Schott GG 455 + Corning CS-4-96)
T_1	6330Å	800Å	(Schott BG 38 + Schott OG 590)
T_2	7885Å	1400Å	(Schott RGN 9)

UGR (or RGU). This is a photographic system deisgned by Becker for the study of open clusters and galactic structure. The R filter matches the E-plates of the Palomar Observatory Sky Survey, and the G filter is a close match to the sensitivity of the POSS O-plates. The system finds little use outside of Switzerland.

Intermediate Band Systems:

The characterization of various photometric systems as broad band, intermediate band, or narrow band systems is specified by the half widths of the filters which define the system, with the smallest value usually taking precedent. In this manner, broad band systems are defined by filters with half-widths of the order of 500Å to 1000Å, intermediate band systems are defined by filters with half-widths of 100Å to 500Å, and narrow band systems are defined by filters with half-widths of less than 100Å. The most important intermediate band systems are listed below:

Walvaren System.

This system, established by Walraven in the Netherlands, uses a quartz prism spectrograph and quartz filters (except for the L filter which is isolated by Schott UG2 (2mm) plus Schott WG2 (2 mm) glass filters) in combination with a 1P21 photomultiplier tube to isolate the spectral bands, which, by definition, generally have sharp wavelength cutoffs. The system is used extensively by Dutch astronomers, and has proven to be useful for Cepheid studies (Pel, Lub), and some galactic astronomy (recent cluster studies). The magnitudes are defined by $W = \log_{10} I_w$, rather than the usual method of $W = -2.5 \log_{10} I_w$, and this makes comparisons with other systems rather difficult. The system also has a different zero-point from the UBV system. The nature of interstellar reddening in this system has not been studied in detail, although the filters are not susceptible to the same problems as are the broad band UBV filters. Unfortunately, narrower filters place brighter limits on useful photometric studies which can be accomplished with this equipment, so standard UBV photometry still advantageous for many types of observational studies.

Filter	λ_{eff}	$\Delta\lambda$ **(half-width)**
W	3270Å	150Å
U	3670Å	260Å
L	3900Å	300Å
B	4295Å	420Å
V	5450Å	850Å

Strömgren System (Four Colour System).

As a consequence of possible ambiguities in the interpretation of intrinsic stellar parameters which arise when using UBV colours, Bengt Strömgren developed an intermediate band system which also uses the RCA 1P21 photomultiplier, but with narrow passband interference filters to isolate all but the ultraviolet wavelength bands (a glass filter was used for the latter). The parameters of the wavelength bands for the uvby, or Strömgren, system are:

Filter	λ_{eff}	$\Delta\lambda$ **(half-width)**
u (ultraviolet)	3500Å	380Å
v (violet)	4100Å	200Å
b (blue)	4700Å	100Å
y (yellow)	5500Å	200Å

Since the u-filter in the Strömgren system does not extend to the wavelength cutoff for the Earth's atmosphere near 3000Å, it proves to be less susceptible to the problems generated by the U-filter in the Johnson system (these were mainly problems in obtaining reliable observations — Johnson specifies a reflecting telescope with aluminized mirrors and an observing altitude of 7000 feet above sea level for UBV photometry). The use of interference filters also reduces some of the problems generated by the effects of atmospheric and interstellar extinction on the effective wavelengths for the various filters.

The effective wavelengths for the Strömgren system were purposely selected to provide as much information of astrophysical interest for stars as possible. Thus, the b and y bands are located in relatively line-free portions of the Paschen continuum, so that the **b–y index** is temperature sensitive. The v band is located on the long wavelength side of the Balmer discontinuity, where the overlapping of lines from metallic atoms and ions, as well as from hydrogen Balmer series members, is noticeable, particularly for A, F, G, and K-type stars. Strömgren designed a specific index to measure the depression of the stellar continuum in the v band. This is called:

$\mathbf{m_1 \equiv (v-b) - (b-y)}$, and is known as the "metallicity" index (m for metallicity).

The u band is located on the short wavelength side of the Balmer discontinuity, and can be combined with the v and b filters to give an index which is sensitive to the size of the Balmer jump, which is gravity dependent for hot O, B, and A-type stars. Strömgren designed another index to measure the size of the Balmer discontinuity from the depression of the stellar continuum in the u band. This is called:

$\mathbf{c_1 \equiv (u-v) - (v-b)}$, and is known as the gravity index (c for the supergiant c designation). This index has very similar properties to the U–B index in the Johnson system, but is not uniquely related to it. The Strömgren system therefore has several colour-colour diagrams of interest. The (c_1, b–y) diagram is similar to the UBV two-colour diagram, while the (m_1, b–y) diagram is fairly unique. The various Strömgren indices are designed to give more precise information about intrinsic stellar parameters than is possible using UBV photometry. However, it is not totally clear that they are suitable for this task.

Reddening-free indices can be formed, once the reddening relations are known:

e.g. $[c_1] = c_1 - 0.20\,(b-y)$, since $E(c_1) = 0.20\,E(b-y)$, typically.

$[m_1] = m_1 + 0.35\,(b-y)$, since $E(m_1) = -0.35\,E(b-y)$ [but note that a factor of 0.18 was adopted initially by Strömgren!].

See the series of calibration papers by Crawford (AJ, 80, 955, 1975 — F-star calibration; AJ, 83, 48, 1978 — B-star calibration; AJ, 84, 1858, 1979 — A-star calibration) for more details.

DDO Five-Colour System.

The DDO photometric system was introduced by McClure and van den Bergh (AJ, 73, 313, 1968) in an effort to supplement UBV photoelectric photometry to obtain more information on temperatures, luminosities, metallicities, etc. for late-type stars. The passbands are defined by the following filter sets, in conjunction with a standard 1P21 photoelectric photometer:

Filter	λ_{eff}	$\Delta\lambda$ (half-width)	
35	3490Å	360Å	(Schott UG11 Filter + WG3)
38	3800Å	172Å	(Thin Films Filter)
41	4166Å	83Å	(Baird Atomic Filter)
42	4257Å	73Å	(Baird Atomic Filter)
45	4517Å	76Å	(Baird Atomic Filter)

The system is actually a narrow band system, but is usually referred to as intermediate band. It proves to be extremely useful for the study of late-type stars since:

C(41–42) brackets the CN break at λ4216Å and blueward, so is luminosity sensitive.

C(42–45) brackets and measures the CH absorption in the G-band at λ4300Å, so is quite sensitive to temperature.

C(38–41) measures the line blanketing in late-type stars.

C(35–38) measures the Balmer jump, so is sensitive to temperature and gravity.

Narrow Band Systems:

Narrow band photometric systems are so-named because they employ very narrow passband filters to isolate specific wavelength regions of interest. The most frequently cited is the the **Hβ photometric system**, which uses two narrow-band filters (a wide filter of half-width 150Å and a narrow filter of half-width 30Å — see Crawford & Mander, AJ, 71, 114, 1966) to provide an index which measures the strength of the hydrogen Balmer Hβ line at λ4861Å in stellar

spectra. This feature proves to be gravity sensitive for stars hotter than spectral type ~A2, and temperature sensitive for cooler stars. It is defined by:

β = 2.5 log I(wide Hβ filter) – 2.5 log I(narrow Hβ filter).

Since both filters are centred on the same wavelength, the index is insensitive to both atmospheric and interstellar reddening (i.e. observations can be made on partly cloudy nights!). Although defined to be insensitive to extinction, practical problems arise with actual filter sets in which the effective wavelengths of the two filters prove not to be identical. As discussed by Kilkenny (AJ, 80, 134, 1975), Muzzio (AJ, 83, 1643, 1978) and Schmidt & Taylor (AJ, 84, 1192, 1979), colour terms may be necessary in the reduction of Hβ photometry when this problem arises. The system is almost always used in conjunction with intermediate band Strömgren system photometry, and often results in the combined observations being erroneously referred to as "narrow band" data.

A narrow band **K-line photometric system** has been employed by Henry (ApJ, 152, L87, 1968; ApJS, 18, 47, 1969) to provide a measure of the Fraunhofer K-line strength due to singly-ionized calcium (Ca II λ3933Å) in stellar spectra. This index is useful as a both a temperature and metallicity indicator, and has been combined with Strömgren system photometry to obtain a metallicity index for A, F, and G-type stars. It proves to be particularly successful at identifying Am and Ap stars photometrically. A similar intermediate band system has been separately established by Maitzen (A&A, 100, 3, 1981) with interference filters of half-width 120Å centred on 5020Å (the g_1 filter) and 5240Å (the g_2 filter) to measure the depression at λ5200Å in Ap stars. It is also a successful predictor of stellar spectral types.

The astronomers at Brigham Young University have also developed a **KHG photometric system**, which uses narrow band filters centred on the Ca II K-line (λ3933Å), the hydrogen Balmer Hδ line (λ4100Å), and the Fraunhofer G-band (due to the CH molecule at λ4305Å) to produce an index which is essentially independent of atmospheric or interstellar reddening, but is very sensituve to the temperatures and metallicities of stars. As described by McNamara et al. (PASP, 82, 293, 1970) and Feltz (PASP, 84, 497, 1972), the appropriate index is:

$$\text{khg} = 2.5 \log \left[\frac{I^2(4100)}{I(3933)I(4305)} \right].$$

The index has proven to be ideally suited to the study of Cepheid reddenings (Turner et al., AJ, 93, 368, 1987) as well as for Baade-Wesselink analyses of these variables.

8. Interstellar Reddening

The wavelength dependence of interstellar extinction is obtained by comparing the monochromatic magnitudes of two stars, one of which is more heavily reddened by interstellar matter than the other. It is assumed that the extinction coefficient is a function of wavelength, i.e. is described by the term A_λ, and that $A_\lambda = 0$ when $\lambda \rightarrow \infty$. **Extinction curves** are derived as a function of $1/\lambda$, and are usually normalized to unity for $A_B - A_V = E_{B-V} = 1.00$, and $A_V = 0.00$. This makes $A_B = 1.00$ for normalized extinction curves. The absolute normalization must be obtained from the value of A_λ for $1/\lambda = 0.00$, and for this one needs observations in the infrared portion of the spectrum.

The extinction in the ultraviolet portion of the spectrum tends to be relatively constant for λ < 1250 Å, although there is a marked extinction dip at λ2200 Å ($1/\lambda \approx 4.5\ \mu m^{-1}$) which is variable in strength and probably originates from the presence of various amounts of small graphite particles in the interstellar dust. In the visible and near infrared, A_λ varies almost linearly with $1/\lambda$. There is a bit of a break at λ = 4430 Å ($1/\lambda = 2.26\ \mu m^{-1}$) due to one specific component of interstellar dust not yet identified There are various other recognized interstellar bands for which the source is not known with certainty. The actual shape of the extinction curve at these wavelengths reflects the nature of the dust grains, in particular the size distribution of the grains, most of which have approximately the same diameters as the wavelengths of visible light. Large particles produce relatively neutral extinction at visible wavelengths, while small particles produce strong increases in A_λ as one observes to shorter wavelengths. The ultraviolet extinction curve

provides further information about the size distribution of interstellar dust particles, and their ranges for a typical galaxy.

In the UBV system, we define the colour excesses:

$E_{B-V} = (B-V)_{observed} - (B-V)_{intrinsic} = (B-V) - (B-V)_o$,

and $E_{U-B} = (U-B)_{observed} - (U-B)_{intrinsic} = (U-B) - (U-B)_o$, and their ratio:

$\frac{E_{U-B}}{E_{B-V}} = X + Y E_{B-V}$ (as expressed in its general form).

The parameter X is the slope of the UBV reddening relation, and Y is the curvature term, which depends upon the amount of reddening. For typical galactic conditions in the plane of the Galaxy, the slope $X \approx 0.75$, but with observed variations from as little as 0.65 in Upper Scorpius to as much as 0.85 in Cygnus and other regions. This parameter has a strong spectral type dependence due to the effects of reddening on the effective wavelengths of the UBV passbands, and increases for later spectral types, becoming ~1.0 for K0 stars and larger for M-type stars. The curvature term, Y, is generally small, and appears to average $Y \approx 0.02$ for most regions of the Galaxy. It can often be ignored in reddening investigations.

The ratio:

$$R = \frac{A_V}{E_{B-V}}$$

is called the ratio of total to selective extinction, and generally is ~3.1 ±0.1 for most regions of the Galaxy. The mean value of R seems to be slightly above the average value (~3.2) towards the anticentre and centre regions of the Galaxy (i.e. looking across spiral arms) and slightly below the average value (~3.0) looking along spiral arms (i.e. in Cygnus, etc.). This can be explained by the preferential alignment (by the Davis-Greenstein mechanism) of dust grains by the magnetic fields associated with spiral arms. Certain localized regions are characterized by values of R of ~5–6, which is the signature of dust pockets containing lots of particles of above-average size. These regions are rare, and their existence is still a matter of debate in some cases (examples are Orion, Carina, etc.). The parameter is important for distance determinations, since:

$V_o - M_V = 5 \log d - 5$.

In the presence of interstellar extinction,

$V = V_o + A_V = V_o + (R \times E_{B-V})$.

$\therefore \quad V-M_V = V_o-M_V + R E_{B-V} = 5 \log d - 5 + R E_{B-V}$,

or $\quad V_o-M_V = V-M_V - R E_{B-V}$,

i.e. an extinction correction is needed to find the true distance to an object in the presence of interstellar reddening. Note the simplification possible for a group of stars of common distance, namely:

$V-M_V = (V_o-M_V) + R E_{B-V} = \text{constant} + R E_{B-V}$.

Clearly, a plot (called a **variable-extinction diagram**) of apparent distance modulus, $V-M_V$, versus colour excess, E_{B-V}, for such a group should produce a linear relationship which has a slope R = the ratio of total to selective extinction. In fact, it has been possible to use clusters and associations of stars in which differential (variable) reddening is present to derive some of the best estimates for the parameter R for galactic regions (see Turner, AJ, 81, 97 & 1125, 1976).

Reddening-Free Indices:

If one supposes that the extinction law is invariant throughout the Galaxy and has no curvature term, then $\frac{E_{U-B}}{E_{B-V}} = X$, a constant. Johnson and Morgan (ApJ, 117, 313, 1953) introduced a Q parameter for the UBV system which took advantage of this invariance property, namely:

$$\begin{aligned} Q &= (U-B) - X(B-V) = (U-B)_o + E_{U-B} - X[(B-V)_o + E_{B-V}] \\ &= (U-B)_o - X(B-V)_o + E_{U-B} - X E_{B-V} \\ &= (U-B)_o - X(B-V)_o + E_{U-B} - \frac{E_{U-B}}{E_{B-V}} E_{B-V} \\ &= (U-B)_o - X(B-V)_o + E_{U-B} - E_{U-B} = (U-B)_o - X(B-V)_o . \end{aligned}$$

i.e. $\quad Q = (U-B) - X(B-V) = (U-B)_o - X(B-V)_o$.

Any parameter which has the same value when it is written in terms of either the reddened or intrinsic colours of an object is referred to as a **reddening-free parameter**. Clearly, the UBV parameter Q satisfies this property, provided that the interstellar extinction law is invariant. Its advantage becomes immediately clear, since it is straightforward to correlate the value of Q with the spectral type or intrinsic colour of a star. As used by Johnson and Morgan, Q was constructed using X = 0.72, the best value available in 1953. However, note that it is the opinion of your instructor that the interstellar extinction law is not invariant, in which case Q-parameters serve no useful purpose.

Reddening-free indices have also been constructed for the Strömgren system, where they are used frequently (and erroneously). The parameters used, and the reddening relations upon which they have been developed, are:

$[c_1] = c_1 - 0.20\,(b-y)$ from $E(c_1) = 0.20\,E(b-y)$,

$[u-b] = (u-b) - 1.50\,(b-y)$ from $E(u-b) = 1.50\,E(b-y)$,

and $[m_1] = m_1 + 0.18\,(b-y)$ from $E(m_1) = -0.18\,E(b-y)$.

But more recent calculations indicate that $E(m_1) = -0.35\,E(b-y)$ on average, so the use of older definitions for $[m_1]$ is particularly open to question. Note also that $[c_1] \neq (c_1)_o$, and $[m_1] \neq (m_1)_o$. As long as the properties of interstellar extinction are known reliably for the region containing a star of interest, then it is always possible to make reddening corrections without reliance on reddening-free indices. Given the dubious validity of reddening-free indices, the use of a reddening relation valid for the field of interest is certainly the correct way of making reddening corrections for stars in that field.

9. Absolute Magnitude Calibrations

Tables of absolute magnitudes for stars as a function of spectral type and luminosity class are constructed in a variety of ways. It is not unusual for several different techniques to be used in the compilation of one table. The three most commonly used techniques for establishing absolute magnitudes of stars are listed below:

i. Statistical Parallaxes.

Recall the relation for tangential velocity,

$$v_T\ (\text{km/s}) = \frac{4.74\,\mu}{\pi},$$

for the proper motion μ in "/yr and the parallax π in arcseconds. This can be rewritten as:

$$\pi = \frac{4.74\,\mu}{v_T}.$$

There is a statistical means of establishing the mean parallax for a group of stars having common properties by making use of the data for their positions in the sky, for their proper motions, and for their radial velocities. The resulting **statistical parallax** for the group is:

$$\langle\pi\rangle = \frac{4.74\,\langle\mu\rangle}{\langle v_T\rangle},$$ where <> denotes mean values.

In general, a randomly distributed group of stars should have $\langle v_T\rangle \approx \langle v_R\rangle$, i.e. one component of space velocity should be similar to another. Thus,

$$\langle\pi\rangle = \frac{4.74\,\langle\mu\rangle}{\langle v_R\rangle}.$$

Actually this is a simplification of the true method. In practice, the true situation is complicated by the sun's peculiar motion relative to the group, as described later in the course notes. Denote (upsilon) υ = the μ-component in the direction of the solar antapex (i.e. the μ-component due to the sun's motion), (tau) τ = the μ-component perpendicular to the direction of the solar antapex (i.e. the μ-component due to the star's peculiar velocity), and (lamda) λ = the angular separation of the star from the solar apex. Then:

$<\pi> = \frac{4.74 <\upsilon \sin \lambda>}{v_\Theta <\sin^2\lambda>}$ is referred to as the **secular parallax** (i.e. the parallax inferred from the sun's space motion), where v_Θ is the solar motion relative to the LSR, and:

$<\pi> = \frac{4.74 <|\tau|>}{<|v_R + v_\Theta \cos \lambda|>}$ is referred to as the **statistical parallax** (i.e. the parallax inferred from the statistical properties of stellar space velocities).

Upsilon components work best when the solar motion dominates the group random velocities, while tau components work best when group motions dominate. Both techniques have been applied to B stars and RR Lyrae variables, which are too distant for direct measurement of their distances by many standard techniques. Both classes of object are also relatively uncommon in terms of their local space densities, yet luminous enough that they can be seen to large distances. Due to the general perturbations from smooth galactic orbits predicted in density-wave theories of spiral structure, the assumptions used in the methods of statistical and secular parallax may not be strictly satisfied for many statistical samples of stars.

ii. Trigonometric Parallaxes.

Parallax data, such as those contained in the General Catalogue of Trigonometric Stellar Parallaxes, have been used to establish luminosities for the various types of stars which are relatively common in the solar neighbourhood, i.e. white dwarfs and late-type dwarf stars of various metallicities. Some examples are Crawford's (AJ, 80, 955, 1975) use of trigonometric parallaxes for F-type stars (with partial inclusion of Lutz-Kelker corrections) to calibrate absolute magnitudes derived from Strömgren photometry (the B-star and A-star calibrations were later tied to the F-star calibration), and Sandage's (ApJ, 162, 841, 1970) use of General Catalogue parallaxes to calibrate the δ(U–B) versus ΔM_V relation for G subdwarfs (this was used to establish a main-sequence calibration for deriving distances to globular clusters). It should be evident from the comments of Hanson (MNRAS, 186, 875, 1979), however, that calibrations of this type are subject to possible systematic errors arising from random errors in stellar parallaxes and the incompleteness of parallax catalogues.

iii. Moving Cluster Parallax and ZAMS Fitting.

Open clusters are ideally suited to the calibration of stellar luminosities since they contain such a wide variety of stars of different spectral types and luminosity classes. The general method of using a calibrated zero-age main-sequence (ZAMS) to derive cluster distances is outlined by Blaauw in Basic Astronomical Data. However, the necessary zero-point calibration involves the independent determination of the distance to a nearby cluster whose unevolved main-sequence stars serve to establish the M_V versus $(B-V)_0$ (or spectral type) relation over a limited portion of the ZAMS. The distance to this zero-point cluster must be derived using the moving cluster method, or one of its many variants.

The requirements for use of the moving cluster method are a sizable motion of the cluster both across the line-of-sight and in the line-of-sight. The technique is most frequently discussed for the case of the Hyades star cluster, which is the standard cluster used for the construction of the empirical stellar ZAMS. However, Ursa Major and Scorpius also contain moving clusters, and recently the Pleiades has attracted renewed attention as a moving cluster. In general, all stars in a moving cluster move together through space with essentially identical space velocities (their peculiar velocities are invariably much smaller by comparison). Once the direction to the cluster convergent point (divergent points are equivalent!) is established on the celestial sphere, the geometry of the situation is established. In particular, the angle θ between the star's space velocity and radial velocity is fixed.

A star's space velocity is given by: $V^2 = V_T^2 + V_R^2$, and $V_T = 4.74\,\mu d$.

But, $V_R = V \cos\theta$, and $V_T = V \sin\theta$. Thus, the distance to the star, $d*$, is given by:

$$\mathbf{d* = \frac{V_T}{4.74\,\mu} = \frac{V \sin\theta}{4.74\,\mu} = \frac{V_R \sin\theta}{4.74\,\mu \cos\theta} = \frac{V_R \tan\theta}{4.74\,\mu}}$$

Once the radial velocity, V_R (in km/s), of a moving cluster star, its proper motion, μ (in "/yr), and angular distance from the cluster convergent point, θ, are known, its distance (in pc) can be obtained from the above equation. The dispersion in radial velocity for stars in an open cluster is typically quite small, no larger than ± 1 to ± 2 km/s. Therefore, for a cluster of stars of common distance, the ratio $\frac{\tan \theta}{\mu}$ must remain essentially constant across the face of the cluster. This means that those stars lying closest to the cluster convergent point will have the smallest proper motions, while those lying furthest from the convergent point will have the largest proper motions. For nearby clusters this feature allows one to determine the relative distances to stars in the cluster by comparing the individual stellar proper motions, μ_*, with the mean cluster proper motion, μ_c, at that value of θ, i.e. $\frac{d_*}{d_c} = \frac{\mu_c}{\mu_*}$. This technique has been used extensively for stars in the Hyades cluster, which has a line-of-sight distance spread on the order of 10% or more of its mean distance.

The moving cluster method can also be pictured in a more general manner, as noted by Upton (AJ, 75, 1097, 1970). In this case, the motion of a cluster like the Hyades away from the sun results in an apparent decrease in the cluster's angular dimensions, even though its actual dimensions are unchanged. By geometry and the assumption that the cluster's actual diameter, D, is relatively constant, we have:

$D \approx r \times \theta$, where θ is the cluster's angular diameter. We have used r to denote the cluster's distance in this instance in order to avoid confusion with the derivative notation.

$$\therefore \quad \theta = \frac{D}{r}, \text{ and } \frac{d\theta}{dt} = -\frac{D}{r^2}\frac{dr}{dt} = -\frac{\theta r}{r^2}\frac{dr}{dt} = -\frac{\theta \langle V_R \rangle}{r}, \text{ since } \langle V_R \rangle \text{ for the cluster} = \frac{dr}{dt}.$$

The term $\frac{1}{\theta}\frac{d\theta}{dt}$ can be determined from the proper motion gradients across the face of the cluster.

i.e. $\frac{1}{\theta}\frac{d\theta}{dt} = \frac{d\mu_\alpha}{d\alpha} = \frac{d\mu_\delta}{d\delta}$. Therefore, the cluster distance is obtained from:

$$\mathbf{r = -\langle V_R \rangle / \left(\frac{d\mu_\alpha}{d\alpha}\right) \quad or \quad r = -\langle V_R \rangle / \left(\frac{d\mu_\delta}{d\delta}\right)}.$$

Since proper motion gradients are easier to measure accurately than is the location of the convergent point, the method is somewhat superior to the convergent point method. The cluster convergent point is not lost by this method, since it is located by the points where the proper motion gradients become zero. Upton noted, however, that it was necessary to transform the α, δ motions of cluster stars on the celestial sphere into their cartesian (flat surface) equivalents in order to obtain meaningful proper motion gradients. For the Hyades cluster, he also found it necessary to account for line-of-sight distance spread.

A further modification to the general method can be made using the original equations given previously, namely:

$$V_R = V \cos\theta, \text{ and } d_c = \frac{V_R \tan\theta}{4.74\,\mu}.$$

$$\therefore \quad \frac{dV_R}{d\theta} = -V \sin\theta = -V_R \tan\theta = -4.74\,\mu\, d_c,$$

$$\text{and} \quad d_c = \frac{-dV_R/d\theta}{4.74\,\mu},$$

i.e. given the mean proper motion of a moving cluster, one can find its distance from the gradient in radial velocities across the face of the cluster. This technique is very difficult to apply, since it requires extremely accurate radial velocities for cluster members which are not biased by the systematic effects of binary companions. The method has been applied in a very sophisticated fashion to the Hyades cluster by Gunn et al. (AJ, 96, 198, 1988), with fairly good results. Current estimates for the distance modulus of the Hyades cluster by all of the various methods used (including trigonometric parallaxes) lie in the range 3.15 to 3.40, or 42.7 pc to 47.9 pc.

The construction of the ZAMS with its zero-point established by Hyades stars is accomplished by overlapping the unreddened (actually dereddened) and unevolved main-sequences of successively younger clusters to that of the Hyades. The general technique described by Blaauw is actually somewhat flawed since it ignores differential reddening in some of the clusters (such as the Pleiades and α Persei clusters) and the presence of serious systematic errors in the photometry for one (NGC 6611). It also assumes that metallicity differences between one cluster and another are unimportant. This assumption is probably safe for the early-type stars in young clusters, since metallicity differences are unlikely to be very important and typically only result in absolute magnitude differences between stars, not colour differences. However, for late-type stars both the absolute magnitude and colour are affected, so it is necessary to properly account for this when establishing a calibrated ZAMS. Turner (PASP, 91, 642, 1979) discusses the case of the Pleiades cluster, which has a metallicity close to that of the sun as well as to that of the average star in the solar neighbourhood, and demonstrates how the Hyades zero-point needs to be adjusted to account for the higher metallicity of Hyades members.

The fitting of open cluster main-sequences from one to another invariably makes allowances for reddening differences as well as the effects of stellar duplicity, evolution away from the main-sequence, and rotational displacements from the ZAMS. Independently-derived ZAMS ridge lines are surprisingly similar from one author to another, and are also in fairly food agreement with the predictions from stellar models. A different approach has been adopted by Garrison (IAU Symp., 80, 147, 1978), who uses MK spectral type rather than unreddened colour as the ordinate for his ZAMS relation. The use of this relationship is clearly predicated upon the availability of good quality spectral classifications for cluster stars, and is consequently fairly limited at the present time.

Open cluster distances obtained by ZAMS fitting have often been used as a means of testing stellar luminosities derived in independent fashion. The hydrogen Balmer Hβ and Hγ line width indicators — the narrow band β-index and Hγ equivalent width — can also be calibrated using trigonometric parallax data (as has been done by Crawford and Millward & Walker, for example), and generally give absolute magnitudes for stars in open clusters which are close to those obtained from ZAMS fitting. Systematic differences have been commented upon at times, but are probably due to the contaminating effects which are produced on the Balmer line profiles by rapid stellar rotation. A proper detailed study of this problem has never been done.

Another method of determining distances for late-type stars is by means of the Wilson-Bappu effect, namely that the width of the central emission component of the Ca II K line in G and K-type stars is directly related to the absolute magnitude of the star — the broader the emission line width, denoted W_2, the more luminous the star. The original calibration of this relationship was based upon optically-measured half-widths of W_2 for the Ca II K line by Olin Wilson using photographic spectra, and was tied to parallaxes from the General Catalogue. The parallax calibration has been reworked a number of times in order to eliminate the effects of catalogue bias on the parallaxes, and has been tested using the derived distances to Hyades K giants. Much effort has also been expended in understanding the theoretical basis for the effect, although it is still regarded as an empirical relationship. Similar relationships have been looked for in the resonance lines of other singly-ionized alkaline metals.

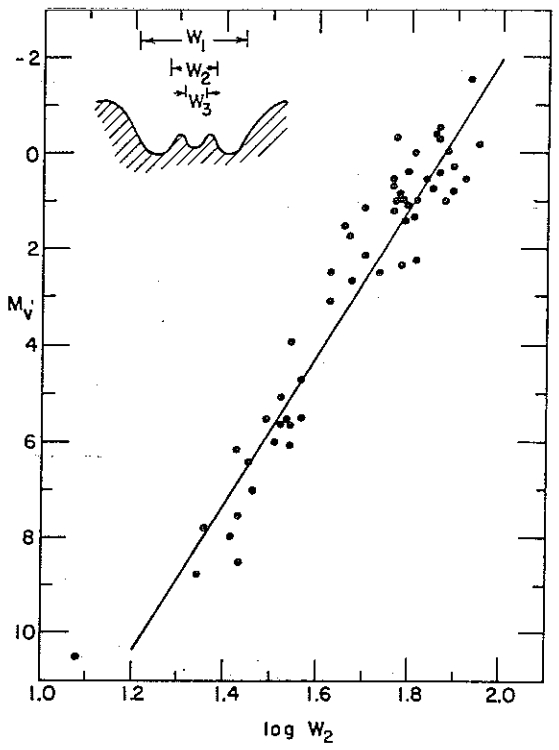

10. Open Clusters, Globular Clusters, and Associations

Major Phases of Stellar Evolution.

Pre-Main-Sequence Evolution

The early stages of star formation tend to be hidden by obscuring clouds of gas and dust (Larson, MNRAS, 145, 271, 1969). In the later stages one detects stars which shine through light produced during gravitational contraction; half of the energy of a star lost through gravitational contraction escapes as radiation, the other half contributes to an increase in the kinetic energy of the gas. The **Hayashi Track** is the evolutionary path in the H-R diagram followed by a contracting star (Hayashi, ARA&A, 4, 171, 1966). The **Hayashi forbidden region** is a region at the cool edge of the H-R diagram where no stable stars can exist. Contracting stars therefore follow evolutionary paths on the hot side of this region.

During the Hayashi track phases newly-formed stars are thoroughly mixed, since convection is the most efficient way of releasing energy from the object. At some stage (earlier for massive stars) the contracting star slows its contraction as the mode of energy escape changes from convective transport to predominantly radiative transport. Studies of polytropes, stellar models described by a single equation of state, show that **radiative tracks** have quite different slopes from **convective tracks**. The individual evolutionary tracks for stars of different mass change slope as the dominant method of energy escape for the star changes. The evolutionary tracks for massive stars quickly become radiative, following which they trace out tracks of rapidly increasing stellar temperature in the H-R diagram. Low mass stars contract without much change in surface temperature, until these stars become radiative as well. Since high mass stars reach the ZAMS at the fastest rate, young clusters can contain many pre-main-sequence stars of low mass. This shows up in the H-R diagrams for young clusters as a lower main-sequence **turnon point**. Many, but not all, pre-main-sequence stars are still associated with the material from which they formed. Often such stars are found to be losing mass and to have emission lines in their spectra originating from circumstellar gas; most are light variable. Pre-main-sequence variable stars are referred to as Orion Population variables. B and A-type pre-main-sequence stars are often found to be Herbig Ae and Be stars. F, G, and K-type pre-main-sequence stars are usually T Tauri variables. Some M dwarfs also show emission lines in their spectra; they are believed to be low-mass stars ($M < 0.5\ M_\odot$) which have only recently reached the main-sequence stage (characterized by hydrogen burning).

Several important nuclear reactions involving light elements take place in stars during their pre-main-sequence phases. These are summarized below:

$D^2 + H^1 \rightarrow He^3$	Critical Temperature $= 5.4 \times 10^5$ °K
$Li^6 + H^1 \rightarrow He^3 + He^4$	Critical Temperature $= 2.0 \times 10^6$ °K
$Li^7 + H^1 \rightarrow He^3 + He^4$	Critical Temperature $= 2.4 \times 10^6$ °K
$Be^9 + 2H^1 \rightarrow He^3 + 2He^4$	Critical Temperature $= 3.2 \times 10^6$ °K
$B^{10} + 2H^1 \rightarrow 3He^4$	Critical Temperature $= 4.9 \times 10^6$ °K
$B^{11} + H^1 \rightarrow 3He^4$	Critical Temperature $= 4.7 \times 10^6$ °K
$He^3 + He^3 \rightarrow He^4 + 2H^1$	Critical Temperature $= 5.0 \times 10^6$ °K

During the pre-main-sequence phases, deuterium (D^2) is converted to He^3 during the convective stages of the Hayashi tracks (Ostriker & Bodenheimer, ApJ, 184, L15, 1973) and the light elements lithium (Li), beryllium (Be), and boron (B) are destroyed during the early stages of the radiative tracks. These reactions add to the He^3 abundance, so that when He^3 is converted to He^4 and H^1 (protons) during the final stages just prior to reaching the main-sequence (Ulrich, ApJ, 165, L95, 1971; ApJ, 168, 57, 1971) the stage can have a significantly long duration. An abundance of $N(He^3)/N(He^3 + He^4) \approx 0.005$ is sufficient to be seen in the H-R diagrams of young clusters as a gap where the pre-main-sequence connects to the ZAMS (see Turner, AJ, 86, 231, 1981). An abundance ratio of $N(He^3)/N(He^3 + He^4) \approx 0.001$ appears to be more typical of open cluster stars.

Post-Main-Sequence Evolution

The post-main-sequence evolution depends critically upon the initial mass of the star.

$M > 1.1\ M_\odot$ (stars with convective cores and radiative envelopes)

The major phases of evolution for these stars are described many standard references (e.g. Iben, ARA&A, 5, 571, 1967). These can be summarized briefly as: H burning, core shrinkage, H shell burning, core shrinkage, He burning in core, core shrinkage, He shell burning, exhaustion of H shell burning, etc. ... carbon burning, oxygen burning etc., depending upon the stellar mass (advanced nuclear reactions are mass dependent, and only occur if the mass is large enough). The **Schönberg-Chandrasekhar limit** is defined as follows. If the isothermal core of a massive star exceeds 10–15% of the total mass of the star, then the contraction of the core following the exhaustion of H burning in the core results in rapid contraction of the core, since the pressure gradient is insufficient to support the star's outer layers. This limit occurs at roughly 1.7 to 2.25 $M_\odot$. Stars with $M > 1.7$ to $2.25 M_\odot$ undergo rapid evolution to the right in the H-R diagram at core H exhaustion. Less massive stars undergo less rapid evolution at this stage. Rapid evolution at core contraction results in a scarcity of such stars in the H-R diagram (A–G supergiants), referred to as the **Hertzsprung Gap**. Convective cores seem to be ~50% larger than predicted from simple theoretical considerations (according to the evidence from open cluster colour-magnitude diagrams), so recent models generally include core overshooting (convetion beyond the standard core region of the star) which increases the core H burning lifetime and affects age estimates for open clusters). The inclusion of realistic amounts of rotation in stellar evolutionary models is still very much in its infancy.

Metallicity can affect the values of T_{eff} reached during core He burning, with lower metallicities resulting in higher T_{eff} during He burning. Classical Cepheids are yellow supergiants which are unstable to radial pulsation (driven by the opacity of He and H in their outer layers). Normal massive stars pass through this region of pulsational instability during the H shell source phase (most rapid) and core He burning and shell He burning stages (slower). Most Cepheids should be burning He in the core or in a thin shell. The standard critical masses for the most important stages of nuclear burning are:

H-burning ~0.1 $M_\odot$
He-burning ~0.35 $M_\odot$
C-burning ~0.8 $M_\odot$.

The major stages of main-sequence nuclear reactions are:

Proton-Proton Reactions — Critical Temperature = 10×10^6 °K

$H^1 + H^1 \rightarrow D^2 + \text{positron}$
$D^2 + H^1 \rightarrow He^3$
$He^3 + He^3 \rightarrow He^4 + 2H^1$

CNO Bi-Cycle — Critical Temperature = 16×10^6 °K

$C^{12} + H^1 \rightarrow N^{13}$
$N^{13} \rightarrow C^{13} + \text{positron}$
$C^{13} + H^1 \rightarrow N^{14}$
$N^{14} + H^1 \rightarrow O^{15}$
$O^{15} \rightarrow N^{15} + \text{positron}$
$N^{15} + H^1 \rightarrow C^{12} + He^4$

The various isotopes of carbon, nitrogen, and oxygen are not destroyed in these reactions, but act as catalysts which make the conversion of hydrogen to helium more efficient. Their relatives abundances tend towards equilibrium values which have nitrogen enhanced at the expense of carbon and oxygen.

The major stages of post-main-sequence nuclear reactions are:

$He^4 + He^4 \rightarrow Be^{8*}$ (unstable)
$He^4 + Be^{8*} \rightarrow C^{12}$ — Critical Temperature = 100×10^6 °K
$C^{12} + He^4 \rightarrow O^{16}$ — Critical Temperature = 200×10^6 °K

$O^{16} + He^4 \rightarrow Ne^{20}$	etc.
$Ne^{20} + He^4 \rightarrow Mg^{24}$, etc.	etc.
$C^{12} + C^{12} \rightarrow Mg^{24}$	Critical Temperature = 1000×10^6 °K
$O^{16} + O^{16} \rightarrow S^{32}$, etc.	Critical Temperature = 2000×10^6 °K

The various possible exothermic nuclear reactions continue in massive stars until an iron core is produced. Thereafter, only endothermic reactions are possible, and these probably occur spontaneously during the implosion of the iron core during a supernova explosion, in which inverse beta decay converts the stellar core to a rich neutron mass, and the release of high neutrino fluxes helps to eject the remaining stellar envelope into space as an expanding (and mass-collecting) supernova remnant. The remaining stellar remnant is likely to be a neutron star, possibly detected as a pulsar; black holes may also be produced.

$M < 1.1\ M_\odot$ (stars with radiative cores and convective envelopes)

The post-main-sequence stages of these stars reflect the gradual depletion of H at the star's centre followed by contraction and heating of the core as H burning moves away from the centre of the star. When He ignites at the centre of a red giant star of this mass, it does so in a degenerate gas. The onset of He burning therefore has no effect on the pressure of the gas, only its temperature, which increases exponentially. Since the rate of He burning is sensitive to temperature, the energy generation rate also increases exponentially as T increases producing a short-lived helium flash as the available He in the star's centre is converted to carbon. This stage is only terminated when the gas temperature becomes high enough to remove the conditions for degeneracy. Massive stars do not develop degenerate gas in their isothermal cores, so their He ignition (and C ignition) is less dramatic. The post He-flash evolution of a red giant star unto the **asymptotic giant branch** is believed to be associated with a superwind which, along with shell helium flashes, induces the formation of planetary nebulae. Stars of 1.5 to 2 $M_\odot$ pass through a **carbon flash** phase which may also assist the production of planetary nebulae. The end fate of planetary nebulae (originally stars of up to ~6 $M_\odot$) are **white dwarfs** ($M < 1.4\ M_\odot$) located in dispersed nebular shells.

$M < 0.4\ M_\odot$ (stars completely convective)

These stars slowly change into He stars as their H content is converted by nuclear reactions. Since the time scale for these reactions is much larger than the age of the universe, the evolution of these stars is of academic interest only. Below $M \approx 0.08\ M_\odot$, no thermonuclear reactions can occur because the gas never reaches a high enough temperature.

Open Clusters.

Open, or galactic, clusters are symmetrical groups of stars found along the major plane of the Galaxy. Globular clusters are richer and older groups of stars populating the halo of the Galaxy. Associations are loose groups of stars in the galactic plane which may be the dispersed remains of young open clusters. There are three different types of associations recognized: OB associations consisting of hot O and B-type stars, R associations consisting mainly of hot B-type stars illuminating reflection nebulosity in the dust clouds with which they are associated, and T associations which are loose groupings of T Tauri variables associated with young dust complexes. The important properties of these various types of stellar groups can be summarized as follows:

	Open Clusters	**Globular Clusters**	**Associations**
Number known in Galaxy...	> 1000	130–150	~100
Stars Contained...	50–5000	1000–1,000,000	10–100
Diameters...	10–25 pc	20–100 pc	25–250 pc
Appearance...	loose concentrations	rich concentrations	open
Shapes...	more-or-less spherical	spherical	irregular
Population Type...	Disk and Pop. I	Pop. II	extreme Pop. I
Ages...	10^6–10^9 yrs	~12–16 $\times 10^9$ yrs	10^6–10^7 yrs
Location in Galaxy...	disk and spiral arms	halo	spiral arms

The formal reference catalogue for star clusters (including globular clusters, associations, and moving groups — which may be the physical remains of dispersed open clusters) is the **Catalogue of Star Clusters and Associations** (Ruprecht et al. 1970, 1981), published in Czechoslovakia. This source is badly in need of updating. Currently the best available source of information on known clusters is the database of the Stellar Data Centre (CDS) at Strasbourg, and the personal database of J.–C. Mermilliod, both of which are accessible electronically.

Trumpler initiated a visual scheme for describing open clusters from their appearance on photographic plates, and this is occasionally used today. The designations in this scheme are:

I. Detached clusters with a strong central concentration of stars.
II. Detached clusters with little central concentration of stars.
III. Detached clusters with no noticeable concentration of stars, but rather a more or less uniformly scattered distribution.
IV. Clusters not well detached from the general star field, which appear more like a small concentration than a true cluster.
1. Most cluster stars are of the same apparent brightness.
2. The brightness of cluster stars covers a medium range.
3. Clusters composed of bright and faint stars, generally only a few very bright stars, but many faint stars.
p. A poor cluster of less than 50 stars.
m. A moderately rich cluster of 50–100 stars.
r. A rich cluster with more than 100 stars.
N. Designates nebulosity involved in the cluster.
U. Identifies the cluster as being unsymmetrical.
E. Designates the cluster as being elongated.

An example of the scheme is the Pleiades cluster, which is designated by Trumpler as II3rN, i.e. a detached cluster of more than 100 stars exhibiting only a mild central concentration, a large range of star brightnesses, and which is associated with nebulosity. Does this match the description of the cluster which you can recall from photographs in introductory textbooks?

A series of papers by your instructor (Turner, AJ, 86, 222, 1981; AJ, 86, 231, 1981; AJ, 98, 2300, 1989) outline the general method used to analyze photometric and spectroscopic data for open cluster stars. The basic problems that are encountered are: (i) the proper separation of cluster stars from field stars in the same line of sight, (ii) making reasonable corrections for the effects of interstellar reddening upon the stellar photometry, and (iii) using the resulting data for cluster stars to determine all of the interesting parameters of the cluster — its age, its distance, chemical composition, peculiarities of member stars, etc. The membership problem is usually tackled using proper motion and/or radial velocity data for cluster stars, but most clusters can also be studied in a reliable manner even without such information.

Reddening corrections require a knowledge of the interstellar reddening law appropriate for the region under study. MK spectral types for stars in cluster fields prove to be invaluable for determining the reddening slopes necessary for making reddening corrections to the colour data of cluster stars. In many cases, this reddening slope will be close to a value of $E_{U-B}/E_{B-V} = 0.75$. Once the correct reddening slope is established, the next step is to apply reddening corrections to the colours of all cluster stars. Field stars which lie well foreground to the cluster are generally less heavily reddened than cluster members, while background stars may be more heavily reddened. Most dust clouds responsible for the reddening in any star field are relatively nearby, and only the closest stars in any field will be found to be unreddened. The more typical case will find both cluster and most field stars reddened by some minimum amount, which can be determined from a two-colour diagram. Two cases are encountered in practice: (i) **homogeneous reddening**, where all stars have the same colour excess, E_{B-V}, except for a small temperature-dependent term, and (ii) **differential reddening**, where the colour excesses vary across the field from one star to another. In the latter case, one normally finds that there is a correlation of the reddening, as measured by the colour excess, with spatial location; in most cases one can actually map the reddening across the face of the star cluster — quite frequently these maps bear a one-to-one relationship to the optical dustiness of the same field, as determined from a visual inspection of

images of the field. Where differential reddening exists, as for example in the fields of many young clusters, it may not always be obvious using photometry alone what the true unreddened colours of a star may be. In certain regions of the UBV two-colour diagram, reddening lines from a star intersect the intrinsic relation more than once. However, even in these instances, one can usually deduce the correct choice of intrinsic colours by referring to a reddening map established using those stars with unique dereddening solutions, or by trying all possible solutions to see which one produces the most reasonable result in the cluster's colour-magnitude diagram.

The practical method of dereddening is to follow the reddening vector for a star from its observed colours to the colours applicable to a star on the main-sequence (or giant and supergiant relations where appropriate) in order to find $(B-V)_0$. The colour excess E_{B-V} follows immediately. The colour excess of a star is one ingredient necessary to correct the star's observed visual magnitude V for the effects of interstellar extinction. The other ingredient is the ratio of total to selective extinction, R. This can often be adopted from the results of Turner (AJ, 81, 1125, 1976), i.e. R = 3.1, with possible variations from 3.0 to 3.2 depending upon the field. Where differential reddening exists in the field, it may even be possible to derive R from a variable-extinction analysis, as described earlier.

The next step is to plot the **reddening-corrected colour-magnitude diagram** for the cluster, which is a plot of V_0 versus $(B-V)_0$. Cluster members usually stand out in this diagram by the manner in which they fall along the evolved and unevolved portions of the main-sequence, or on the red giant or red supergiant branches. Field stars will be found randomly scattered throughout the diagram, although there is a tendency for their numbers to increase with magnitude as well as with increasing colour index. Experience plays a prominent role at this stage of the analysis, although inexperienced researchers generally do not have too much difficulty in determining which stars are cluster members. In sophisticated analyses, star counts are sometimes used to place the membership selection on a more quantitative basis. Most humans have a tendency to be rather conservative with regard to cluster member candidate selection.

The distance of the cluster can be found from **ZAMS fitting**, which involves fitting a standard ZAMS to the unevolved cluster main-sequence, either by eye or by the preferred mathematical method of averaging the dereddened distance moduli, V_0-M_V, of true ZAMS stars. These objects are the least-luminous stars on the ZAMS. Since close binaries are typically unresolved at the distance of the cluster, these stars, evolved cluster members, and rapidly-rotating stars fall above the ZAMS in the colour-magnitude diagram. Such objects must be taken into account for the proper placement of the ZAMS on the cluster main-sequence.

The age of the cluster is usually determined from the main-sequence turnoff point, the location of which, in terms of unreddened colour $(B-V)_0$ or luminosity M_V, can be readily calibrated using stellar evolutionary models. Stellar models are constantly being improved, so estimates of cluster ages do change with time as the models produce different values for the age of stars at the same cluster turnoff location. A true absolute scale of ages for open clusters is a goal currently unreachable due to the present state of evolutionary models.

Globular Clusters.

One of the most difficult parameters to derive for a globular cluster is its space reddening. This is because the most luminous stars in a globular cluster are its red giants, the intrinsic colours of which are generally rather uncertain and are very sensitive to the metallicity of the stars. New CCD detectors are capable of obtaining photometry for main-sequence stars in these clusters.e also However, the intrinsic colours of these G dwarfs depend upon their metallicity. Older studies of globular clusters made use of reddening estimates obtained from a comparison of the integrated colours of the clusters with their integrated spectral types, from colour excesses derived for member RR Lyrae variables in the clusters (when they were present!), and from the galactic cosecant law.

Since most globular clusters are located in the galactic halo where there are no interstellar dust clouds to produce obscuration along the line of sight, their reddening arises locally in the galactic plane. If the galactic plane is considered to be a plane parallel sheet of uniform absorbing material, then the reddening of a globular cluster lying outside the galactic plane should depend

upon its galactic latitude. In particular, if X is the thickness of the galactic disk above the sun's location, then the reddening of a cluster located away from the plane at galactic latitude b must be given by $E_{B-V} = X/\sin b = X \csc b$. Harris (AJ, 81, 1095, 1976) quotes a slightly different relation, $E_{B-V} = 0.06 (\csc |b| - 1)$ as a better fit to the observed reddening of $E_{B-V} \approx 0.00$ at the galactic poles. Current practice is to make use of cosecant law reddenings in conjunction with reddening estimates based upon the observed column densities of neutral hydrogen towards the clusters (from the work of Burstein). Neither method is particularly reliable, although this is not very important since most globulars tend to have rather small colour excesses.

Main-sequence fitting for globular clusters is very difficult, since it requires reliable magnitudes and colours for cluster main-sequence stars. The severe crowding suffered by stars in most globular cluster fields has important effects upon the derivation of such data, although Peter Stetson feels that current versions of his DAOPHOT routines are sufficient for the task. More importantly, the observed data must be compared with main-sequences for stars of similar metallicity. Observationally such sequences are subdwarf sequences, which are poorly calibrated in luminosity (they depend upon older trigonometric parallaxes). Theoretical sequences can also be constructed (see Hesser et al., PASP, 99, 739, 1987; Hesser, ASP Conf. Series, 1, 161, 1988; Stetson et al., AJ, 97, 1360, 1989), but these rely heavily upon the validity of the models. This field is still progressing.

Distances to globular clusters are derived in several different ways, as summarized by Harris (AJ, 81, 1095, 1976). Current studies aim to establish a distance scale for globular clusters which relies entirely upon fits to synthetic main-sequences. This may be dangerous given the current state of modelling for low-mass stars.

No two globular clusters seem to have identical colour-magnitude diagrams, mainly because of the differences in metallicity from one cluster to another. In most clusters it appears that the horizontal branch lies a "fixed" distance of $3^m.5$ above the main-sequence turnoff. Some general characteristics have been noted which seem to depend upon metallicity. One is the slope of the giant branch, which is steepest for metal-poor clusters. The quantity used to measure this parameter is ΔV = the difference in magnitude between the horizontal branch (at the RR Lyrae gap) and the red giant branch at $(B-V)_0 = 1.40$. Another parameter is the population of the horizontal branch as measured using the ratio (B–R)/(B+V+R), where B is the number of stars on the blue portion of the horizontal branch, R is the number on the red portion, and V is the number of RR variable stars in the RR Lyrae gap. In general it is found that mostly blue stars populate the horizontal branch in metal-poor clusters, while mostly red stars populate the horizontal branch in metal-rich clusters. The relative population of the horizontal branch also dictates whether or not there will be any stars located in the region of the instability strip. Globular clusters with the richest populations of RR Lyrae variables tend to be intermediate-metallicity clusters. This parameterization can be summarized as follows:

Metallicity Type	ΔV	HB Stars	RR Lyraes	Example
Metal-Rich	~2.1	mostly red	few	47 Tuc
Intermediate	~2.5	red and blue	moderately rich	M3
Metal-Poor	~3.0	mostly blue	moderate	M15

The HR diagrams of globular clusters differ from those of old open clusters mainly due to the effects of lower metallicity and smaller average stellar masses, although other effects may also be important. There are only ~150 globular clusters known in the Galaxy, compared with ~300 in M31, a difference presumably related to the overall more massive nature of M31. The luminosity distribution of globular clusters in the Galaxy (and in other galaxies) has a Gaussian-like shape, and ranges from $\langle M_B \rangle \approx -9$ to -5, with a peak near $\langle M_B \rangle = -7.5$. The high-luminosity cutoff is probably affected by an upper mass limit to clusters, as well as to the evaporation of cluster stars during their lifetimes. The low-luminosity cutoff may be due to the evaporation of any previously-existing low-mass clusters. Most galactic clusters have evaporated by the time they reach ages of $\sim 10^9$ years. Only very rich globulars could survive to the ages of $\sim 10^{10}$ or more years which are found for them.

Associations.

OB associations are extremely loose groupings of stars, with all stars of similar age, distance, and origin, which locally may be spread over 5° to 10° of sky, or more. They have diameters of up to 200 pc, beyond which they seem to lose their identify as a coeval group. Blaauw's (ARA&A, 2, 213, 1964) classic study of OB associations pointed out that they seem to consist of subgroups of different ages, with the youngest subgroups being the most compact and the oldest subgroups (with ages of $\sim 2.5 \times 10^7$ years) being the most dispersed. OB associations are unstable to galactic tidal effects and do not last long. They appear to be the dispersed remains of young open clusters which are no longer bound together by gravitational forces, a property well supported by proper motion and radial velocity studies of these groups. The relationship of one subgroup to another has been explained by Elmegreen & Lada (ApJ, 214, 725, 1977), who envision a progression of star formation through a giant molecular cloud induced by the expanding shock fronts of stellar winds and expanding H II regions from previously-created clusters. Most associations seem to fit this pattern, although there are many details which remain unexplained.

The term "association" was introduced by Ambartsumian in 1947, but subsequent catalogues often varied in their nomenclature of the groups. Such variations as I Ori and Cyg II represent two older schemes developed in the 1950's by Morgan and others. Following the designations introduced by Ruprecht in 1966 for the IAU, OB associations are now named for the constellation in which they (or most of their stars) are found, with an Arabic numeral (not Roman numeral) appended, e.g. Ori OB1, Per OB2, etc. The older schemes are no longer in use, except perhaps by radio astronomers who seem to be unaware of the current literature.

R associations, as noted by van den Bergh (AJ, 71, 990, 1966), are loose groups of stars of common age and distance which are associated with dust complexes. They get their names from the reflection nebulosity which each star illuminates — blue refelection nebulosity for B-type stars, yellow reflection nebulosity for G and K supergiants. R associations rarely contain O-type stars, and seem to be low-mass groups of newly-formed stars. Herbst and Assousa (ApJ, 217, 473, 1977) and Herbst (IAU Symp., 85, 33, 1980) present evidence that a few R associations were formed from the accumulated material marking the expanding shock fronts of supernova remnants. Their designations are similar to those of OB associations, e.g. Vul R1.

T associations are loose associations of T Tauri variables all associated with dark clouds. Since T Tauri variables seem to be pre-main-sequence objects of low mass, T associations represent low-mass groups of stars located in the dust clouds associated with star-forming complexes. They are not well studied. Their designations are as above, e.g. Tau T1.

Stellar rings (Isserstedt, Vistas, 19, 123, 1975) are a now-discredited concept, although in the early 1970's there was considerable debate about their existence. In hindsight it appears that most are simple illusions created by the eye's tendency to form geometrical patterns from random stellar distributions. Actually, a few may be real. The Orion Ring, fro example, is the stellar asterism formed by the stars lying around ε Orionis, the central star in Orion's Belt. Not only is this a real physical group of stars located in the Ori OB1b association, but it also has the appearance of a cluster caught in the final stages of dissolution into the general field. Perhaps other stellar rings are of similar nature.

Moving groups (Eggen, Galactic Structure, Chapter 6, 1965) are believed to be the actual dissolved remains of open clusters located in close proximity to the sun. Eggen has been fanatical in finding and studying stellar groups using the available proper motion, trigonometric parallax, and radial velocity data for nearby stars. Unfortunately, detailed chemical composition studies of group members tend to find that their compositions vary greatly from those found for members of open clusters. It therefore seems that the membership in moving groups is much less well-established than Eggen believes. However, the concept upon which moving groups are based is sound enough, and many such dispersed star clusters are undoubtably real enough, even if group membership is not firmly established for all potential members. A recent paper discussing the membership of the nearby Ursa Major moving group has been published by Soderblom & Mayor (AJ, 105, 226, 1993), with results for other clusters to follow.

11. Star Count Analysis (see Mihalas & Routly, Galactic Astronomy)

Define, for a particular area of sky:
N(m) = the total number of stars brighter than magnitude m per ~~square degree of sky~~ in the area under consideration, and
A(m) = the total number of stars of apparent magnitude $m \pm \frac{1}{2}\Delta m$ in the same area.
[Usually Δm steps of 1 magnitude are used, which is why A(m) is defined in this manner.]
Clearly, N(m) increases by the amount $A(m)\Delta m$ for each increase Δm in magnitude m.

$$\therefore \quad dN(m) = A(m)\, dm,$$

$$\text{or} \quad A(m) = \frac{dN(m)}{dm}.$$

Star counts in restricted magnitude intervals are usually made over a ~~restricted~~ specific area of sky which subtends a solid angle = ω. The entire sky is contained in a solid angle of 4π steradians = 4π $(\text{radian})^2 = 4\pi\ (57.2957795)^2$ square degrees = 41,252.96 square degrees ≈ 41,253 square degrees. Thus, 1 steradian = $41{,}253/4\pi$ square degrees = 3283 square degrees.

In order to consider the density of stars per unit distance interval of space in the same direction, it is necessary to consider the star counts as functions of distance, i.e. N(r), A(r). If the space density distribution is D(r) = number of stars per cubic parsec at the distance r in the line of sight, then:

$$N(r) = \int_0^r \omega r^2 D(r)\, dr.$$

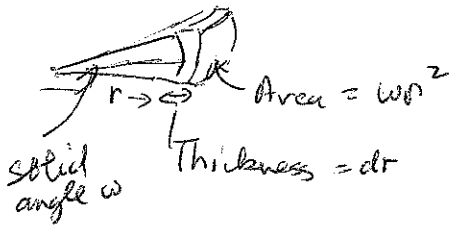

If D(r) = constant = D, then:

$$N(r) = \int_0^r \omega r^2 D\, dr = \omega D \int_0^r r^2 dr = \tfrac{1}{3}\omega D r^3.$$

Therefore, cumulative star counts in a particular area of sky should increase as r^3 for the case of a uniform density of stars as a function of distance. Recall that, for no absorption:

$$m - M = 5 \log r - 5.$$

$$\therefore \quad 0.2(m - M) + 1 = \log r, \quad \text{or} \quad r = 10^{[0.2(m-M)+1]}.$$

$$\text{Thus,} \quad N(m) = \tfrac{1}{3}\omega D 10^{[0.2(m-M)+1]\times 3}$$

$$= \left(\tfrac{1000}{3}\right)\omega D 10^{[0.6(m-M)]}$$

$$= \left(\tfrac{1000}{3}\right)\omega D 10^{-0.6M}\, 10^{0.6m}$$

$$= 10^{0.6m + C}, \text{ if M and D are constant.}$$

$$\text{i.e.} \quad \log N(m) = 0.6m + C.$$

$$A(m) = \frac{dN(m)}{dm} = \frac{d}{dm}\left[10^C\, 10^{0.6m}\right] = (0.6)(10^C)(\log_e 10)10^{0.6m} = C' 10^{0.6m}.$$

Denote l_0 = the light received from a star with m = 0.

$$\therefore \quad l(m) = l_0 10^{-0.4m} \text{ [Recall that } m_1 - m_2 = -2.5 \log l_1/l_2\text{]}.$$

$$\text{or} \quad -0.4\, m = \log \frac{l(m)}{l_0}.$$

The total light received from stars of magnitude m is therefore given by:

$$L(m) = l(m)\, A(m) \text{ (per unit interval of sky)}$$

$$= l_0 C' 10^{-0.4m + 0.6m} = l_0 C' 10^{0.2m}.$$

The total light received by all stars brighter than magnitude m is given by:

$$L_{tot}(m) = \int_{-\infty}^{m} L(m')\, dm' = l_0 C' \int_{-\infty}^{m} 10^{0.2m'} dm' = K\, 10^{0.2m}, \text{ where K is a constant.}$$

Thus, $L_{tot}(m)$ diverges exponentially as m increases (Olber's Paradox).

The results from actual star counts in various galactic fields are:

i. Bright stars are nearly uniformly distributed between the pole and the plane of the Galaxy, but faint stars are clearly concentrated towards the galactic plane.
ii. Most of the light from the region of the galactic poles comes from stars brighter than m ≈ 10, while most of the light from the galactic plane comes from fainter stars (maximum at m ≈ 13).
iii. Increments in log A(m) are less than the value predicted for a uniform star density, no interstellar extinction, and all stars of the same intrinsic brightness. This implies that D(r) could decrease with increasing distance (a feature of the local star cloud which could very well be true according to the work of Bok and Herbst), or interstellar extinction could be present (or both!).

Recall the true relation for distance modulus in the presence of interstellar extinction:

$m - M = 5 \log r - 5 + a(r)$. ← simple assumption, not necessarily true

$\therefore \quad \log r + 0.2\, a(r) = 0.2\,(m - M) + 1$.

Define the **apparent distance of a star**, ρ, in such a way that:

$\log \rho = 0.2\,(m - M) + 1 = \log r + 0.2\, a(r)$.

$\therefore \quad \log \rho - \log r = 0.2\, a(r)$, or $\rho = r\, 10^{0.2\, a(r)}$.

Thus, for example, if $a(r) = 1^m.5$, then $\rho = r\, 10^{0.3} \approx 2r$, so that the distance is overestimated by a factor of two. Since the volume varies as r^3, star densities derived from star counts should decrease strongly in the presence of interstellar extinction, as they are observed to do. However, Bok pointed out in 1937 that even reasonable allowances for interstellar extinction still produced an apparent density decrease with distance from the sun for star counts in the solar neighbourhood. This local star density enhancement is referred to as the "**local system**" (Herbst & Sawyer, ApJ, 243, 935, 1981).

McCuskey (Galactic Structure, Chapter 1, 1965) summarizes the results for studies of the distribution of common stars in the galactic plane, and Mihalas provides information on the galactic latitude dependence for these stars. The noteworthy features are the marked concentration of O, B, and A-type stars towards the galactic plane, and the weaker concentration of K-type stars to the plane. F, G, and M-type stars exhibit a more-or-less random distibution, with no concentration towards the plane or poles. Bright O and B-type stars are not aligned with the galactic plane, but concentrate towards a great circle inclined to the plane by ~16°. This feature is known as **Gould's Belt**, and is interpreted as a Venetian blind effect due to the tilt of the local spiral feature to the galactic plane, with the tilt being below the plane in the direction of the anticentre and above the plane in the direction of the galactic centre. Investigations of the distribution of dark clouds by Lynds (ApJS, 7, 1, 1962) for the northern hemisphere sky survey (POSS) and by Feitzinger & Stuwe (AAS, 58, 365, 1984) for the southern hemisphere sky survey (ESO-UK Schmidt) indicate that there is a distinct clumpiness in their distribution, which imples that the run of interstellar extinction with distance is also unlikely to be smooth. This is confirmed by the study of Neckel & Klare (AAS, 42, 251, 1980) on the distribution of interstellar reddening material.

Fundamental Equation of Star Count Analysis.

Define the general luminosity function as follows:

$\phi(M)$ = the number of stars per cubic parsec in the solar neighbourhood of absolute magnitude M.

$\phi(M,S)$ = the number of stars per cubic parsec in the solar neighbourhood of absolute magnitude M and spectral class S.

i.e. $\phi(M) = \sum_S \phi(M,S)$, over all spectral classes.

Define D(r) = the star density as a function of r relative to that at the sun's location, and $D_S(r)$ = the star density as a function of r for stars of spectral class S, relative to the sun's location,

i.e. $D(r) \to 1$ and $D_S(r) \to 1$ as $r \to 0$.

Recall the definition of A(m) = the number of stars per square degree of sky of magnitude m. This number can be obtained for any direction by considering the contributions from all stars of different absolute magnitude M at different distances r along the line of sight.

e.g. $A(m) = \sum \phi(M)\, D(r)\, \Delta V(r)$, where $\Delta V(r)$ is the volume element at distance r.

In differential notation,

$\Delta V(r) = \omega r^2 dr$.

$$\therefore \quad A(m) = \int_0^\infty \phi(M)D(r)\omega r^2 dr = \omega \int_0^\infty \phi(M)D(r)r^2 dr .$$

If the counts are made over a specific surface area Ω, they must be reduced to equivalent counts per square degree using the factor $4\pi\Omega/41{,}253$. Now, $M = m + 5 - 5 \log r - a(r) = m + 5 - 5 \log \rho$.

$$\therefore \quad \mathbf{A(m) = \omega \int_0^\infty \phi[m + 5 - 5 \log r - a(r)]D(r)r^2 dr}$$, which is the **fundamental equation of star counts.**

$$\text{or} \quad \mathbf{A(m,S) = \omega \int_0^\infty \phi[m + 5 - 5 \log r - a(r),S]D(r)r^2 dr} .$$

For stars of one specific spectral type and luminosity class, Malmquist demonstrated in 1925 and 1936 that the luminosity function could be assumed to be Gaussian,

$$\text{i.e.} \quad \phi(M,S) = \frac{1}{\sigma\sqrt{2\pi}} e^{[-(M-M_o)^2/2\sigma^2]},$$

where M_o is the average absolute magnitude for the group and σ is the dispersion of M about M_o. Under such conditions, it is sometimes possible to obtain an analytical solution for D(r) using star count data of the type A(m,S) — see Reed (A&A, 118, 229, 1983) and references therein.

When absorption is clearly present in the star counts, as occurs for most directions of the galactic plane, the fundamental equation can be rewritten in terms of the apparent distance ρ.

$\mathbf{A(m) = \omega \int_0^\infty \phi[m + 5 - 5 \log \rho]\Delta(\rho)\rho^2 d\rho}$, where $\Delta(\rho)$ is the density distribution as a function of apparent distance. Clearly, $D(r)r^2dr = \Delta(\rho)\rho^2 d\rho$.

$$\therefore \quad D(r) = \Delta(\rho) \frac{\rho^2}{r^2} \frac{d\rho}{dr} .$$

Since $\rho = r\, 10^{0.2a(r)}$,

$$\therefore \quad \frac{d\rho}{dr} = 10^{0.2a(r)} + 0.2r \times \log_e 10 \frac{da(r)}{dr} 10^{0.2a(r)} .$$

$$\therefore \quad D(r) = \Delta(\rho)\, 10^{0.6a(r)} \left[1 + 0.2r \times \log_e 10 \frac{da(r)}{dr} \right]. \quad \log_e 10 = 2.3025851...$$

$$\therefore \quad D(r) = \Delta(\rho) \left[1 + 0.4605\, r \frac{da(r)}{dr} \right] 10^{0.6a(r)}.$$

If, as an example, $a(r) = kr$, where k is known (e.g. $k = 1^m/\text{kpc} = 0^m.001/\text{pc}$),
then $D(r) = \Delta(\rho)\,[1 + 0.00046\, r]\, 10^{0.0006r}$ (see Mihalas).

12. Stellar Density Functions

It is possible to derive stellar density variations in certain regions of the sky using a knowledge of the luminosity function and information on the reddening dependence, a(r).

(m, log π) Tables.

Rewrite the integral equation for the magnitude function as a summation over finite shells:

$$\mathbf{A(m) = \sum_{k=1}^{\infty} \phi[m + 5 - 5 \log \rho_k]\Delta(\rho_k)\Delta V_k} ,$$

where ΔV_k is the volume of the kth shell.

Shells can be selected for ease of computation such that their midpoints have apparent distances given by:

$$\log \rho_k = -\log \pi_k = \frac{2k}{10}$$, i.e. midpoints lie at $\log \pi_k = -0.2, -0.4, -0.6, ...$

The corresponding edges of the shells lie at:
Shell 1: Inner edge = the sun. Outer edge, $\log \pi = -0.3$.
Shell 2: Inner edge, $\log \pi = -0.3$. Outer edge, $\log \pi = -0.5$.
Shell 3: Inner edge, $\log \pi = -0.5$. Outer edge, $\log \pi = -0.7$.
... etc.
The volume element ΔV_k refers to the volume of the shell for an angle of 1 square degree subtended on the sky. Recall that the volume of a sphere is given by $4\pi r^3/3$, and 4π steradians = 41,253 square degrees.

$$\therefore \quad \Delta V_k = \frac{1}{41{,}253} \frac{4\pi}{3} (\rho_{k,o}{}^3 - \rho_{k,i}{}^3) ,$$

$$\text{e.g.} \quad \Delta V_k = \frac{4\pi}{3 \times 41{,}253} (\rho_{k+1/2}{}^3 - \rho_{k-1/2}{}^3) .$$

For the kth shell, $\log \rho_k = \frac{2k}{10}$ and $M = m + 5 - 5 \log \rho_k = m + 5 - 5\,(k/5) = m + 5 - k$. One can now construct an (m, log π) table using the luminosity function, where the entries in the table are $\phi[m + 5 - k]\, \Delta V_k$.

(*m*, log π) Table Van Rhijn's Luminosity Function

$\log \pi_k = -\log \rho_k$	*Values of* m_{pg}												log *V*
	8	9	10	11	12	13	14	15	16	17	18	19	
−1.0	0	0											−0.69
−1.2	0	0											−0.22
−1.4	.01	0.01	0.01										0.38
−1.6	.02	0.03	0.03	0.03	0.04	0.06	0.08	0.09	0.10	0.12	0.13		0.98
−1.8	.05	0.08	0.10	0.12	0.13	0.16	0.25	0.30	0.34	0.42	0.49	0.54	1.58
−2.0	.14	0.21	0.32	0.40	0.46	0.51	0.63	1.00	1.18	1.35	1.66	1.95	2.18
−2.2	.26	0.58	0.85	1.26	1.58	1.82	2.04	2.52	3.98	4.72	5.38	6.60	2.78
−2.4	.58	1.05	2.29	3.40	5.00	6.30	7.25	8.14	10.0	15.8	18.8	21.4	3.38
−2.6	.66	2.29	4.18	9.13	13.5	19.9	25.1	28.9	32.4	39.8	63.0	74.8	3.98
−2.8	.60	2.63	9.14	16.6	36.3	53.8	79.4	100	115	129	158	251	4.58
−3.0	.60	2.40	10.5	36.4	66.0	144	214	316	398	458	513	630	5.18
−3.2	.76	2.40	9.55	41.7	145	262	575	853	1260	1580	1820	2040	5.78
−3.4	.96	3.02	9.55	38.0	166	575	1040	2290	3400	5000	6300	7250	6.38
−3.6	.60	3.80	12.0	38.0	151	660	2290	4170	9130	1.35+4	1.99+4	2.51+4	6.98
−3.8	.30	2.40	15.1	47.8	151	604	2630	9140	1.66+4	3.63+4	5.38+4	7.94+4	7.58
−4.0	.15	1.20	9.55	60.4	190	604	2400	1.05+4	3.64+4	6.60+4	1.45+5	2.14+5	8.18
−4.2	0	0.60	4.78	37.9	240	760	2400	9550	4.17+4	1.45+5	2.62+5	5.75+5	8.78
−4.4	0	0	2.4	15	151	955	3020	9550	3.80+4	1.66+5	5.75+5	1.05+6	9.38
−4.6	0	0	0	9.6	76	600	3800	1.20+4	3.80+4	1.51+5	6.66+5	2.29+6	9.98

Note: 1.35+4 = 1.35×10^4, etc.

TOTALS 5.69 22.70 ... ...

For each value of m, the entries reach a maximum at some value of log π_k. The summation of the entries for each column gives the values for:

$$A_o(m) = \sum_{k=1}^{\infty} \phi[m + 5 - 5 \log \rho_k] \Delta(\rho_k) \Delta V_k .$$

These values can be compared with the actual counts in a particular area, and will usually be too high. They must be reduced by the values for the apparent density function $\Delta(\rho_k)$ for each shell. It is therefore necessary to reconstruct the (m, log π) table including an estimated $\Delta(\rho_k)$ function. A solution for the observed counts generally requires a number of iterations with a variable $\Delta(\rho_k)$ function until a best match is obtained. Experience is particularly helpful here. Once a solution for $\Delta(\rho_k)$ is obtained, one still needs to know a(r) to obtain D(r) from the results. Such a(r) estimates can come from various sources, e.g. Neckel & Klare (A&AS, 42, 251, 1980).

Wolf Diagrams and Dark Cloud Distances

Wolf diagrams are used to analyze the extinction in dark clouds which are transparent enough to transmit the light of background stars. The technique is to use (m, log π) tables to deduce the $\Delta(\rho_k)$ function for a nearby reference region which is relatively free of dust extinction, and then to determine where in the table one can hang a "dimming" curtain of dust — i.e. Δm magnitudes of extinction — to reproduce the A(m) values for the region of the dark cloud. The extinction curtain in the (m, log π) table will produce a shift of m + Δm for all the entries in the table beyond log $\pi_k = -0.2x + 0.1$. Thus, the cloud's inner edge lies at log $\rho_k = 0.2x - 0.1$, or at log r + 0.2a(r) = 0.2x – 0.1. If the run of general extinction with distance, a(r), can be established for the region under investigation, it is possible to solve for the distance r of the cloud.

Problems:

1. The comparison region must be as close as possible to the cloud region.
2. The comparison region must be relatively unobscured.
3. The cloud region should only have a single cloud in the line-of-sight.
4. The general luminosity function (GLF) gives very little magnitude resolution, since slight changes in $\Delta(\rho_k)$ can produce equally valid A(m) curves. The preferred technique is to obtain spectroscopic information so that one can use A(m,S) data in the analysis. This generally provides much better distance resolution for the dust curtain.
5. The a(r) dependence must be known extremely well.

Wolf diagrams, when carefully analyzed, can also be used to study the ratio of total-to-selective extinction, R, in dark clouds. Blue light counts give ΔB for each cloud, while red light counts give ΔV. Thus,

$$R = \frac{A_V}{E_{B-V}} = \frac{A_V}{(A_B - A_V)} = \frac{\Delta V}{(\Delta B - \Delta V)} .$$

Schalén (A&A, 42, 251, 1975) has made such an analysis for several nearby dark clouds, and has obtained a mean value of R = 3.1 ±0.1 for the dust in these clouds.

Recent Improvements

Herbst & Sawyer (ApJ, 243, 935, 1981) present an interesting technique based upon star counts in **opaque** dust clouds associated with clusters and associations of known distance to obtain a function dependence of N_{ct} with distance r. They used CO observations to identify clouds likely to be totally opaque to blue light on the Palomar Observatory Sky Survey (POSS), then normalized their counts in only the opaque regions of these clouds to the equivalent value of N_{ct}, the number of foreground stars per square degree of sky. They found a resulting functional dependence for their counts of the form:

$r = 320\ N_{ct}^{0.57}$ (pc) , from their calibrating clouds of known distance.

A careful analysis of the variations in star density as a function of distance for these clouds has confirmed a result noted much earlier by Bok and later by McCuskey (Galactic Structure), namely that the sun appears to be located in a region of local density maximum in the Galaxy. The results of McCuskey suggest that this density maximum may be the local Cygnus spiral arm.

Density Variations Perpendicular to the Galactic Plane

In the direction perpendicular to the plane, the GLF may not apply (see Bok's lecture notes presented below). However, the results with regard to density variations are almost independent of any variations in this function. Typically the density function $D_S(z)$ for stars of a specific spectral type S exhibits an exponential decline with increasing distance z away from the galactic plane.

i.e. $D_S(z) = D_S(0)\, e^{-z/\beta_S}$, or $\log D_S(z) = \log D_S(0) - \frac{z}{\beta_S}$.

where β_S represents the scale height of the stellar distribution. Fits of this type of dependence to the observed density variations for different types of stars can be used to obtain their scale heights relative to the galactic plane. The results for stars of different spectral types can be used to analyze the different population types for each group. Specific results are summarized by Mihalas, and are reproduced below:

Object	Population	Type	β(pc)	
O stars		I	50	
B stars		I	60	
A stars		I	115	
F stars		Mixed	190	
dG stars		Mixed	340	
dK stars		Mixed	350	
dM stars		Mixed	350	
gG stars		Mixed	400	
gK stars		Mixed	270	
Dust and Gas		I	175	
Classical Cepheids		I	45	
Open clusters		I	80	
Novae		Disk II	200	
Planetary Nebulae		Disk II	190–250	Zijlstra & Pottasch, A&A, 243, 478, 1991
RR Lyraes (P < 0d.5)		Disk II	900	
RR Lyraes (P > 0d.5)		Halo II	3000	
Type II Cepheids		Halo II	2000	
Extreme Subdwarfs		Halo II	3000	
Globular Clusters		Halo II	4000	

13. The Luminosity Function

The General Luminosity Function

Notes Prepared by Bart J. Bok for a Lecture delivered at the University of Toronto, April, 1979.

Luminosity Functions

Every astronomer deals almost daily with luminosity functions of some sort. In a way the most basic of these functions is the **general luminosity function** (GLF), which gives us the distribution function of absolute magnitude, **M**, for the average unit volume in the vicinity of the sun. We require this basic distribution function to describe not only the stellar distribution in our immediate galactic surroundings, but also to serve as a basis from which we explore how it varies from one point in our galaxy to another. We can trace it back into time, and, on the basis of some simple assumptions about evolutionary trends, figure out how it must have appeared in earlier phases of galactic evolution. Again, with our local GLF as a firm basis, we can explore its variations in the galactic plane and especially at right angles to the galactic plane, where we are led gently into the largely yet unknown luminosity functions that prevail in our elusive galactic halo, or in the central regions of the Galaxy. We can break our GLF into its component parts and derive luminosity functions for separate spectral or colour subdivisions, or for groups of stars; Cepheid variables or RR Lyrae stars may serve as examples. Or, we may compare luminosity functions for comparable groups of stars with differing metallicities. With proper care, we can make comparative studies of the brighter ends of luminosity functions in our vicinity and in nearby galaxies, starting with the Star Clouds of Magellan. There are many practicable problems which, for their solution, require a good background knowledge of luminosity functions. For example, if we wish to study the space distribution of stars of separate spectral subdivisions, then we can only hope to construct the basic (m, log π) table required for such an analysis after we possess solid information on the luminosity function of the stars under investigation. When we study dark nebulae, such as the great complexes in Ophiuchus and in Taurus, or the Souther Coalsack, we can find their distances and photographic extinctions best from analyses in which the basic (m, log π) tables play key roles.

In a couple of lectures in a "mini course", one cannot hope to cover fully the details of how we have obtained our present knowledge of the GLF and of the luminosity functions for special groups or classes of stars. But I can — in a short time — outline in broad terms the different approaches that have been used and provide a key to some of the basic literature in the field.

1. The Road to Gröningen Publications 30, 34, 38, and 47

J. C. Kapteyn, the first director of the famous Laboratory of Statistical Astronomy in Gröningen, Holland, amd his successor, P. J. van Rhijn, gave us through their work in the first third of the twentieth century the basic GLF that still serves us at the present time. For the range of observable absolute magnitudes, $-4 < M < +16$, for M_B and M_V, the curve shows, for successive values of M−1/2 to M+1/2, the logarithm of the number of stars per cubic parsec in successive intervals of absolute magnitude. We have one curve for blue magnitudes, another for visual magnitudes. Kapteyn and van Rhijn saw from the start two basic approaches to the problem of determining the luminosity function. The first approach follows the path of statistical analysis based principally upon proper motions and radial velocities, making effective use of mean parallaxes and the distribution of derived parallaxes about their means. In the second approach — developed beautifully by van Rhijn after Kapteyn's death — full use is made of the growing body of trigonometric parallaxes of high precision. The study, which was assiduously pursued between 1902 and 1925, culminated in the publication by van Rhijn (1925) of Gröningen Publication 38. Every young astronomer today should take the time to read van Rhijn's treatment. I shall describe briefly the methods used for deriving the GLF of Gröningen Publication 38.

Method 1. This is the method that Kapteyn saw as the best one to obtain the GLF.

a) In Gröningen Publication 30, a great effort had been made to obtain values of $N_{m,\mu}$, the numbers of stars per 10,000 square degrees in the sky between set limits of apparent magnitude m−1/2 to m+1/2, and set limits of total annual proper motion 0".000 to 0".020, 0".020 to 0".040, ..., 0".100 to 0".150, 0".150 to 0".200, ... , etc.

b) In Gröningen Publication 34, there are two types of useful basic tabulations. The first of these lists values of the **mean parallaxes**, $<\pi_{m,\mu}>$, for stars within relatively small ranges of apparent magnitude m and total proper motion μ. These mean parallaxes had been obtained in various ways, especially through the use of **secular parallaxes**, which were found by combining radial velocity data — which yielded the reflex of the solar motion in km/s — and proper motions — which yielded the same reflex of the solar motion in seconds of arc per year. The second type of tabulation gave the probable distribution of true parallaxes about the mean values $<\pi_{m,\mu}>$. Tables 1 and 2 of Gröningen Publication 38 show samples of the tables prepared by van Rhijn.

TABLE 1. NUMBERS OF STARS PER 10000 SQUARE DEGREES AND MEAN PARALLAXES OF THE APPARENT MAGNITUDE 5.45 TO 6.44; GALACTIC ZONE — 20° TO + 20°.

Limits μ.	Numbers	$\bar{\pi}_{m,\mu}$	Limits μ	Numbers	$\bar{\pi}_{m,\mu}$
" "		"	" "		"
.000 to .020	648	0.0048	.400 to .500	7	0.0466
.020 to .040	486	.0078	.500 to .600	8	.0539
.040 to .060	248	.0105	.600 to .700	2.6	.0609
.060 to .080	103	.0129	.700 to .800	1.9	.0675
.080 to .100	74	.0151	.800 to .900	1.9	.0739
.100 to .150	112	.0182	.900 to 1.00	1.5	.0801
.150 to .200	45	.0230	1.00 to 1.50	4.3	.094
.200 to .300	40	.0304	1.50 to 2.00	0.4	.120
.300 to .400	17	.0388	> 2.00	1.1	.180

[1] *Gron. Publ.* 30 table 19, 1920.

[2] *Gron. Publ.* 34, table 19. 1923.

[3] *Op. cit.* Formulae (42) and (43) on page 43, where $r = 0.19$ $a = 0.22$.

TABLE 2. DISTRIBUTION OF THE TRUE PARALLAXES OF THE 648 STARS
$m = 5.45$ TO 6.44 $\mu = ".000$ TO $".020$.

Limits π	Number
$> ".251$	
.251 to .158	
.158 to .100	
.100 to .0631	
.0631 to .0398	
.0398 to .0251	1
.0251 to .0158	4
.0158 to .0100	25
.0100 to .00631	95
.00631 to .00398	207
.00398 to .00251	229
.00251 to .00158	84
.00158 to .00100	3
	648

— INTERMEZZO —

Please note that, in Gröningen Publications 30, 34, and 38, the absolute magnitudes listed are:

$$M = m + 5 \log \pi .$$

In Gröningen Publication 47, van Rhijn adopted the presently used:

$$M = m + 5 + 5 \log \pi .$$

TABLE 3. NUMBER OF STARS PER 10000 SQUARE DEGREES BETWEEN THE MAGNITUDES 5.45 TO 6.44, AND GALACTIC LATITUDES $-20°$ TO $+20°$.

Limits μ \ Limits π / M	$0".158$	$0".100$	$0".0631$	$0".0398$	$0".0251$	$0".0158$	$0".0100$	$0".00631$	$0".00398$	$0".00251$	$0".00158$	$0".00100$	
	+2.72	+1.42	+0.43	−0.55	−1.53	−2.52	−3.50	−4.50	−5.48	−6.46	−7.45	−8.44	
".000 to ".020					0.6	4.	26.	95.	207.	229.	84.	3.	
.020 „ .040				0.5	3.4	21.	76.	159.	168.	56.	1.		
.040 „ .060				1.0	5.9	27.	66.	93.	51.	4.			
.060 „ .080			0.1	0.9	5.4	18.	36.	34.	9.				
.080 „ .100			0.1	1.3	6.0	17.	27.	19.	3.				
.100 „ .150		0.1	0.6	3.8	15.2	35.	39.	17.	1.				
.150 „ .200		0.1	0.7	3.3	10.0	17.	12.	2.					
.200 „ .300		0.2	1.6	6.0	12.9	14.	5.						
.300 „ .400		0.4	1.5	4.2	6.4	4.	1.						
.400 „ .500	0.1	0.3	1.0	2.2	2.5	1.							
.500 „ .600	0.1	0.5	1.5	2.8	2.5	1.							
.600 „ .700	0.1	0.2	0.7	1.0	0.6								
.700 „ .800	0.1	0.2	0.5	0.8	0.4								
.800 „ .900	0.1	0.3	0.6	0.7	0.3								
.900 „ 1.00	0.1	0.2	0.5	0.5	0.1								
1.00 „ 1.50	0.4	1.0	1.6	1.1	0.2								
1.50 „ 2.00	0.1	0.1	0.1	0.0	0.0								
> 2.00	0.4	0.4	0.2	0.0	0.0								
Sum	1.5	4.0	11.3	30.1	72.2	159.	288.	419.	439.	289.	85.	3.	

For each range of apparent magnitude (see Table 3 of Gröningen Publication 38 as a sample), the data from tables such as Table 1 and Table 2 are combined in a master table (see Table 3) listing the numbers for successive intervals of total proper motion μ. The sum line at the bottom of Table 3 shows how the stars for the given range of apparent magnitude are distributed over successive parallax "bins", which are strictly "bins" of narrow intervals in absolute magnitude.

In the final tabulation, Table 4 of Gröningen Publication 38, the summations in the bottom line of each Table 3 are combined. Table 4 is really a (M, π) tabulation in which each series of numbers for a given range of aparent magnitude contributes a diagonal line.

TABLE 4. LOGARITHM OF THE NUMBER OF STARS PER CUBIC PARSEC.
The weights are between parentheses.

M	−9.43	−8.44	−7.45	−6.46	−5.48	−4.50	−3.50	−2.52	−1.53	−0.55	+0.43	+1.42	+2.40	+3.39	+4.37	+5.36	+6.35	Log. Vol. (10.000 square degr.)
Galactic latitude 0° to ± 20°																		
Limits π.																		
.00100 to .00158						5.476 (4.)	6.113 (7.)	6.581 (2.)										8.575
.00158 » .00251				4.468 (4.9)	5.184 (23.0)	5.820 (16.)	6.404 (8.)	6.840 (9.)	7.229 (3.7)									8.275
.00251 » .00398		3.261 (0.51)	4.178 (4.2)	4.783 (7.3)	5.427 (12.0)	6.020 (39.)	6.526 (23.)	6.947 (7.)	7.278 (6.3)	7.589 (1.5)								7.679
.00398 » .00631	3.465 (0.19)	3.645 (0.31)	4.322 (1.5)	5.020 (7.3)	5.563 (12.0)	6.102 (25.)	6.593 (39.)	6.985 (15.)	7.293 (3.7)	7.524 (2.6)	.756 (0.5)							7.079
.00631 » .0100		3.963 (0.27)	4.535 (0.7)	5.081 (2.1)	5.662 (8.2)	6.143 (10.)	6.599 (12.)	6.991 (23.)	7.312 (7.7)	7.591 (1.5)	.626 (0.8)	7.790 (0.2)						6.479
.0100 » .0158			4.877 (0.3)	5.253 (0.8)	5.647 (2.0)	6.158 (7.)	6.580 (7.)	6.947 (6.)	7.248 (10.)	7.540 (3.2)	.693 (0.7)	7.666 (0.8)	7.752 (0.2)					5.879
.0158 » .0251				5.420 (0.3)	5.762 (0.6)	6.126 (2.)	6.551 (4.)	6.925 (8.)	7.192 (2.7)	7.422 (4.5)	.681 (3.2)	7.659 (0.8)	7.591 (0.5)	7.620 (0.73)	7.562 (1.5)	7.395 (1.1)		5.279
.0251 » .0398					5.783 (0.2)	6.184 (1.)	6.522 (2.)	6.855 (3.)	7.180 (6.0)	7.366 (3.1)	.522 (6.9)	7.729 (1.8)	7.648 (0.7)	7.486 (0.33)	7.579 (0.37)	7.408 (0.27)	7.161 (0.17)	4.679
.0398 » .0631						6.383 (0.2)	6.544 (0.5)	6.880 (1.)	7.103 (1.8)	7.400 (3.7)	.503 (1.4)	7.607 (2.9)	7.692 (0.6)	7.635 (0.32)	7.458 (0.16)	7.434 (0.11)	7.253 (0.05)	4.079
.0631 » .100							6.366 (0.04)	6.800 (0.2)	7.211 (0.7)	7.306 (0.8)	.374 (1.3)	7.597 (0.9)	7.651 (1.0)	7.688 (0.20)	7.521 (0.09)	7.407 (0.06)		3.479
.100 » .158									6.966 (0.1)	7.483 (0.4	.301 (0.4)	7.723 (0.6)	7.652 (0.4)	7.640 (0.41)	7.612 (0.05)			2.879
> .158											.451 (0.2)	7.720 (0.2)	7.735 (0.2)	7.609 (0.12)	7.545 (0.13)			2.409
											1	2	3	4	5	6	7	8	9	10	11	12	13	14

Table 4 yields for each shell of distance the derived GLF for that shell. Please note that the GLF derived from Table 4 is reasonably well fixed for the range in absolute magnitude $-2 < M < +10$. In other words, the analysis based upon proper motions and radial velocities yields **no** information about the faint end of the GLF, $M > +10$!

Method 2.

Van Rhijn wished very much to obtain information about the faint end of the GLF, $+10 < M < +16$. The proper analysis indicated that the function might possibly have a maximum near $M = +8$, and that it would turn over after that. Van Rhijn decided to make what use he could (in the early 1920's!) of the growing body of measured trigonometric parallaxes, correcting statistically for the known biases of astronomers engaged in the measurement of trigonometric parallaxes. Parallax observers all use a uniform technique of measurement and reduction established (about 1904) by Frank Schlesinger. How did they select the stars to be placed on their parallax programs? They naturally chose the stars most likely to have large trigonometric parallaxes. Large total proper motion may indicate that the star is a nearby one. So van Rhijn decided that there was in parallax work a strong selection effect favouring the placing of stars of largest proper motion on parallax observing lists. So few stars of small total proper motion are on the lists of selected parallax stars that van Rhijn decided to consider in his statistics only stars with $\mu \geq 0".200$.

Van Rhijn knew from his counts in proper motion catalogues the number of stars with proper motions in, say, the range $0".200 < \mu < 0".400$ for successive intervals of apparent magnitude. He also knew what fraction of these stars had their trigonometric parallaxes measured. Since the program selection had been based only upon total proper motion, every stars with a measured trigonometric parallax had to count as representative for f stars, where f is defined as the ratio of the number $N_{m,\mu}$ (from Table 1 of Gröningen Publication 39) divided by the number of stars in the (m, μ) bin for which a trigonometric parallax had been obtained. Hence,

$$f = \frac{N_{m,\mu}}{N_{\pi,m\mu}} ,$$

where $N_{\pi,m\mu}$ is the number of stars with measured trigonometric parallax in "bin" (m, π). Table 15 of Gröningen Publication 38 shows how every star with a measured parallax in the proper motion interval $0".200 < \mu < 0".400$ and with $6.45 < m < 7.45$ has to count for 13 stars ($f = 13$) in the statistical tabulations for the GLF.

TABLE 15. DERIVATION OF THE PLENITUDES OF THE PARALLAX STARS GALACTIC LATITUDE $\pm 40°$ $\pm 90°$; MAGNITUDE 6.45 TO 7.44.

Limits of μ	Number		Plen.	$\frac{1}{\text{Plen.}} = f$
	π stars	G. P. 30		
0".200 to .400	8	102	0.078	13
.400 to .800	9	33	.273	3.7
.800 to 2.00	7	7.2	.97	1.0
> 2.00	3	1.0	3.0	0.3

A second correction factor must be applied to correct for the omission of the stars with $\mu <$ 0".200, which van Rhijn deliberately omitted. The correction factor K is defined as:

$$K = \frac{\text{Total number in parallax group } \pi_1 \text{ to } \pi_2}{\text{Number in same group with } \mu > 0".200}.$$

If we assume that all stars in the group π_1 to π_2 have the mean parallax of the group, $\langle\pi\rangle = \frac{\pi_1 + \pi_2}{2}$, then the linear velocity corresponding to $\mu > 0".200$ is $V_{lin} > \frac{4.74 \times 0.200}{\langle\pi\rangle}$ km/s. Van Rhijn did possess tabulations (based upon radial velocities of faint stars) to show what fraction of the stars had linear velocities in excess of this velocity, so the factors of K could be derived with reasonable accuracy. With the factors f and K firmly fixed, van Rhijn could correct his statistics for "missing" stars, and the faint end of the GLF could be obtained in a manner very similar to the procedure used to obtain Table 4.

Van Rhijn went further on the problem between 1925 and 1936, when — in Gröningen Publication 47, Table 6 — he published his final impressions of the GLF, side by side for photographic and visual magnitudes. There are in the literature many accounts of the work of Kapteyn and van Rhijn. The one I like best is by S. W. McCuskey in Vistas, 7, 141, 1966. The van Rhijn curves are shown in Figures 2 and 3 of McCuskey's paper. It is amazing to see how nicely the early van Rhijn values agree with more recent determinations of the GLF.

TABLE 6. ADOPTED LUMINOSITY CURVE FOR PHOTOGRAPHIC AND VISUAL MAGNITUDES IN THE GALAXY.

$\varphi(M)$ = number of stars per cubic parsec near the sun between the absolute magnitudes $M - \frac{1}{2}$ and $M + \frac{1}{2}$.

M	$\log \varphi(M)$ photogr.	visual	M	$\log \varphi$ (M) photogr.	visual	M	$\log \varphi$ (M) photogr.	visual
— 6.0	2.10	1.63	+ 2.0	6.77	6.71	+ 10.0	7.64	7.84
— 5.0	3.07	2.77	+ 3.0	6.86	6.98	+ 11.0	7.81	7.99
— 4.0	3.65	3.58	+ 4.0	7.19	7.29	+ 12.0	7.97	8.02
— 3.0	4.25	4.12	+ 5.0	7.35	7.40	+ 13.0	8.01	8.05
— 2.0	4.75	4.71	+ 6.0	7.49	7.45	+ 14.0	8.06	
— 1.0	5.07	5.32	+ 7.0	7.53	7.45			
0.0	5.68	5.98	+ 8.0	7.46	7.55			
+ 1.0	6.34	6.59	+ 9.0	7.49	7.75			

2. Luyten's Studies of the Faint End of the GLF

To Willem J. Luyten, now a Professor Emeritus of the University of Minnesota, goes the credit of having given the astronomical world the most precise information on the faint end of the GLF. There is an excellent summary of Luyten's work in McCuskey's (1966) article. Luyten has summarized his work in two more recent papers (MNRAS, 139, 221, 1968; IAU Symp., 80, 63, 1978).

As a basis for his work, Luyten completed two gigantic surveys leading to the discovery of thousands of stars with total annual proper motions in excess of 0".500. The first of these was based on early epoch and more recent photographs taken with Harvard Observatory's 24-inch Bruce refractor in South Africa. The first survey was begun in the late 1920's, and continued into the early 1940's. In 1962 a program was initiated to repeat the early red survey plates photographed with the Palomar 48-inch Schmidt telescope, a survey which — for the areas covered — yields proper motions for 50,000 or more stars, including, by 1968, 4,000 stars with total annual proper motions in excess of μ = 0".500. The limit of the Palomar survey is about photographic apparent magnitude 19.

Since no radial velocities or parallaxes are available for these stars, Luyten sorted them statistically according to absolute magnitude by the quantity:

$H = m + 5 + 5 \log \mu$, which can be written as:

$H = m + 5 + 5 \log T$,

where T is the tangential velocity expressed in A.U. per year (i.e. units of 4.74 km/s). Information on the distribution of the tangential velocities, T, must be obtained from data for brighter stars.

In his 1968 paper, Luyten could announce that the GLF continues to increase to photographic absolute magnitude M_{pg} = +15, but that a maximum in the frequency function is reached at M_{pg} = +15.7. Since the Luyten survey (based now upon proper motions for 115,000 stars brighter than 21st photographic magnitude) reaches well beyond the value M_{pg} = +15.7, the maximum in the frequency function of absolute magnitude seems well established. Figures 2 and 3 and Table 3 of McCuskey's paper show how nicely the Luyten data extend the van Rhijn GLF. However, many uncertainties remain. In this connection, reference should be made to a recent paper by J. F. Wanner (MNRAS, 155, 463, 1972).

The Bruce and Palomar proper motion surveys, carried out almost single handed by Luyten, followed by his analysis leading to the firm establishment of the faint end of the GLF, will continue to be recognized as one of the great achievements of twentieth century astronomy. The name of W. J. Luyten is firmly established in the annals of astronomy.

PHOTOGRAPHIC MAGNITUDES [Solar Neighborhood]

M	$\log \varphi(M_v)$	$\log \varphi(M_{pg})$	M	$\log \varphi(M_v)$	$\log \varphi(M_{pg})$
−6	2·23:	—	+ 6	7·66	7·47
−5	2·97:	—	+ 7	7·48	7·55
−4	3·60	3·65	+ 8	7·58	7·65
−3	4·10	4·27	+ 9	7·72	7·72
−2	4·80	4·83	+10	7·88	7·80
−1	5·54	5·36	+11	7·97	7·88
0	6·16	5·88	+12	8·00	7·95
+1	6·60	6·35	+13	8·05	7·98
+2	6·83	6·70	+14	8·05	8·00
+3	7·07	7·00	+15	8·02	7·96
+4	7·25	7·21	+16	7·96	7·90
+5	7·56	7·36	—	—	—

TABLE 3. THE STELLAR LUMINOSITY FUNCTION FOR PHOTOGRAPHIC MAGNITUDES

M_{pg}	$\log \varphi(M_{pg}) + 10$		M_{pg}	$\log \varphi(M_{pg}) + 10$	
	van Rhijn	Luyten		van Rhijn	Luyten
−6	2·10:	—	+ 5	7·35	7·34
−5	3·07:	—	+ 6	7·49	7·46
−4	3·65:	—	+ 7	7·53	7·57
−3	4·25	—	+ 8	7·46	7·68
−2	4·75	—	+ 9	7·49	7·76
−1	5·07	—	+10	7·64	7·84
0	5·68	—	+11	7·81	7·91
+1	6·34	—	+12	7·97	7·96
+2	6·77	6·89	+13	8·01	8·01
+3	6·86	7·04	+14	8·06	8·04
+4	7·19	7·18	+15	8·04	—

3. Spectral Colour-Magnitude Surveys and the GLF

In Section 4 of McCuskey's (1966) paper, there is an excellent summary of the contributions to our knowledge of the GLF for intermediate absolute magnitudes ($-2 < M_{pg} < +7$) that has been made via surveys of selected Milky Way fields. These studies are based on spectral classification plus data on colours and magnitudes for the stars under investigation. The most significant investigations in this area are those made at the Warner and Swasey Observatory under the direction of S. W. McCuskey for selected fields along the northern and the southern Milky Way. The availability of colour indices, magnitudes, and spectral-luminosity classes for the stars in each field permit an evaluation of the galactic extinction characteristics for each field, which makes it possible to correct for galactic extinction effects in each field. The analysis for each group of stars proceeds on the basis of assumed mean values for the absolute magnitudes of the stars in each subdivision. Table 6 of McCuskey's paper lists the mean absolute magnitudes (per unti volume) for each spectral group, and the dispersions in absolute magnitude about these means. By combining the results from the separate groups, a GLF can be obtained for all stars within 100 (or 200) parsecs of the sun for each field, and these can be compared with van Rhijn's standard function. Figures 2 and 3 of McCuskey's paper show nicely how the various spectral surveys complement the information contained in the curves by van Rhijn and by Luyten.

4. Epilogue

Table 8 of McCuskey's paper summarizes nicely our present-day knowledge of the GLF. Figures 2 and 3 give the much-needed pictorial representation.

We indicated earlier that a sound knowledge of the GLF serves as a basis for many related studies. Sections 5, 6, and 7 of McCuslkey's paper, and the references for these sections, describe the more important of these related studies; I shall devote a brief paragraph to each or some of these.

a) **Initial Luminosity Function.** Salpeter (1955) was the first to derive the Initial General Luminosity Function, or ILF (now known as the Salpeter Function) on the basis of a few simple assumptions formulated following well-established evolutionary trends. The book by Schwarzschild (1958) has a good discussion of the ILF. See also the recent treatment by V. C. Reddish in his book *Stellar Formation* (Pergamon Press, Oxford, 1978, Chapter 3).

b) **Variations in the Galactic Plane.** McCuskey and his associates have analyzed their material on spectra, colours, and magnitudes for selected Milky Way fields to obtain GLF's at various distances from the sun for each field under investigation. Figure 5 and Table 9 of McCuskey's paper show the sort of variations that occur in, or very near to, the central galactic plane.

M	log φ (M)			
	$b = 0° \pm 20°$	$\pm 20° \pm 40°$	$\pm 40° \pm 90°$	$0° \pm 90°$
— 8.0	4.56			4.140
— 7.0	5.25	4.73	4.56	4.860
— 6.0	5.662	5.471	5.400	5.511
— 5.0	5.982	5.745	5.972	5 900
— 4.0	6.486	6.276	6.365	6.376
— 3.0	6.775	6.620	6.781	6.735
— 2.0	7.230	6.802	7.075	7.037
— 1.0	7.385	7.152	7.273	7.270
0.0	7.417	7.283	7.505	7.402
+ 1.0	7.523	7.285	7.609	7.472
+ 2.0	7.314	7.123	7.503	7.313
+ 3.0	7.672	7.110	7.670	7.484
+ 4.0	7.719	7.923	7.692	7.778
+ 5.0		7.382		7.382
+ 6.0		7.922		7.922

c) **Variations Perpendicular to the Galactic Plane.** In 1941, Bok and MacRae (Annals of the N.Y. Academy of Sciences, 42, 219, 1941) made a careful analysis of density distributions and luminosity functions at positions well above or below the central galactic plane. The derived GLF's at high z–values (z is the height above or below the galactic plane) are very different from the function in the plane, since the more luminous stars show decreases in space density with z that are far steeper than those found for the less luminous stars. The Joint Discussion on High Latitude Problems held (in 1976) at the IAU General Assembly in Grenoble shows clearly that the GLF in the galactic halo is quite different depending upon the height z above or below the galactic plane.
d) **Central Regions of our Galaxy.** For the present, we must admit that we have essentially **no** information on the GLF that prevails within 5,000 parsecs of the centre of our Galaxy.

Much of the original work on the study of star densities in the Galaxy used Kapteyn's luminosity function of 1920, which was a simple Gaussian function with $M_o = +7.69$ and $\sigma = \pm 2^m.5$. Later work made use of van Rhijn's luminosity function (described above), and later modifications of it (van Rhijn, Galactic Structure, Chapt. 2, 1965; McCuskey, Vistas, 7, 141, 1966; Mihalas, Galactic Astronomy).

As noted in Bok's lecture, the procedure used to derive the GLF is rather involved, and requires a detailed statistical approach. The various parameters used in deriving the GLF are:
i. **Mean Parallaxes**, $\langle \pi_{m,\mu} \rangle$, for groups of common m ±0.5 and μ ±0".01/annum. In this case radial velocity data and proper motions are used to establish secular parallaxes for the stars. In addition, the results can sometimes be supplemented by measured trigonometric parallaxes, after corrections for the effects of bias in the samples of parallax stars (see Mihalas).
ii. **Trigonometric Parallaxes**, once adjusted for statistical effects due to errors in parallax measurements, and for the effects of incompleteness in parallax catalogues, provide useful information on the frequency of stars of different absolute magnitudes.
iii. **Spectroscopic Parallaxes**, which are derived from spectroscopic surveys of Milky Way fields, form the basis for the establishment of absolute magnitudes for primarily distant, luminous stars. These data are most useful for establishing the $\phi(M,S)$ functions, but also provide supplementary information for the GLF.
iv. **Mean Absolute Magnitudes**, as defined by Luyten (see Bok's notes), are derived using the following relationships:

$$m - M = -5 \log \pi - 5, \quad v_T = \frac{4.74\mu}{\pi}.$$

$$\therefore \quad M = m + 5 + 5 \log \pi = m + 5 + 5 \log \frac{4.74\mu}{v_T}.$$

Define $T = \frac{v_T}{4.74}$ (i.e. the tangential velocity in A.U./annum).

Then, $H = m + 5 + 5 \log \mu = M + 5 \log T$.

Luyten found, using stars of measured trigonometric parallax, that the absolute magnitudes of stars were related to the parameter H in linear fashion,

i.e. $\langle M(H) \rangle = a + b H$, if $\langle T \rangle$ is roughly constant for the group.

Luyten assumed that this type of relationship could be extended to faint stars for which no radial velocity or trigonometric parallax data were available, namely for the stars with m > 15 for which he obtained proper motions using POSS and Bruce survey plates. In this manner, the GLF which was defined to $M_{pg} \approx +14$ in the Gröningen Publications was extended to $M_{pg} \approx +20$ by Luyten. The resulting GLF $\phi(M)$ appears to reach a maximum near $M_{pg} \approx +15.7$, although this is questioned by Wanner (MNRAS, 155, 463, 1972), who finds a peak in $\phi(M)$ at $M_{pg} \approx +12$.

Variations in the GLF

Population II stars are mainly old stars of relatively low metallicity, so their luminosity function should differ in a straightforward fashion from the GLF derived for stars in the disk of the Galaxy. In particular, $\phi(M)$ is steeper at the bright end due to the lack of high luminosity, massive stars, and exhibits a local maximum associated with the luminosity of giants and horizontal branch

stars. Studies of the Population II GLF have been made from investigations at the galactic poles, where stars of this type are preferentially encountered. Studies have also been made of $\phi(M)$ for other nearby galaxies, in particular for the Magellanic Clouds and M31. Differences are apparent which are population dependent.

Initial Luminosity Function (Salpeter Function)

The main-sequence lifetime of a star is proportional to the mass of the star and its luminosity,

i.e. $t_{ms} \sim \frac{M}{L}$, where M is its mass.

It is possible to use $\phi(M)$, the general luminosity function, to obtain $\phi_{ms}(M)$, the main-sequence luminosity function, by calculating the fraction of stars at each luminosity which lie on the main-sequence, or in the main-sequence band (which includes subgiant and giant stars lying just above the zero-age main-sequence). The function defined in this manner is the initial luminosity function, denoted $\psi(M)$. It should be clear that:

$\psi(M) = \phi_{ms}(M)$, for t_{ms} > the age of the Galaxy,

and $\psi(M) \sim \phi_{ms}(M)/t_{ms}$, for t_{ms} < the age of the Galaxy.

One can also investigate $\psi(M)$ using stars in open clusters, and also derive the **Initial Mass Function**, IMF, from a knowledge of the masses and luminosities of main-sequence stars.

i.e. $M_{ms} = f(M_{ms})$.

Salpeter Function $\xi(m) = c(m/M_\odot)^{-2.35}$ but exponents of -2 or -1 are common

-1.25 for low mass

-3.2 for high mass?

Problems:

i. Open clusters are subject to the preferential evaporation of low-mass stars through the energy exchange which occurs in stellar encounters. Thus, $\psi(M)$ for most clusters should be biased towards the brighter, more massive stars, and will underrepresent the low-mass stars.

ii. High-mass stars in open clusters seem to be very dispersed over the fields of some clusters, often lying in cluster coronal regions. This feature may result in their being undersampled in some cluster studies, which tend to concentrate on the denser cluster nuclear regions. This effect may also result in bias for $\psi(M)$.

iii. The IMF may differ from region to region in the Galaxy, since the creation of high-mass stars requires larger amounts of material than does the creation of low-mass stars. Whether or not there is any dependence of $\psi(M)$ on location in the Galaxy, or possibly on cluster initial mass, are questions which have never been thoroughly investigated.

iv. The initial conditions in clusters — things like high or low metallicity, high or low rotation rates, and high or low binary frequencies — may combine to influence the magnitude distribution of stars on cluster main-sequences, invariably in ways which will lead to spurious results for $\psi(M)$.

14. The Chemical Composition of the Galaxy

Halo

The study of peculiarities in the chemical composition of globular clusters as a function of location in the Galaxy seems to be an ongoing process without a final resolution. It is recognized that the metal-rich globulars are located close to the galactic centre, while the metal-poor globulars are more evenly distributed throughout the halo. Captured extragalactic globulars may even be included in the Milky Way sample. It is recognized that there may be subtle effects in spectroscopic studies of the metallicity of globular cluster stars arising from the fact that these studies invariably sample cluster red giants, for which the original surface composition has been altered by deep convective mixing of core heavy element-enriched material to the surface. The alternate use of CMD's for determining globular cluster metallicities invariably runs up against the problem of fitting model isochrons for differing cluster metallicity and age as two dependent parameters, neither of which may be uniquely determined. The overall metallicity and age of Population II stars in the halo clearly differ from those of old disk stars. Population II stars are typically metal-poor (lower by as much as a few orders of magnitude from the solar metallicity)

and old ($> 10^{10}$ years, with current estimates lying in the range $12–15 \times 10^9$ years) in comparison with the oldest known disk stars. There are some globular clusters, however, where the metallicities are more comparable to the solar values.

Bulge

The spectroscopic studies by Morgan (AJ, 64, 432, 1959) using the integrated spectra of stars in the galactic bulge region established that the dominant stars in the galactic bulge are K giants of solar or above-solar metallicity. It has also been noted that RR Lyrae variables are common in the bulge, but much less so than M giants and Mira variables, which are more typical of the red giant evolution of metal-rich stars. The observational CMD of the galactic bulge region appears to resemble that for the old open cluster NGC 188 rather than those of globulars. It is therefore inferred that bulge stars are both old and metal-rich.

Disk

There is considerable evidence available that there is an abundance gradient apparent in the disk, with proportionately more objects of high metallicity being found closer to the galactic centre than the solar circle. An increase in the overall metallicity of stars and gas towards the galactic centre is the expected result of increasing star densities towards the galactic centre, since the overall metallicity of the Galaxy is gradually increasing through the dispersion of nuclear-processed material from stellar cores and nuclear-generated R-process elements by supernovae. Nebular studies appear to show this result most clearly (Shaver et al., MNRAS, 204, 53, 1983), although not without some criticism. Evidence for such a gradient in the stellar component has also been found in open cluster studies, although there are many difficulties which exist in the interpretation of such data. Chemical composition studies of open clusters are really only in their infancy, and much work has yet to be done. However, detailed studies of nearby stars, using ultraviolet excesses to supplement curve-of-growth studies, do confirm the existence of a disk metallicity gradient.

15. The Solar Motion

The Fundamental Standard of Rest

The galactic centre defines the fundamental reference point for the Galaxy. Its distance is not known precisely, but its direction is very well established from both radio and optical (IR) studies. The velocities of objects in the solar neighbourhood are usually defined in terms of their components relative to the galactic plane and the direction of the galactic centre, in particular:

- Π is the velocity measured in a positive sense towards the galactic anticentre, i.e. towards (l, b) = (180°, 0°). In some sources this is designated as –U.
- Θ is the velocity which is measured in a positive sense in the direction of the sun's orbital motion about the galactic centre, i.e. towards (l, b) = (90°, 0°). In some sources this is designated as V.
- Z is the velocity which is measured in a positive sense towards the north galactic pole (NGP), i.e. towards (l, b) = (any, +90°). In some sources this is designated W.

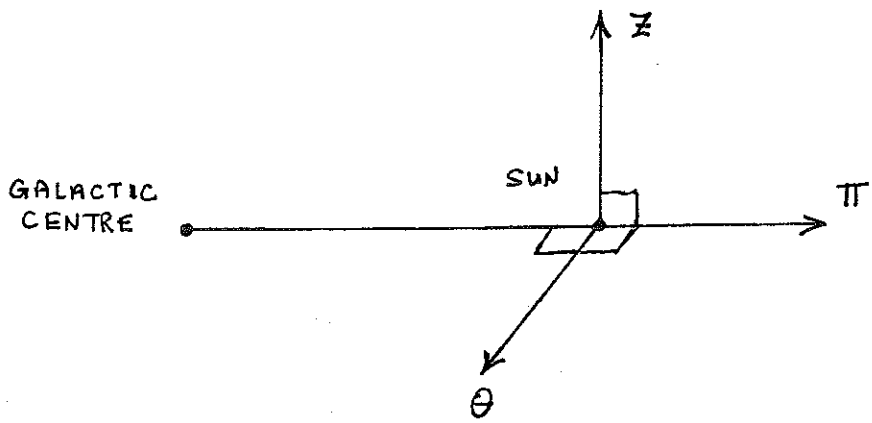

The Local Standard of Rest

In the gravitational field of the Galaxy, the stars near the sun orbit the galactic centre with velocities which are close to that of the local circular velocity Θ_c. In other words, a star at the sun's location in the Galaxy which describes a circular orbit about the galactic centre has velocity components:

$(\Pi, \Theta, Z) = (0, \Theta_c, 0)$ km/s.

A velocity system which is centred on such a fictitious object is used to define the **local standard of rest or LSR**. That is, the LSR is defined by an axial system aligned with the Π, Θ, and Z axes and with an origin which describes a circular orbit about the galactic centre with a velocity Θ_c.

i.e. $(\Pi, \Theta, Z)_{LSR} = (0, \Theta_c, 0)$ km/s.

Nearby stars have peculiar velocities relative to the LSR described by:

$u = \Pi - \Pi_{LSR} = \Pi$,
$v = \Theta - \Theta_{LSR} = \Theta - \Theta_c$,
$w = Z - Z_{LSR} = Z$.

The peculiar velocity of the sun is therefore given by:

$(u_\odot, v_\odot, w_\odot) = (\Pi_\odot, \Theta_\odot - \Theta_c, Z_\odot)$.

The velocity of any star with respect to the sun must have three components:
i. a peculiar velocity relative to the star's LSR (which differs from the sun's LSR),
ii. the peculiar velocity of the sun with respect to the sun's LSR, and
iii. the differential velocity of the LSR at the star with respect to the solar LSR due to differential galactic rotation (this is usually negligible). Under the assumption that component (iii) is indeed negligible (which is typically valid for $d \leq 100$ pc), the observed velocity of a star relative to the sun is given by the velocity vector (U_*, V_*, W_*), where:

$U_* = u_* - u_\odot = \Pi_* - \Pi_\odot$,
$V_* = v_* - v_\odot = \Theta_* - \Theta_\odot$,
$W_* = w_* - w_\odot = Z_* - Z_\odot$.

The Solar Motion

For any particular group of stars belonging to the disk and having nearly identical kinematical properties, one can define a **kinematic centroid** of their velocities by:

$$\langle u_* \rangle = \frac{1}{N} \sum_{i=1}^{N} u_{*i},$$

$$\langle v_* \rangle = \frac{1}{N} \sum_{i=1}^{N} v_{*i},$$

$$\langle w_* \rangle = \frac{1}{N} \sum_{i=1}^{N} w_{*i}.$$

For disk stars which are not drifting either perpendicular to the galactic plane or in the direction of the galactic centre, it is reasonable to expect that:

$\langle u_* \rangle \equiv 0$ and $\langle w_* \rangle \equiv 0$.

However, $\langle v_* \rangle \neq 0$, since a typical group of stars selected observationally will always tend to lag behind the solar LSR. The reason for this is fairly straightforward. A group of stars chosen spectroscopically will include objects of various origins, unless the group is so young that the stars have not had time to travel far from their places of formation. The increasing density gradient in the disk of the Galaxy towards the galactic centre implies that the majority of stars in the sun's neighbourhood originated at points which lie on average somewhat closer to the galactic centre than the sun, i.e. most of them are currently near apogalacticon. Since the **apogalacticon velocity** of stars in elliptical orbits is less than the local circular velocity Θ_c, any mix of elliptical orbits for nearby stars will find the majority travelling at less than Θ_c in the direction of the sun's orbital motion. It follows that locally-defined kinematic groups of stars should, in general, tend to lag behind the LSR motion. This **asymmetric drift** is well-observed in such groups, and must be taken into account in any determination of the sun's LSR velocity.

The lag of a kinematic group of stars relative to the solar LSR, namely its asymmetric drift, is defined by:

$\langle v_* \rangle = \langle \Theta_* \rangle - \Theta_c = -x$, where x is the lag velocity.

Thus, $u_\odot = \langle u_* \rangle - \langle U_* \rangle = -\langle U_* \rangle$,

$v_\odot = \langle v_* \rangle - \langle V_* \rangle = -x - \langle V_* \rangle$,

$w_\odot = \langle w_* \rangle - \langle W_* \rangle = -\langle W_* \rangle$.

Define $v'_\odot \equiv -\langle V_* \rangle$ for a particular kinematic group, i.e. $v'_\odot = v_\odot + x$. The sun's velocity with respect to such a group is therefore given by:

$$S_\odot \equiv (u_\odot^2 + v'^2_\odot + w_\odot^2)^{1/2} ,$$

with its direction of motion determined by the inverse of the motion of the centroid of the group.

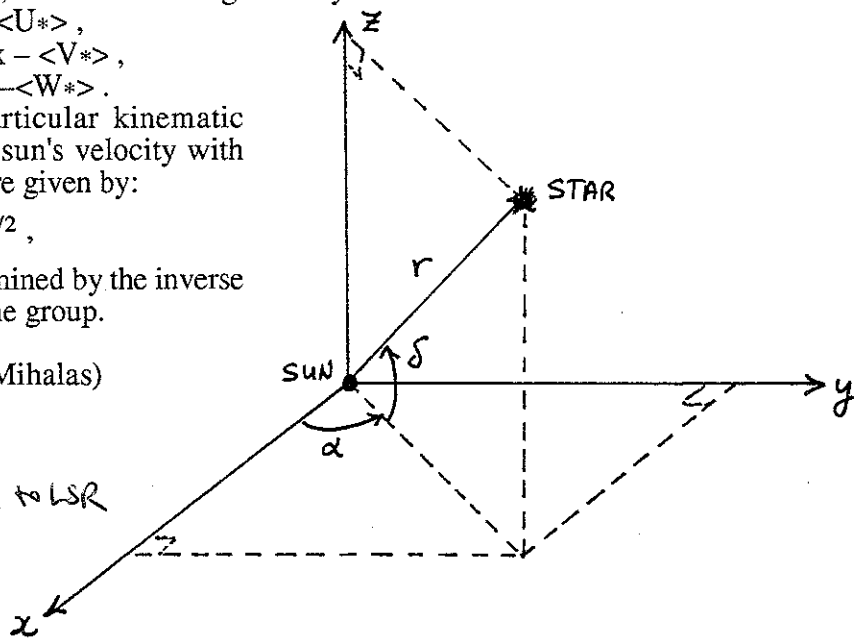

Mathematical Solutions (see Mihalas)

Define a system of coordinates identical to the equatorial system, i.e. relative to LSR

$$x = r \cos\delta \cos\alpha ,$$
$$y = r \cos\delta \sin\alpha ,$$
$$z = r \sin\delta .$$

The velocity components of a star with respect to the sun are $X_*-X_\odot$, $Y_*-Y_\odot$, and $Z_*-Z_\odot$, which can be derived from the temporal derivatives of these basic equations.

where x, y, z represent velocities relative to LSR

$$\text{i.e.} \quad X_*-X_\odot = \frac{dx}{dt} = \cos\delta\cos\alpha\frac{dr}{dt} - r\sin\delta\cos\alpha\frac{d\delta}{dt} - r\cos\delta\sin\alpha\frac{d\alpha}{dt} ,$$

$$Y_*-Y_\odot = \frac{dy}{dt} = \cos\delta\sin\alpha\frac{dr}{dt} - r\sin\delta\sin\alpha\frac{d\delta}{dt} + r\cos\delta\cos\alpha\frac{d\alpha}{dt} ,$$

$$Z_*-Z_\odot = \frac{dz}{dt} = \sin\delta\frac{dr}{dt} + r\cos\delta\frac{d\delta}{dt} .$$

Clearly, the terms in $\frac{dr}{dt}$ are equivalent to the radial velocities V_R, while the terms in $\frac{d\alpha}{dt}$ and $\frac{d\delta}{dt}$ are equivalent to the proper motions μ_α and μ_δ. The above equations can therefore be simplified and inverted by matrix algebra to the following form:

$$\begin{bmatrix} V_R \\ r\,\mu_\delta \\ r\,\mu_\alpha\cos\delta \end{bmatrix} = \begin{bmatrix} dx/dt \\ dy/dt \\ dz/dt \end{bmatrix} \begin{bmatrix} \cos\delta\cos\alpha & \cos\delta\sin\alpha & \sin\delta \\ -\sin\delta\cos\alpha & -\sin\delta\sin\alpha & \cos\delta \\ -\sin\alpha & \cos\alpha & 0 \end{bmatrix} .$$

Mihalas demonstrates how the equations can be rearranged to permit least squares solutions for $X_\odot$, $Y_\odot$, and $Z_\odot$ from radial velocities as well as similar solutions for $X_\odot/K$, $Y_\odot/K$, and $Z_\odot/K$ from proper motions. The solutions involve the fact that the velocity components X_*, Y_*, and Z_* for a group of stars must average to zero because they are measured relative to the LSR. Therefore, the components X_*, Y_*, and Z_* of dx/dt, dy/dt, and dz/dt in the above equations can be eliminated from the equations when averaged over a large enough group of stars which are randomly distributed across the celestial sphere. Likewise, any averages of terms which involve the components X_*, Y_*, and Z_* must be equated with zero. This greatly simplifies the resulting series of equations involving the various terms for the equatorial positions, radial velocities, proper motions, and distances of stars in a typical kinematic group. The resulting series of equations to obtain a least squares solution for the solar motion relative to a kinematic stellar group uses radial velocities and positions only, and is given by:

$$\begin{bmatrix} X_\odot \\ Y_\odot \\ Z_\odot \end{bmatrix} \begin{bmatrix} \sum_{i=1}^{N} \cos^2\delta_i \cos^2\alpha_i & \sum_{i=1}^{N} \cos^2\delta_i \cos\alpha_i \sin\alpha_i & \sum_{i=1}^{N} \cos\delta_i \sin\delta_i \cos\alpha_i \\ \sum_{i=1}^{N} \cos^2\delta_i \cos\alpha_i \sin\alpha_i & \sum_{i=1}^{N} \cos^2\delta_i \sin^2\alpha_i & \sum_{i=1}^{N} \sin\delta_i \cos\delta_i \sin\alpha_i \\ \sum_{i=1}^{N} \cos\delta_i \sin\delta_i \cos\alpha_i & \sum_{i=1}^{N} \cos\delta_i \sin\delta_i \sin\alpha_i & \sum_{i=1}^{N} \sin^2\delta_i \end{bmatrix}$$

$$= \begin{bmatrix} -\sum_{i=1}^{N} V_{R_i} \cos\delta_i \cos\alpha_i \\ -\sum_{i=1}^{N} V_{R_i} \cos\delta_i \sin\alpha_i \\ -\sum_{i=1}^{N} V_{R_i} \sin\delta_i \end{bmatrix}, \text{ which can be solved for } X_\odot, Y_\odot,, \text{ and } Z_\odot.$$

The equations involving the proper motions are somewhat more complicated, since they involve the unknown distances to the stars in the group. A solution in this case yields the values $X_\odot/K$, $Y_\odot/K$, and $Z_\odot/K$, which are also of considerable value (see Mihalas for details).

In the case of a radial velocity solution or a proper motion solution for the solar motion, the **apex of the solar motion** (direction of motion of the sun relative to the group) is given by:

$$\tan\alpha_{apex} = \frac{Y_\odot}{X_\odot} = \frac{Y_\odot/K}{X_\odot/K},$$

$$\tan\delta_{apex} = \frac{Z_\odot}{(X_\odot^2 + Y_\odot^2)^{1/2}} = \frac{Z_\odot/K}{[(X_\odot/K)^2 + (Y_\odot/K)^2]^{1/2}},$$

and the velocity of the solar motion is given by:

$$S_\odot = (X_\odot^2 + Y_\odot^2 + Z_\odot^2)^{1/2} = K \times [(X_\odot/K)^2 + (Y_\odot/K)^2 + (Z_\odot/K)^2]^{1/2}.$$

Note that the velocity of the sun relative to a group cannot be determined using only proper motion data unless the distances to the stars in the group are also known so that K is specified.

All results for the solar motion which make use of least squares solutions for these equations are **kinematic estimates** for the solar motion. The problem of deriving the **dynamical motion** of the sun relative to the LSR makes use of such kinematic results in conjunction with mathematical expectations for the rotation of the galactic disk.

From strictly qualitative arguments it is expected that the asymmetric drift for any group of stars must depend directly upon the nature of the orbits for the stars in the group. For **stars in nearly circular orbits no asymmetric drift is expected**, while for stars having a mix of very eccentric orbits the asymmetric drift should be fairly significant. A group of stars having the latter properties will also exhibit a fairly large dispersion in the component of their orbital motions directed along the line-of-sight to the galactic centre, the Π velocities, whereas stars in strictly circular orbits have no such component of their orbital motion. This **correlation of asymmetric drift with the dispersion in Π velocities,** σ_Π^2, for various kinematic groups is also predicted from quantitative arguments, and proves to be a valuable tool for determining the exact parameters for the sun's LSR velocity.

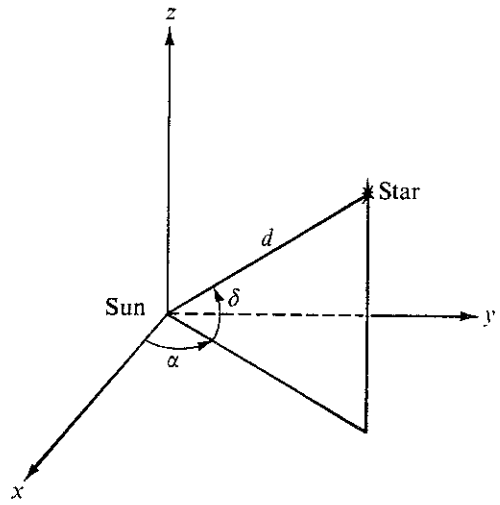

FIG. 5-5. Equatorial rectangular coordinate system.

$$\begin{aligned} x &= d \cos \delta \cos \alpha \\ y &= d \cos \delta \sin \alpha \\ z &= d \sin \delta \end{aligned} \tag{5-2}$$

Differentiating equations (5-2) gives the components of the velocity of the star relative to the sun:

$$\begin{aligned} \dot{x} &= X_* - X_\odot = \dot{d} \cos \delta \cos \alpha - \dot{\delta} d \sin \delta \cos \alpha - \dot{\alpha} d \cos \delta \sin \alpha \\ \dot{y} &= Y_* - Y_\odot = \dot{d} \cos \delta \sin \alpha - \dot{\delta} d \sin \delta \sin \alpha + \dot{\alpha} d \cos \delta \cos \alpha \\ \dot{z} &= Z_* - Z_\odot = \dot{d} \sin \delta + \dot{\delta} d \cos \delta \end{aligned} \tag{5-3}$$

where X_*, Y_*, and Z_* and $X_\odot$, $Y_\odot$, and $Z_\odot$ are the velocity components of the star and the sun, respectively, relative to the LSR. The quantity $\dot{d}$ stands for the radial velocity in kilometers per second, and $\dot{\delta} d$ and $\dot{\alpha} d \cos \alpha$ are transverse velocities in kilometers per second, if $\dot{\alpha}$ and $\dot{\delta}$ are expressed in radians per second and d is expressed in kilometers.

Equations (5-3) can easily be solved for $\dot{d}$, $\dot{\alpha}$, and $\dot{\delta}$ by direct inversion of the matrix of coefficients, which is orthogonal, so that the inverse of the matrix equals its transpose. We thus find

$$\dot{x} \cos \delta \cos \alpha + \dot{y} \cos \delta \sin \alpha + \dot{z} \sin \delta = \dot{d} \tag{5-4a}$$

$$-\dot{x} \sin \delta \cos \alpha - \dot{y} \sin \delta \sin \alpha + \dot{z} \cos \delta = d\dot{\delta} \tag{5-4b}$$

$$-\dot{x} \sin \alpha + \dot{y} \cos \alpha = d\dot{\alpha} \cos \alpha \tag{5-4c}$$

SOLAR MOTION FROM RADIAL-VELOCITY DATA

We shall now see how equation (5-4*a*) can be used to derive the solar motion from radial-velocity data alone. The velocity components X_*, Y_*, and Z_* of the stars must average to zero, since they are referred to the LSR. Thus, when averages are taken in equation (5-4*a*) over a large number of

stars, the terms in X_*, Y_*, and Z_* on the left-hand side drop out, leaving only the terms in $X_\odot$, $Y_\odot$, and $Z_\odot$. Suppose we observe N stars and have N equations of the form (5-4*a*). We can then use these equations to determine $X_\odot$, $Y_\odot$, and $Z_\odot$ by the method of *least squares*. This method requires that we multiply each equation by the coefficient of $\dot{x}$ and then sum over all N. In this way we obtain

$$\sum_{i=1}^{N} \dot{x}_i \cos^2\delta_i \cos^2\alpha_i + \sum_{i=1}^{N} \dot{y}_i \cos^2\delta_i \cos\alpha_i \sin\alpha_i + \sum_{i=1}^{N} \dot{z}_i \cos\delta_i \sin\delta_i \cos\alpha_i = \sum_{i=1}^{N} \dot{d}_i \cos\delta_i \cos\alpha_i$$

Now consider the term

$$\sum_{i=1}^{N} \dot{x}_i \cos^2\delta_i \cos^2\alpha_i = \sum_{i=1}^{N} X_{*i} \cos^2\delta_i \cos^2\alpha_i - X_\odot \sum_{i=1}^{N} \cos^2\delta_i \cos^2\alpha_i$$

By hypothesis, all averages over X_* are zero; hence the first sum on the right-hand side of the equation directly above is zero, and we have

$$\sum_{i=1}^{N} \dot{x}_i \cos^2\delta_i \cos^2\alpha_i = -X_\odot \sum_{i=1}^{N} \cos^2\delta_i \cos^2\alpha_i \tag{5-2}$$

In a similar manner we can show that

$$\sum_{i=1}^{N} \dot{y}_i \cos^2\delta_i \cos\alpha_i \sin\alpha_i = -Y_\odot \sum_{i=1}^{N} \cos^2\delta_i \cos\alpha_i \sin\alpha_i$$

and

$$\sum_{i=1}^{N} \dot{z}_i \cos\delta_i \sin\delta_i \cos\alpha_i = -Z_\odot \sum_{i=1}^{N} \cos\delta_i \sin\delta_i \cos\alpha_i \tag{5-3}$$

Therefore the net effect of multiplying equation (5-4*a*) by the coefficient of $\dot{x}$ and summing over all N stars is

$$X_\odot \sum_{i=1}^{N} \cos^2\delta_i \cos^2\alpha_i + Y_\odot \sum_{i=1}^{N} \cos^2\delta_i \cos\alpha_i \sin\alpha_i + Z_\odot \sum_{i=1}^{N} \cos\delta_i \sin\delta_i \cos\alpha_i = -\sum_{i=1}^{N} \dot{d}_i \cos\delta_i \cos\alpha_i \tag{5-5}$$

We can now repeat this entire procedure using the coefficients of $\dot{y}$ and $\dot{z}$ in equation (5-4*a*) to obtain

$$X_\odot \sum_{i=1}^{N} \cos^2\delta_i \cos\alpha_i \sin\alpha_i + Y_\odot \sum_{i=1}^{N} \cos^2\delta_i \sin^2\alpha_i + Z_\odot \sum_{i=1}^{N} \sin\delta_i \cos\delta_i \sin\alpha_i = -\sum_{i=1}^{N} \dot{d}_i \cos\delta_i \sin\alpha_i \tag{5-6}$$

$$X_\odot \sum_{i=1}^{N} \cos\delta_i \sin\delta_i \cos\alpha_i + Y_\odot \sum_{i=1}^{N} \cos\delta_i \sin\delta_i \sin\alpha_i + Z_\odot \sum_{i=1}^{N} \sin^2\delta_i = -\sum_{i=1}^{N} \dot{d}_i \sin\delta_i \tag{5-7}$$

We end up with three linear equations, which may be solved directly for $X_\odot$, $Y_\odot$, and $Z_\odot$, since $\dot{d}_i$, α_i, and δ_i are presumed known for each star. This kind of an analysis can be carried out for different spectral classes, and the detailed results are given in Table 5-3; typically, we find $v_\odot \approx 20$ km/sec in the direction $\alpha \approx 18^h$ and $\delta \approx 30°$.

SOLAR MOTION FROM PROPER MOTIONS ALONE

Consider now equations (5-4*b*) and (5-4*c*). Let us first convert d, $\dot{\alpha}$, and $\dot{\delta}$ to the usual observational units: d, normally measured in parsecs, equals $1/\pi''$, where π'' is the parallax in seconds of arc. Thus $d = (1/\pi'') \times 206{,}265 \times 1.497 \times 10^8$ km. The proper motions μ_δ and $\mu_\alpha \cos\delta$ are normally expressed in seconds of arc per year. Thus, for example, $\dot{\delta}$ in radians per second is $\mu_\delta''/(206{,}265 \times 3.156 \times 10^7)$, so that $\dot{\delta}d = 4.74\mu_\delta''/\pi''$. A similar expression holds for $\dot{\alpha}$, namely, $\dot{\alpha}d = 4.74\mu_\alpha'' \cos\delta/\pi''$. Therefore, after substituting in equations (5-4*b*) and (5-4*c*), we have

$$-\dot{x}\sin\delta\cos\alpha - \dot{y}\sin\delta\sin\alpha + \dot{z}\cos\delta = \frac{4.74\mu_\delta''}{\pi''} \tag{5-8}$$

$$-\dot{x}\sin\alpha + \dot{y}\cos\delta = \frac{4.74\mu_\alpha''\cos\delta}{\pi''} \tag{5-9}$$

Let us now proceed to find the solar motion. Consider a small area of sky, so that all stars in the area have essentially the same α and the same δ. Again we argue that all averages over terms in X_*, Y_*, and Z_* will be zero, since the motions of the stars are assumed random relative to the LSR. Therefore, averaging over the stars in the chosen region we obtain

$$X_\odot\sin\delta\cos\alpha + Y_\odot\sin\delta\sin\alpha - Z_\odot\cos\delta = \frac{4.74}{N}\sum_{i=1}^{N}\frac{\mu_{\delta_i}''}{\pi_i''}$$

$$X_\odot\sin\alpha - Y_\odot\cos\alpha = \frac{4.74}{N}\sum_{i=1}^{N}\frac{\cos\delta\mu_{\alpha_i}''}{\pi_i''}$$

The parallaxes π_i'' of the individual stars are in general unknown. If we assume the stars to lie at some mean distance d_0, however, we can replace π_i'' by π_0'', the parallax corresponding to d_0. In practice, to assure the validity of this assumption, we would initially choose stars of a given spectral type which lie within a narrow apparent-magnitude range. Now, writing $\bar{\mu}_\alpha = \sum \mu_\alpha/N$ and $\bar{\mu}_\delta = \sum \mu_\delta/N$, we have

$$X_\odot\sin\delta\cos\alpha + Y_\odot\sin\delta\sin\alpha - Z_\odot\cos\delta = \frac{4.74\bar{\mu}_\delta}{\pi_0} \equiv K\bar{\mu}_\delta$$

$$X_\odot\sin\alpha - Y_\odot\cos\alpha = \frac{4.74\bar{\mu}_\alpha\cos\delta}{\pi_0} \equiv K\bar{\mu}_\alpha\cos\delta$$

If there are R regions, we have R sets of such equations, which we again can

solve by the
We thus obt

$$X_\odot \sum_{i=1}^{R}$$

$$X_\odot \sum_{i=1}^{R}$$

$$X_\odot \sum_{i=1}^{R}$$

$$X_\odot \sum_{i=1}^{R}$$

$$X_\odot \sum_{i=1}^{R}$$

Finally, if v
the proper-r
of the form

$$a_1X_\odot +$$
$$a_2X_\odot +$$
$$a_3X_\odot +$$

which we m

$$\tan\alpha_\odot$$

and

$$\tan\delta_\odot$$

giving the d
of the solar

SOLAR

If we k
their obser

solve by the least-squares method by taking moments as described previously. We thus obtain

$$X_\odot \sum_{i=1}^{R} \sin^2 \delta_i \cos^2 \alpha_i + Y_\odot \sum_{i=1}^{R} \sin^2 \delta_i \sin \alpha_i \cos \alpha_i - Z_\odot \sum_{i=1}^{R} \sin \delta_i \cos \delta_i \cos \alpha_i = K \sum_{i=1}^{R} \bar{\mu}_{\delta_i} \sin \delta_i \cos \alpha_i \quad (5\text{-}10)$$

$$X_\odot \sum_{i=1}^{R} \sin^2 \delta_i \sin \alpha_i \cos \alpha_i + Y_\odot \sum_{i=1}^{R} \sin^2 \delta_i \sin^2 \alpha_i - Z_\odot \sum_{i=1}^{R} \sin \delta_i \cos \delta_i \sin \alpha_i = K \sum_{i=1}^{R} \bar{\mu}_{\delta_i} \sin \delta_i \sin \alpha_i \quad (5\text{-}11)$$

$$X_\odot \sum_{i=1}^{R} \sin \delta_i \cos \delta_i \cos \alpha_i + Y_\odot \sum_{i=1}^{R} \sin \delta_i \cos \delta_i \sin \alpha_i - Z_\odot \sum_{i=1}^{R} \cos^2 \delta_i = K \sum_{i=1}^{R} \bar{\mu}_{\delta_i} \cos \delta_i \quad (5\text{-}12)$$

$$X_\odot \sum_{i=1}^{R} \sin^2 \alpha_i - Y_\odot \sum_{i=1}^{R} \sin \alpha_i \cos \alpha_i = K \sum_{i=1}^{R} \bar{\mu}_{\alpha_i} \sin \alpha_i \cos \delta_i \quad (5\text{-}13)$$

$$X_\odot \sum_{i=1}^{R} \sin \alpha_i \cos \alpha_i - Y_\odot \sum_{i=1}^{R} \cos^2 \alpha_i = K \sum_{i=1}^{R} \bar{\mu}_{\alpha_i} \cos \alpha_i \cos \delta_i \quad (5\text{-}14)$$

Finally, if we add equations (5-10) to (5-13) and (5-11) to (5-14) to utilize the proper-motion information as fully as possible, we obtain three equations of the form

$$\begin{aligned} a_1 X_\odot + b_1 Y_\odot + c_1 Z_\odot &= K g_1 \\ a_2 X_\odot + b_2 Y_\odot + c_2 Z_\odot &= K g_2 \\ a_3 X_\odot + b_3 Y_\odot + c_3 Z_\odot &= K g_3 \end{aligned} \quad (5\text{-}15)$$

which we may solve for $X_\odot/K$, $Y_\odot/K$, and $Z_\odot/K$. Then, clearly,

$$\tan \alpha_\odot = \left(\frac{X_\odot}{K}\right) \Big/ \left(\frac{Y_\odot}{K}\right)$$

and

$$\tan \delta_\odot = \frac{\left(\frac{Z_\odot}{K}\right)}{\left[\left(\frac{X_\odot}{K}\right)^2 + \left(\frac{Y_\odot}{K}\right)^2\right]^{1/2}} \quad (5\text{-}16)$$

giving the direction of the solar motion. Note that we get only the direction of the solar motion, but not its magnitude.

SOLAR MOTION FROM SPACE MOTIONS

If we know the distances to the stars under consideration, we can convert their observed proper motions to transverse velocities, which, coupled with

their radial velocities, yield the complete space motions of the stars with respect to the sun. We may resolve each derived space velocity along the axes of the standard coordinate system defined in Figure 5-1. We thus obtain

$$\Pi_{obs} = \Pi_* - \Pi_\odot$$
$$Z_{obs} = Z_* - Z_\odot$$
$$\vartheta_{obs} = \Theta_* - \Theta_\odot$$

It should be emphasized at this stage that the direct observations give us no information on Π_*, Z_*, Θ_*, $\Pi_\odot$, $Z_\odot$, or $\Theta_\odot$ themselves, but only on their differences. Moreover, we should recall that Θ_* and $\Theta_\odot$ contain dominant terms due to the overall rotation of the Galaxy. Reserving Θ as a general symbol for any tangential velocity about the Galactic center, we shall use ϑ to denote differences in Θ. Thus it follows that ϑ_{obs} is independent of Galactic rotation.

If we now average over a large number of stars, we obtain

$$\begin{aligned} \langle \Pi_{obs} \rangle &= \langle \Pi_* \rangle - \Pi_\odot \\ \langle Z_{obs} \rangle &= \langle Z_* \rangle - Z_\odot \\ \langle \vartheta_{obs} \rangle &= \langle \Theta_* \rangle - \Theta_\odot \end{aligned} \tag{5-17}$$

It is reasonable to suppose that both $\langle \Pi_* \rangle$ and $\langle Z_* \rangle$ are zero. This simply asserts that we expect no net radial expansion or contraction of the Galaxy near the sun, nor do we expect any systematic drift of stars away from the Galactic plane. Therefore, from equation (5-17), we have directly

$$\Pi_\odot = -\langle \Pi_{obs} \rangle$$
$$Z_\odot = -\langle Z_{obs} \rangle$$

The situation with respect to the Θ components is considerably more complicated and requires further clarification. Let us write $\Theta_* = \Theta_0 + \vartheta_*$ and $\Theta_\odot = \Theta_0 + \vartheta_\odot$, where Θ_0 represents the rotation velocity of the LSR around the Galactic center. If we insert these terms into equation (5-17), we have

$$\langle \vartheta_{obs} \rangle = \langle \vartheta_* \rangle - \vartheta_\odot$$

If we now use the *kinematical* definition of the LSR, the stars have no net motions relative to it, so that $\langle \vartheta_* \rangle = 0$ and we can write

$$\vartheta_\odot = -\langle \vartheta_{obs} \rangle \equiv \vartheta_0 \tag{5-18}$$

This value of $\vartheta_\odot$ depends solely upon observations and is unambiguously determined. However, as mentioned before, in dynamical studies it is convenient to define the LSR as moving on a circular orbit around the Galactic center. With this *dynamical* definition of the LSR there is no longer a guarantee that $\langle \vartheta_* \rangle = 0$; it will be zero if and only if all stars in the group are moving precisely on circular orbits. In fact this is not true, and the dynamical treatment given in Chapter 12 will show that, on the average, stars tend to lag slightly behind the circular velocity, and $\langle \vartheta_* \rangle$ is really a small negative

quantity. If
write

$$\vartheta_\odot = \langle \vartheta$$

The reasons
and (5-19) sl
actual value

5-5. Sum

A large num
a wide variet

TABLE 5·

Stellar type
Supergiants
O–B5
F–M
Giants
A
F
G
K0
K3
M
Main sequence
B0
A0
A5
F5
G0
G5
K0
K5
M0
M5

Source:
Structure, Chic

gives both t
velocity com
in Chapter 7

quantity. If we wish to use the dynamical definition of the LSR, we must write

$$\vartheta_\odot = \langle \vartheta_* \rangle - \langle \vartheta_{\text{obs}} \rangle \equiv \vartheta_1 \tag{5-19}$$

The reasons for introducing the special symbols ϑ_0 and ϑ_1 in equations (5-18) and (5-19) should now be obvious. We shall discuss in Section 5-6 how the actual value of $\langle \vartheta_* \rangle$ is determined.

5-5. Summary of Results

A large number of determinations of the solar motion have been made using a wide variety of stellar types. The results are summarized in Table 5-3, which

TABLE 5-3. Solar Motion and Velocity Dispersions

Stellar type	*Solar motion (km/sec)*			*Velocity dispersions (km/sec)*			
	$\Pi_\odot$	ϑ_0	$Z_\odot$	$\langle \Pi^2 \rangle^{1/2}$	$\langle \vartheta^2 \rangle^{1/2}$	$\langle Z^2 \rangle^{1/2}$	$\langle \vartheta^2 \rangle^{1/2} / \langle \Pi^2 \rangle^{1/2}$
Supergiants							
O–B5	−9.0	13.4	3.7	12	11	9	0.92
F–M	−7.9	11.7	6.5	13	9	7	0.69
Giants							
A	−13.4	11.6	10.3	22	13	9	0.59
F	−19.7	18.5	9.5	28	15	9	0.54
G	− 7.2	11.1	6.9	26	18	15	0.69
K0	−10.6	18.6	6.5	31	21	16	0.68
K3	− 9.0	17.6	6.4	31	21	17	0.68
M	− 4.5	18.3	6.2	31	23	16	0.74
Main sequence							
B0	− 9.6	14.5	6.7	10	9	6	0.90
A0	− 7.3	13.7	7.2	15	9	9	0.60
A5	− 8.5	7.8	7.4	20	9	9	0.45
F5	−10.1	12.3	6.2	27	17	17	0.63
G0	−14.5	21.1	6.4	26	18	20	0.69
G5	− 8.1	22.1	4.3	32	17	15	0.53
K0	−10.8	14.9	7.4	28	16	11	0.57
K5	− 9.5	22.4	5.8	35	20	16	0.57
M0	− 6.1	14.6	6.9	32	21	19	0.65
M5	− 9.8	19.3	8.6	31	23	16	0.74

Source: Adapted from J. Delhaye, in A. Blaauw and M. Schmidt (eds.), *Galactic Structure*, Chicago: University of Chicago Press, 1965, p. 71, by permission.

gives both the solar motions and the dispersions of the stars' individual velocity components (the significance of these dispersions will be explained in Chapter 7). The plots in Figure 5-6 show the observed velocity components

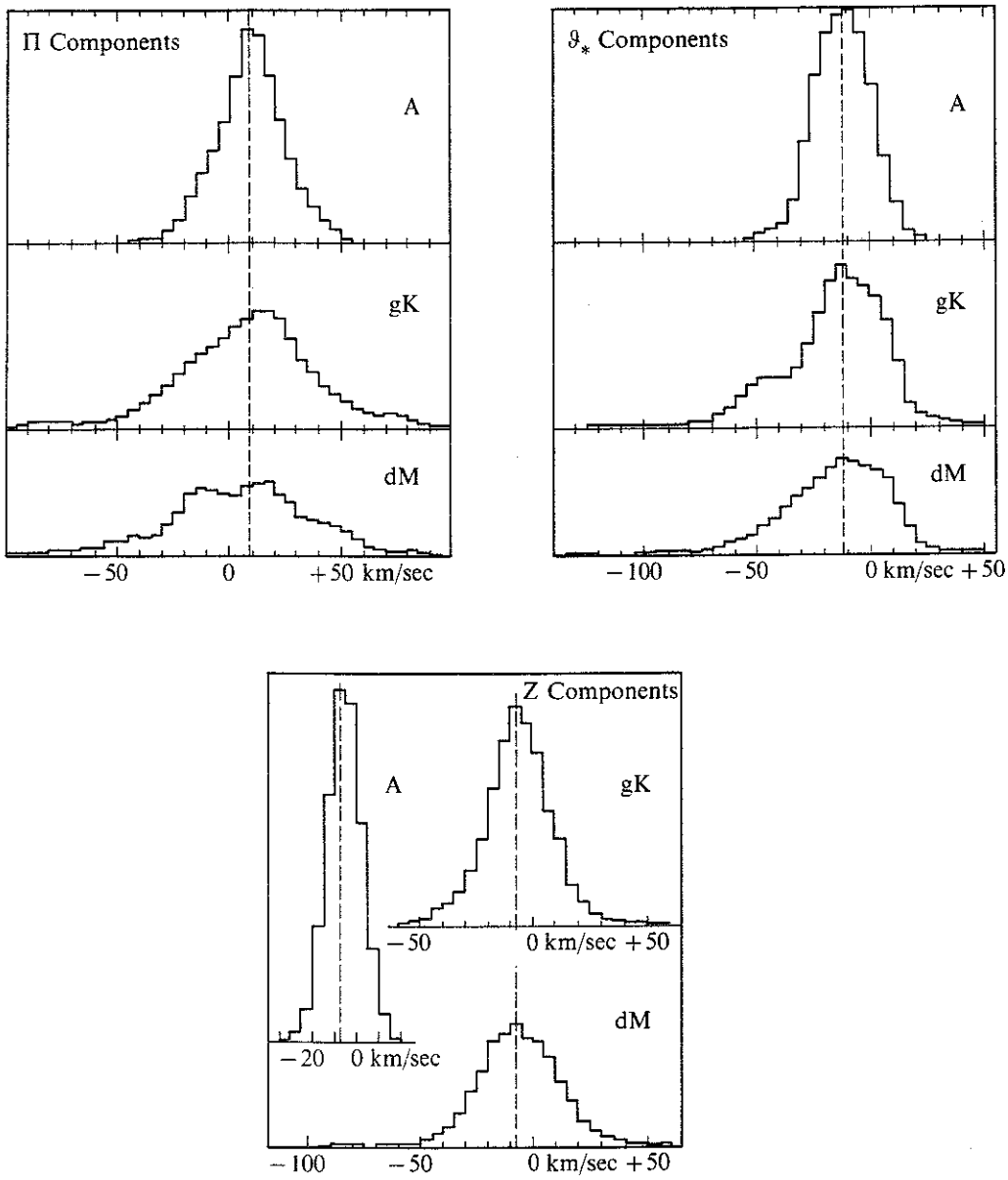

FIG. 5-6. Observed distribution of Π, ϑ_*, and Z components for A, gK, and dM stars. The dotted vertical lines show $\Pi_\odot$, ϑ_0, and $Z_\odot$. Note in the distribution of ϑ_* components the excess of stars with large negative velocities. [From J. Delhaye, in A. Blaauw and M. Schmidt (eds.), *Galactic Structure*, Chicago: University of Chicago Press, 1965, chap. 4, by permission.]

for A, gK, and dM stars, and their adopted mean values, which are the negatives of $\Pi_\odot$, $Z_\odot$, and ϑ_0.

The means of all spectral types in Table 5-3 yields

$$\Pi_\odot = -9.2 \pm 0.3 \text{ km/sec}$$
$$Z_\odot = +6.9 \pm 0.2 \text{ km/sec} \qquad (5\text{-}20)$$

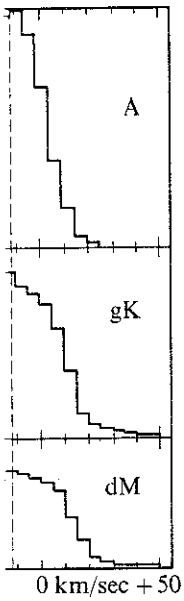

A mean for ϑ_0 is not physically significant over so large a range in spectral types, as will be discussed in Section 5-6.

STANDARD SOLAR MOTION

The standard solar motion is defined to be the solar motion relative to the majority of stars in general catalogs of radial velocity and proper motion (types A through G, including dwarfs, giants, and supergiants). We find

$$\begin{aligned} \Pi_{\text{std}} &= -10.4 \text{ km/sec} \\ \vartheta_{\text{std}} &= 14.8 \text{ km/sec} \\ Z_{\text{std}} &= 7.3 \text{ km/sec} \end{aligned} \tag{5-21}$$

These values lead to $v_\odot = 19.5$ km/sec in the direction $l^{\Pi}_{\text{std}} = 56°$, $b^{\Pi}_{\text{std}} = 23°$.

BASIC SOLAR MOTION

The basic solar motion is defined by the velocities occurring most frequently among the stars in the solar neighborhood. It is in good agreement with the solar motion derived from A, gK, and dM stars. These three groups give almost the same results, namely,

	Π_{basic}	ϑ_{basic}	Z_{basic}
A	−9.4	+ 9.9	+5.6
gK	−9.3	+10.7	+6.7
dM	−8	+10	+6

Thus we adopt

$$\begin{aligned} \Pi_{\text{basic}} &= -9 \text{ km/sec} \\ \vartheta_{\text{basic}} &= 11 \text{ km/sec} \\ Z_{\text{basic}} &= 6 \text{ km/sec} \end{aligned} \tag{5-22}$$

which corresponds to $v_\odot = 15.4$ km/sec in the direction $l^{\Pi}_{\text{basic}} = 51°$ and $b^{\Pi}_{\text{basic}} = 23°$.

5-6. Determination of the Drift between the Kinematical and Dynamical LSR

As mentioned previously, while we can determine $\Pi_\odot$, $Z_\odot$, and ϑ_0, we cannot find ϑ_1 directly. The difference between ϑ_0 and ϑ_1 arises because the stars we observe may have a systematic drift relative to the dynamical LSR. Dynamical theory allows us to untangle the effects of this drift. We shall see later, in Chapter 12, that

$$\langle \Theta \rangle - \Theta_0 = \vartheta_1 - \vartheta_0 = \frac{\langle \Pi^2 \rangle}{2(A - B)} \left[\frac{\partial \ln \nu}{\partial r} + \frac{1}{R_0} \left(1 - \frac{\langle \vartheta^2 \rangle}{\langle \Pi^2 \rangle} \right) \right] \tag{5-23}$$

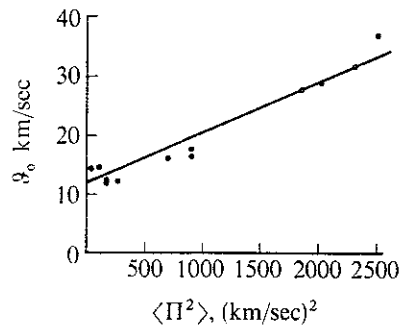

FIG. 5-7. Correlation of ϑ_0 with $\langle \Pi^2 \rangle$. We see that the observed value of ϑ_0 is a linear function of $\langle \Pi^2 \rangle$ as predicted by equation (5-23). Extrapolating to $\langle \Pi^2 \rangle = 0$, we estimate $\vartheta_1 = 12$ km/sec. [From J. Delhaye, in A. Blaauw and M. Schmidt (eds.), *Galactic Structure*, Chicago: University of Chicago Press, 1965, by permission.]

so that ϑ_0 has essentially the form, $\vartheta_0 = \vartheta_1 + C\langle \Pi^2 \rangle$, where $\langle \Pi^2 \rangle$ represents the velocity dispersion in the Π direction for stars of different spectral classes. Thus, if we were to plot ϑ_0 against $\langle \Pi^2 \rangle$, we should find a linear relation, with the intercept on the $\langle \Pi^2 \rangle = 0$ axis equal to ϑ_1. When such a plot is carried through, say with the data of Table 5-3, we obtain a diagram such as that shown in Figure 5-7. A linear fit to the points gives $\vartheta_1 = 12$ km/sec. Thus, with the adopted means in the Π and Z directions given in equation (5-20), we have

$$\Pi_\odot = -9.2 \text{ km/sec} \qquad \vartheta_1 = 12 \text{ km/sec} \qquad Z_\odot = 6.9 \text{ km/sec}$$

It must be emphasized that these velocity components represent the magnitude and direction of the solar motion relative to the dynamical LSR, in contrast to the kinematical LSR. The values agree with the basic solar motion to within the observational accuracies. (For further details see Ref. 3, chap. 4.)

5-7. Motion of the LSR around the Center of the Galaxy

We would very much like to estimate Θ_0, the tangential velocity of the LSR due to Galactic rotation. The difference between the kinematical and dynamical LSR's is negligible compared to the observational errors involved in the determination of this rotational velocity, and we shall not distinguish here between the two definitions. Basically, we must determine the velocity of the sun relative to some inertial frame in the Galaxy. Two attempts have thus far been made to define such an inertial frame.

GLOBULAR CLUSTERS

If we assume that the system of globular clusters does not rotate, on the average, relative to an inertial frame in the Galaxy, then by measuring the

radial velocities of the individual clusters (corrected for the solar motion), we may determine Θ_0. Such radial velocities were obtained by N. U. Mayall (*Astrophys., J.*, **104,** 291, 1946) for fifty globular clusters with the following result:

$$\Theta_0 = 200 \pm 25 \text{ km/sec}$$

in the direction ($l^{II} = 87°$, $b^{II} = 0°$). Additional data were later obtained By T. D. Kinman (*M.N.*, **119,** 559, 1959) who, from a discussion of velocities for seventy clusters, obtained

$$\Theta_0 = 167 \pm 30 \text{ km/sec}$$

in the direction perpendicular to the direction to the Galactic center.

LOCAL GROUP OF GALAXIES

If the galaxies in the Local Group (see Ref. 1, chap. 31) move at random relative to our own Galaxy, then they also can be used to define an inertial frame. Again, if we observe the radial velocities of these galaxies, we can derive the velocity of the LSR due to galactic rotation. In this way Mayall found

$$\Theta_0 = 300 \pm 25 \text{ km/sec}$$

in the direction ($l^{II} = 87°$, $b^{II} = 0°$). A more recent study by M. L. Humason and H. D. Wahlquist (*Astron. J.*, **60,** 254, 1955) yielded

$$\Theta_0 = 292 \pm 32 \text{ km/sec}$$

in the direction approximately ($l^{II} = 106°$, $b^{II} = -6°$).

Thus we infer that the rotation velocity of the LSR is about 250 km/sec in the direction ($l^{II} = 90°$, $b^{II} = 0°$); that is, the local standard of rest appears to be executing a pure motion of revolution around the Galactic center in the Galactic plane. This result is in agreement with our previous qualitative arguments that an overall rotation of the Galaxy might be expected. We shall discuss the detailed properties of Galactic rotation in Chapter 8. The velocity estimates given above should be regarded as only qualitative indicators of Θ_0, since there may actually be systematic motions present in both globular clusters and the Local Group. In the first case, for example, there is no *a priori* reason why the globular-cluster system must be at rest relative to the Galaxy and might not possess some net rotation about the Galactic center. Indeed, if we adopt the figure $\Theta_0 = 250$ km/sec, then Kinman's measures imply that the globular-cluster system has, in fact, a rotation of about 80 km/sec with respect to the Galactic center. Alternatively, our own Galaxy may have a characteristic motion relative to other Local Group members, which could also affect the derived value of Θ_0.

Standard Solar Motion

The solar motion relative to stars forming the majority of objects in general catalogues of radial velocity and proper motion is referred to as the **standard solar motion**. It is based upon the derived space velocities of A to G-type dwarfs, giants, and supergiants, which yield:

$u_{std} = -10.4$ km/s , [Gomez et al. (1990) find -10.9 ± 0.5 km/s]

$v'_{std} = +14.8$ km/s , [$= v_{LSR} + x$]

$w_{std} = +7.3$ km/s , [Gomez et al. (1990) find $+7.1 \pm 0.3$ km/s]

corresponding to S = 19.5 km/s towards $l_{std} = 56°$, $b_{std} = +23°$. It not identical to the sun's motion relative to the LSR, but is neverthelesss an interesting parameter. Many radio astronomers have erroneously adopted it as the LSR motion of the sun, and many studies of galactic structure have subsequently been based upon this value. The inhomogeneity of the stars defining this motion for the sun is evident in their large velocity dispersions. They do not represent a sample of stars which is in circular motion about the galactic centre.

Basic Solar Motion

A more representative value for the sun's motion relative to nearby stars is defined by the most frequently occurring velocities among stars in the solar neighbourhood. The appropriate values are those found for A stars, K giants, and M dwarfs, namely:

Type	$u_\odot$	$v_\odot$	$w_\odot$
A stars	–9.4 ±0.5 km/s	+9.9 km/s	+5.6 ±0.2 km/s
K giants	–9.3 ±0.9 km/s	+10.7 km/s	+6.7 ±0.5 km/s
M dwarfs	...	+12.6 km/s	...
M dwarfs	–8 ±2 km/s	+10 km/s	+6 ±2 km/s

The resulting basic solar motion is given by the components:

$u_{bsc} = -9$ km/s ,

$v'_{bsc} = +11$ km/s ,

$w_{bsc} = +6$ km/s ,

corresponding to S = 15.4 km/s towards $l_{bsc} = 51°$, $b_{bsc} = +23°$. This value is closer to the solar motion relative to the dynamical LSR, but is not identical to it.

Solar Motion Relative to the Dynamical LSR

As pointed out previously, the asymmetric drift of local groups of stars relative to the LSR results in values for v'_Θ which are larger than v_Θ. Dynamical theory can be used to relate the drift of a group with respect to the local circular velocity to the local galactic rotation constants A and B, the distance R_o to the galactic centre, the local density gradient of stars $\rho(R_o)$, and the measured dispersions σ_Π, σ_Θ , and σ_Z in the Π, Θ, and Z velocities. As derived in Mahalas:

$$-x = \langle v_* \rangle = \langle \Theta_* \rangle - \Theta_c = \frac{\sigma_\Pi^2}{2(A-B)}\left[\frac{\partial \ln \rho}{\partial r} + \frac{\partial \ln \sigma_\Pi^2}{\partial r} + \frac{1}{R_o}\left(1 - \frac{\sigma_\Theta^2}{\sigma_\Pi^2}\right) + \frac{1}{R_o}\left(1 - \frac{\sigma_Z^2}{\sigma_\Pi^2}\right)\right].$$

In other words, $\langle v_* \rangle \sim \sigma_\Pi^2$, so that a plot of $\langle V_* \rangle$ ($= \langle v_* \rangle - v_\Theta$) versus σ_Π^2 for various kinematical groups in the disk should be linear with an intercept for $\sigma_\Pi^2 = 0$ given by $-v_\Theta$. The actual situation is somewhat more complicated than this owing to the spiral density wave of the Galaxy, and ideally only well-mixed groups which have orbited the galactic centre at least once appear to yield an uncontaminated value for v_Θ. Evidence for the distinct nature of older stars from those which have not travelled far from their places of birth can be found in **Parenego's discontinuity**, which marks a distinct increase in the velocity dispersions of main-sequence stars of spectral types F5 and later relative to hotter stars. A similar break is evident for giant stars of spectral types G and later. The best results for the components of the solar motion relative to the dynamical LSR found from a proper consideration of all factors are (from Turner):

$u_\odot = -8.2 \pm 0.6$ km/s

$v_\odot = +5.1 \pm 0.5$ km/s

$w_\odot = +7.0 \pm 0.2$ km/s

corresponding to S = 11.9 km/s towards $l_{lsr} = 32°$, $b_{lsr} = +36°$.

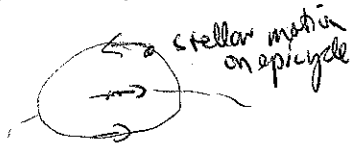

Solution to collisionless Boltzmann Equation (eqn. of motion + fluid eqns) in cylindrical coordinates for local velocity ellipsoid - epicycle motion

Methods of Calculating Θ_0

The parameter $\Theta_0 = \Theta_c$ is the circular velocity at the sun's distance R_0 from the galactic centre. Most current estimates for it concentrate between values of 220 km/s and 250 km/s. There are several methods available for deriving Θ_0, namely:

i. by determining the peculiar motion of the LSR with respect to the halo population. Since even **halo stars** are in orbit about the galactic centre, however, the value of Θ_0 derived in this manner may be a lower limit. The result of such an analysis yield a value of $\Theta_0 \geq 220$ km/s.

ii. by extrapolating the $<V*>$ versus σ_Π^2 curve to its extreme values for globular clusters. This technique also has uncertainties owing to the unknown rate of rotation for the **globular cluster system** about the galactic centre, as well as to the possible existence of two distinct groups of globulars. An analysis of this type gives a value of $\Theta_0 \geq 230$ km/s.

iii. by examining the orbits of **high velocity stars**. High velocity stars are halo stars in the solar neighbourhood which have high apparent velocities relative to the sun owing to the fact that most of their orbital motion is along the direction to the galactic centre. The results of such an analysis depend upon the assumption that all such stars are bound to the Galaxy, and that their orbits are governed by the mass of the Galaxy concentrated inside of the solar circle. The implied value of Θ_0 is between 275 and 300 km/s with this last assumption, but may be ~50 km/s smaller (i.e. Θ_0 between 225 and 250 km/s) if one allows for a flat rotation curve.

iv. by searching for the gap in the distribution of Θ_0-velocities for high velocity stars caused by **plunging disk stars**. Such stars have plunging orbits about the galactic centre, so that they are perturbed into much different orbits (possible even gaining escape velocity from the Galaxy) during their perigalacticon passage. Such a gap is observed in the distribution of Θ_0-velocities for nearby stars (Carlberg & Innanen, AJ, 94, 666, 1987), and corresponds to $\Theta_0 = 245 \pm 10$ km/s.

v. by determining the **peculiar velocity** of the sun relative to nearby galaxies in the **Local Group**. This is not as simple a task as it might seem, owing to the intrinsic velocities of other galaxies in the system. A recent estimate of the local circular velocity from such an analysis is that of Arp (A&A, 156, 207, 1986), who finds $\Theta_0 = 246 \pm 17$ km/s.

vi. by using the best estimates for the **Oort constants** A and B, since $\Theta_0 = (A - B)R_0$. Clearly, an analysis of this type depends upon a concurrent best estimate for R_0, and assumes that both A and B are well-determined. Most current estimates for R_0 lie in the range 7–10 kpc, while Oort's A and B constants appear to lie in the range 10 km/s/kpc $\leq A \leq$ 20 km/s/kpc and –15 km/s/kpc $\leq B \leq$ –7 km/s/kpc, i.e. 119 km/s $\leq \Theta_0 \leq$ 350 km/s. With the more recent best estimates of A = 12.32–14.22 km/s/kpc and B = –11.85 km/s/kpc derived by Schwan (A&A, 198, 116, 1988), this range is further reduced to 169 km/s $\leq \Theta_0 \leq$ 261 km/s.

16. Statistical Parallaxes and Secular Parallaxes

Trigonometric parallaxes are derived from the observable annual parallactic displacements of stars in the sky resulting from the Earth's orbital motion about the sun. The systematic motion of the sun with respect to the local system of stars results in secular displacements in the sky of the observed positions of nearby stars, namely a large part of their observable proper motions. The proper motion of any star therefore has two components — one which is a reflection of the sun's motion relative to it, and the other which is due to its own peculiar motion.

Denote a star's coordinates (right ascension and declination) by α and δ, and the coordinates of the solar apex by A and D. Denote the angular distance of a star from the solar apex by λ, and let ψ represent the angle between the great circles joining the star to the north celestial pole (NCP) and the solar apex, where the angle is positive if measured from north through west (see diagram). According to the relations for a spherical triangle:

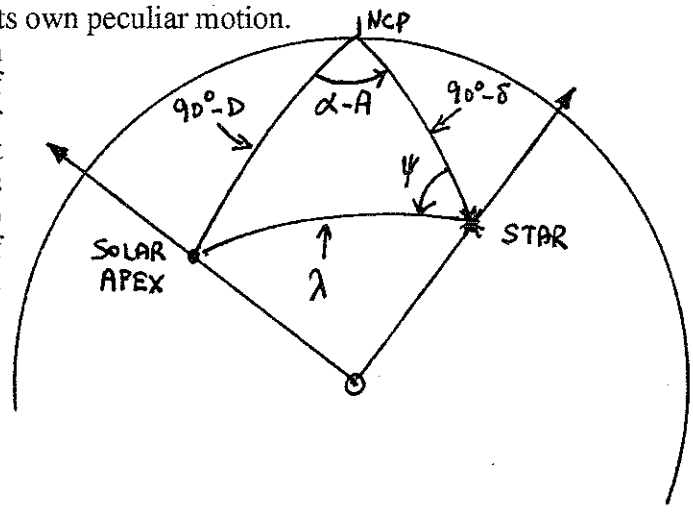

$$\cos\lambda = \cos(90°-\delta)\cos(90°-D) + \sin(90°-\delta)\sin(90°-D)\cos(\alpha-A) \quad \text{[Cosine Law]},$$

or $$\mathbf{\cos\lambda = \sin\delta \sin D + \cos\delta \cos D \cos(\alpha - A)} .$$

Also, $$\frac{\sin(\alpha-A)}{\sin\lambda} = \frac{\sin\psi}{\sin(90°-D)} \quad \text{[Sine Law]},$$

or $$\mathbf{\sin\psi \sin\lambda = \cos D \sin(\alpha - A)} .$$

By the Four-Parts equation:

$$\sin\lambda\cos\psi = \cos(90°-D)\sin(90°-\delta) - \sin(90°-D)\cos(90°-\delta)\cos(\alpha-A) ,$$

or $$\mathbf{\cos\psi \sin\lambda = \cos\delta \sin D - \sin\delta \cos D \cos(\alpha - A)} .$$

These three equations can be used to establish values for λ and values and quadrants for ψ from a knowledge of the direction of the solar apex in combination with a star's coordinates.

The components of a star's proper motion which are normally given in position catalogues are $\mu_\alpha \cos\delta$ and μ_δ. It is more useful to consider the different components υ (upsilon) and τ (tau), where υ is the component of the star's proper motion which reflects the sun's motion through space (it is measured along λ towards the solar antapex) and τ is the component perpendicular to this (it is measured perpendicular to λ northwards). The situation can be envisaged on the celestial sphere, as shown at right. Clearly,

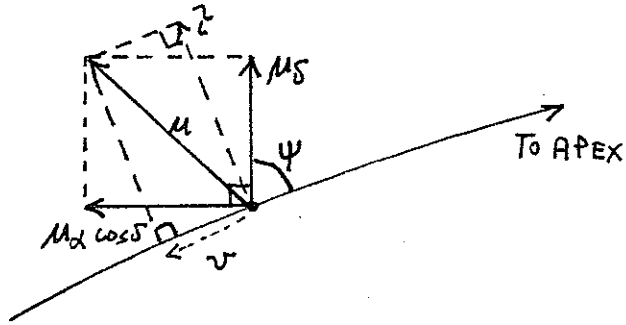

$$\upsilon = \mu_\alpha \cos\delta \cos(90°-\psi) - \mu_\delta \cos\psi ,$$

or $$\upsilon = \mu_\alpha \mathbf{\cos\delta \sin\psi} - \mu_\delta \mathbf{\cos\psi} ,$$

and $$\tau = \mu_\alpha \mathbf{\cos\delta \cos\psi} + \mu_\delta \mathbf{\sin\psi} .$$

The upsilon components of proper motion clearly depend upon the distances to stars and the sun's motion relative to them, while the tau components depend mostly upon the random space motions of stars.

Secular Parallax (The Use of Upsilon Components)

Consider the situation described in the figure at right. Denote the peculiar velocity of the sun relative to a group of stars by $v_\odot$. Recall the relation for stellar tangential velocity:

$$v_T \text{ (km/s)} = \frac{4.74\,\mu}{\pi},$$

for μ in "/yr and the parallax π in arcseconds. This can be rewritten as:

$$\mu = \frac{\pi v_T}{4.74} .$$

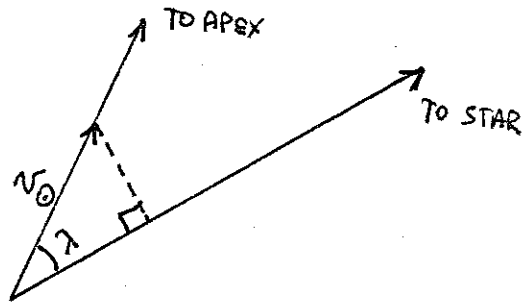

For any star the υ proper motion component is composed of two terms, one which is purely a reflection of the solar motion, and the other which results from the star's peculiar velocity in that direction, i.e.

$$\upsilon = \upsilon^* + \frac{\pi v_\odot \sin\lambda}{4.74} .$$

If we consider a homogeneous group of stars distributed at random around the sky, it is possible to derive a mean parallax $\langle\pi\rangle$ for the stars in the group through careful use of the above equation. A proper statistical analysis of a homogeneous sample of stars would assign statistical weights to

each star in the sample dependent upon the star's distance from the solar antapex, i.e. $w_i = \sin\lambda_i$. Thus, the equation for υ given above can also be rewritten:

$$\sum_{i=1}^{N} \upsilon_i \sin\lambda_i = \sum_{i=1}^{N} \upsilon_{*i} \sin\lambda_i + \frac{4.74}{4.74} v_\odot \sum_{i=1}^{N} \sin^2\lambda_i .$$

If the group of stars is truly randomly distributed in space, then we expect that:

$$\sum_{i=1}^{N} \upsilon_{*i} \sin\lambda_i = 0.$$

$$\therefore \quad \pi = \frac{4.74 \sum_{i=1}^{N} \upsilon_i \sin\lambda_i}{v_\odot \sum_{i=1}^{N} \sin^2\lambda_i} .$$

A solution for $<\pi>$ in this instance requires only a knowledge of the proper motions and positions of stars and the direction of the apex of motion (A, D) and velocity of the sun $v_\odot$ relative to the stars in the group. It is somewhat easier to use the terminology:

$$<x> = \sum_{i=1}^{N} x_i / N .$$

The **equation for secular parallax** with this terminology is therefore:

$$\pi_{sec} = \frac{4.74 <\upsilon \sin\lambda>}{v_\odot <\sin^2\lambda>} .$$

This relationship can be used to estimate the mean absolute magnitudes of stars in such a group using the standard equation for distance modulus:

i.e. $<V_0> - <M_V> = -5\log<\pi> - 5$,

so $<M_V> = <V_0> + 5\log<\pi> + 5$.

Statistical Parallax (The Use of Tau Components)

The tau components of proper motion contain no component due to the sun's motion relative to the group, only the single component due to the star's random space motion projected in that direction. The component of the star's tangential velocity originating from this component of its peculiar velocity is therefore given by:

$$|v_T| = \frac{4.74|\tau|}{\pi} ,$$

where absolute values have been used to isolate the magnitude of this component of the tangential velocity. Note that the total space velocity of a star also contains a component in the direction of the solar antapex.

Stellar radial velocities v_R also contain two components, one due to the star's peculiar space velocity v_{*R}, and one due to the solar motion, namely $v_\odot \cos\lambda$.

i.e. $v_R = v_{*R} - v_\odot \cos\lambda$, or $v_{*R} = v_R + v_\odot \cos\lambda$ (see figure on previous page).

A solution for the mean parallax of a group of stars using their tau components can be derived from the equation in the previous paragraph,

i.e. $\pi = \frac{4.74 <|\tau|>}{<|v_T|>}$.

On average, however, $<|v_T|> = <|v_{*R}|> = <|v_R + v_\odot \cos\lambda|>$, if the stellar peculiar velocities are randomly distributed.

$$\therefore \quad \pi_{sec} = \frac{4.74 <|\tau|>}{<|v_R + v_\odot \cos\lambda|>} .$$

A solution for the mean parallax of a group of stars using the method of statistical parallax requires a knowledge of the positions, proper motions, and radial velocities of the stars in the sample, as well as a knowledge of the apex of motion (A, D) and velocity of the sun $v_\odot$ relative to the stars in the group.

Which method works best for any particular group of stars depends upon the particulars of the group. Upsilon components appear to work best when the solar motion dominates the group random velocities (i.e. $v_\odot > <|v_{*R}|>$), while tau components work best when group motions dominate ($<|v_{*R}|> > v_\odot$). Both techniques have been applied to B stars and, in particular, to RR Lyrae variables (e.g. Clube & Jones, MNRAS, 190, 591, 1980; Heck & Lakaye, MNRAS, 184, 17, 1978; see review by Stothers, ApJ, 274, 20, 1983), which are too distant for direct measurement of their distances by standard techniques. Both classes of object are also relatively uncommon in terms of their local space densities, yet luminous enough that they can be seen to large distances. Due to the general perturbations from smooth galactic orbits predicted in density-wave theories of spiral structure, the assumptions used in the methods of statistical and secular parallax may not be strictly satisfied by many statistical samples of stars. A knowledge of the sun's motion relative to stars in the group is an important ingredient of statistical analyses of this type, and should clearly be determined beforehand as accurately as possible. Differential galactic rotation for distant stars may also be an important complicating factor.

17. Kinematic Groups

Once the LSR velocity of the sun is established, it is possible to plot the space motions of various types of stars relative to the LSR. The corresponding u, v, and w velocities always exhibit scatter, i.e. the velocities have associated dispersions σ_u, σ_v, and σ_w, typically such that $\sigma_u > \sigma_v$ and $\sigma_u > \sigma_w$. The resulting distribution of LSR velocities describes an ellipsoidal cloud with the w-axis (Z-axis) directed towards the galactic poles. This observed distribution of space velocities relative to the LSR is referred to as the **velocity ellipsoid**.

The standard method of examining the velocity ellipsoid of nearby stars is to plot the space velocities as projected on the galactic plane. The resulting distribution of u and v velocities is expected to display an elliptical form with $\sigma_u > \sigma_v$ and with the principal axis directed towards the galactic centre. The actual distibution of velocities is elliptical, but with its principal axis generally skewed towards $l = 30°–45°$, instead of towards $l = 0°$. This skew angle is referred to as the **vertex deviation**, and its cause is not fully known, although Eggen believes that it may be partly due to the contamination of the nearby star sample by members of moving groups.

Moving groups, or superclusters, are collections of stars which apparently share common galactic orbits with open clusters. They are therefore believed to represent the extended clouds of stars which are associated with star cluster evaporation, or the dispersed remains of previously-existing open (or, in one case, globular) clusters. In order for these stars to be still identified with open clusters within the region of space including the solar neighbourhood, it is necessary that all group members have common v-velocities (to within ±1 km/s for older groups, ±2 km/s for younger groups) and similar u-velocities (to within ±10 km/s, generally — this representing the original dispersion of velocities in the parent cluster), with no restriction on w-velocities (which are decoupled from the other components due to the gravitational attraction of the galactiic plane). Details are given by Wooley (1965) and Eggen (1965) in Galactic Structure.

Since the derivation of the space velocity components u, v, and w for a star requires a knowledge of the exact distance to the star, it is clearly necessary to have distance information available for a group of stars before searching for common space velocities of some of them. Many of Eggen's moving groups were delineated by allowing the unknown distance of each star to be a floating variable. Usually, trigonometric parallaxes are available for enough stars with measured proper motions and radial velocities that any potential moving groups can be detected by their common v-velocities and similar u-velocities. Eggen proceeded to add candidate members to these recognized groups, as well as to his newly delineated groups, by inferring distances for the candidates in the first instance so that they fit well into a common colour-magnitude diagram for the "group", then adjusting the distance within standard constraints so that the u and v-velocities for all

stars are "suitably close". Most of his moving group members have therefore not been selected on the basis of exact distance data, and it should not be surprising to learn that follow-up studies of some of them have not confirmed the expected chemical compositon homogeneity of group stars. It appears that many field stars are collected in Eggen's tables of moving group "members". The reality of some of Eggen's moving groups may therefore be open to question, although the general concept of moving groups being composed of escaped members of open clusters is quite valid.

High-velocity stars are stars in the solar neighbourhood which have high space velocities relative to the LSR (see Roman, Galactic Structure, 1965). They are identified by their large u, v, and w velocities with respect to the LSR, generally space velocities >> 50 km/s. Such stars actually lag behind the LSR in its orbital motion about the galactic centre, and have rather low v-components of their orbital velocities relative to the galactic centre. Their peculiar space motions therefore originate in the unusual nature of their galactic orbits, which is due to population differences. High-velocity stars are all metal-poor, ultraviolet excess objects generally categorized as being of intermediate Population II age and composition. They appear to be relatively old F, G, K, and M subdwarfs and K giants somewhat more metal-rich than typical globular cluster stars, which dynamically represent objects in highly elliptical orbits about the galactic centre. None have orbital velocities which lag behind the LSR velocity by more than ~365 km/s, which is used to constrain the local escape velocity, and no high-velocity stars are found moving ahead of the LSR in the direction of galactic rotation (their velocity vectors trail behind the local galactic rotation). Their proportion among nearby stars is listed in the following table:

Object	**Proportion of High-Velocity Members**
Globular Clusters	100%
RR Lyrae Variables	72%
M Dwarfs	47%
K Dwarfs	18%
G Dwarfs	16%
K Giants	6%
G Giants	4%
F Dwarfs	3%
M Giants	2%

Note that stars have to be relatively metal-rich to reach the low effective temperatures typical of M giants, so very few stars of this type are metal-poor high-velocity objects.

18. Galactic Rotation

The flatness of the Milky Way system, as evidenced for example by the narrow band of the Milky Way visible from Earth, suggests that the Galaxy has been influenced by general rotation about an axis perpendicular to the galactic plane. The expected rotation of the Galaxy should be similar to what is found for any central force law (e.g. the solar system), namely **differential rotation**. That is, the angular velocity of rotation, $\omega = v/r$, should depend upon r, the distance from the centre of the Galaxy. In some galaxies and in the innermost regions of our own Galaxy, **solid body rotation** occurs; here ω = constant = X, and $v = Xr$, i.e. v increases linearly with increasing r. For Keplerian motion, $v \sim 1/\sqrt{r}$, i.e. $\omega \sim 1/r^{3/2}$.

Assume simple circular orbits about the centre of the Galaxy in the galactic plane, and define Θ = the circular velocity at some distance R from the centre of the Galaxy, Θ_0 = the circular velocity at R_0 = the sun's distance from the centre of the Galaxy, and l = the galactic longitude of any object of interest in the galactic plane. The coordinates used here are defined so that the velocities in the direction of the sun's motion, away from the galactic centre, and towards the north galactic pole are Θ, Π, and Z, respectively. The observed radial velocity of the object at l relative to the **local standard of rest** (**LSR** = the reference frame centred on the sun and orbiting the galactic centre in the galactic plane at the local circular velocity) is given by (see diagram):

$v_R = \Theta \cos\alpha - \Theta_0 \cos(90°-l)$
$= \Theta \cos\alpha - \Theta_0 \sin l$.

According to the Sine Law:

$$\frac{\sin l}{R} = \frac{\sin(90°+\alpha)}{R_0} = \frac{\cos\alpha}{R_0}.$$

$$\therefore \cos\alpha = \frac{R_0}{R}\sin l.$$

$$\therefore v_R = \frac{\Theta R_0}{R}\sin l - \Theta_0 \sin l$$

$$= R_0\left[\frac{\Theta}{R} - \frac{\Theta_0}{R_0}\right]\sin l.$$

Since $\frac{\Theta_0}{R_0} = \omega_0$ and $\frac{\Theta}{R} = \omega$,

$$\therefore \mathbf{v_R = R_0(\omega - \omega_0)\sin l}.$$

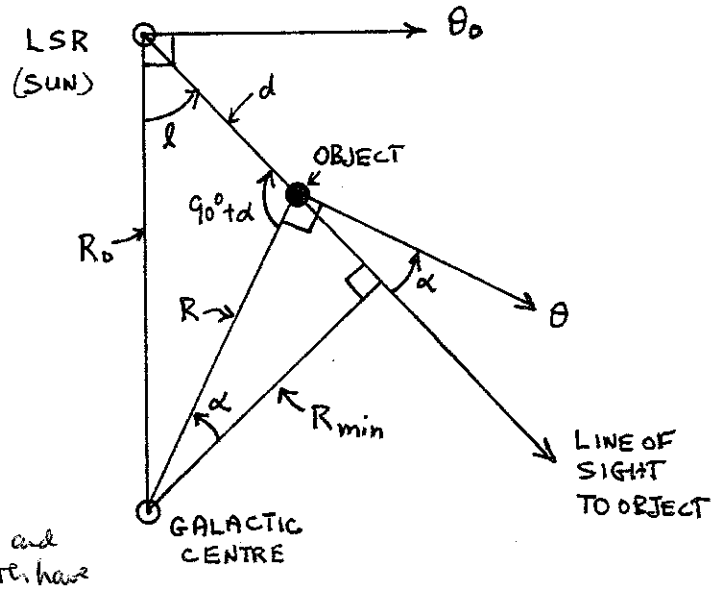

Outside the galactic plane this becomes:

$$\mathbf{v_R = R_0(\omega - \omega_0)\sin l \cos b}.$$

Since θ and θ_0 both have cos b terms.

The observed tangential velocity of this object relative to the LSR is given by:
$v_T = \Theta \sin\alpha - \Theta_0 \cos l$ (where v_T is measured positively in the direction of galactic rotation).
But $R\sin\alpha = R_0 \cos l - d$, where d is the distance to the object.

$$\therefore \sin\alpha = \frac{R_0}{R}\cos l - \frac{d}{R}.$$

$$\therefore v_T = \frac{\Theta}{R}(R_0\cos l - d) - \Theta_0\left(\frac{R_0}{R_0}\right)\cos l = R_0\left[\frac{\Theta}{R} - \frac{\Theta_0}{R_0}\right]\cos l - \frac{\Theta}{R}d = R_0(\omega - \omega_0)\cos l - \omega d.$$

i.e. $\mathbf{v_T = R_0(\omega - \omega_0)\cos l - \omega d}$.

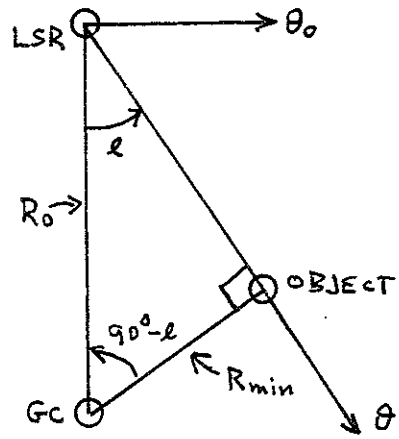

These equations are the general equations of galactic rotation. If ω decreases with increasing distance from the galactic centre, then for any given value of l in the first ($0° < l < 90°$) and fourth ($270° < l < 360°$) quadrants, the maximum value of ω occurs at the tangent point along the line-of-sight, i.e. at $R_{min} = R_0 \sin l$. This is evident from the diagram at right, where:

$d = R_0 \cos l$.
$R_{min} = R_0 \cos(90°-l) = R_0 \sin l$.
$v_R(max) = \Theta(R_{min}) - \Theta_0 \sin l$.

Some approximations to the general formulae are possible for the situation where $d << R_0$. If one expands the term $(\omega - \omega_0)$ in a Taylor series expansion and omits higher order terms then:

$$(\omega - \omega_0) = (R - R_0)\left[\frac{d\omega}{dR}\right]_{R_0} + \frac{1}{2}(R - R_0)^2\left[\frac{d\omega}{dR}\right]^2_{R_0} + \ldots \approx (R - R_0)\left[\frac{d\omega}{dR}\right]_{R_0}.$$

and $\omega d \approx d\left\{\omega_0 + (R - R_0)\left[\frac{d\omega}{dR}\right]_{R_0}\right\} \approx \omega_0 d$ (to a first approximation).

But $\frac{d\omega}{dR} = \frac{d}{dR}\left[\frac{\Theta}{R}\right] = \frac{1}{R}\frac{d\Theta}{dR} - \frac{\Theta}{R^2}$, $\therefore \left[\frac{d\omega}{dR}\right]_{R_0} = \frac{1}{R_0}\left[\frac{d\Theta}{dR}\right]_{R_0} - \frac{\Theta_0}{R_0^2}$.

Also, for $d << R_0$, $R_0 - R \approx d\cos l$.

Thus, for relatively nearby objects in the galactic plane:

$$v_R \approx R_0\left[\frac{1}{R_0}\left[\frac{d\Theta}{dR}\right]_{R_0} - \frac{\Theta_0}{R_0^2}\right](R - R_0)\sin l = \left\{\frac{\Theta_0}{R_0} - \left[\frac{d\Theta}{dR}\right]_{R_0}\right\} d \sin l \cos l$$

$$= \frac{1}{2}\left\{\frac{\Theta_0}{R_0} - \left[\frac{d\Theta}{dR}\right]_{R_0}\right\} d \sin 2l .$$

because $R - R_0$ also contains a $\cos b$ term

i.e. $\mathbf{v_R = A\, d \sin 2l}$, or $\mathbf{v_R = A\, d \sin 2l \cos^2 b}$ **outside of the plane,**

where $\mathbf{A = \frac{1}{2}\left\{\frac{\Theta_0}{R_0} - \left[\frac{d\Theta}{dR}\right]_{R_0}\right\}}$.

$\cos 2x = 2\cos^2 x - 1$

$\therefore \cos^2 x = \frac{1}{2}(1 + \cos 2x)$

Also, $v_T \approx R_0\left[\frac{1}{R_0}\left[\frac{d\Theta}{dR}\right]_{R_0} - \frac{\Theta_0}{R_0^2}\right](R - R_0)\cos l - \omega_0 d$

$$= \left\{\frac{\Theta_0}{R_0} - \left[\frac{d\Theta}{dR}\right]_{R_0}\right\} d \cos^2 l - \frac{\Theta_0}{R_0} d = \frac{1}{2}\left\{\frac{\Theta_0}{R_0} - \left[\frac{d\Theta}{dR}\right]_{R_0}\right\} d\,(1 + \cos 2l) - \frac{\Theta_0}{R_0} d$$

$$= A\, d \cos 2l - \frac{1}{2}\left\{\frac{\Theta_0}{R_0} + \left[\frac{d\Theta}{dR}\right]_{R_0}\right\} d .$$

i.e. $\mathbf{v_T = A\, d \cos 2l + B\, d}$, where $\mathbf{B = -\frac{1}{2}\left\{\frac{\Theta_0}{R_0} + \left[\frac{d\Theta}{dR}\right]_{R_0}\right\}}$.

$\therefore \mathbf{v_T = d(A \cos 2l + B)}$, $\mu_l = \dfrac{\mathbf{(A \cos 2l + B)}}{\mathbf{4.74}}$ (proper motion in galactic longitude).

The two constants A and B are referred to as **Oort's constants.**

i.e. $\mathbf{A = \frac{1}{2}\left\{\frac{\Theta_0}{R_0} - \left[\frac{d\Theta}{dR}\right]_{R_0}\right\}}$ and $\mathbf{B = -\frac{1}{2}\left\{\frac{\Theta_0}{R_0} + \left[\frac{d\Theta}{dR}\right]_{R_0}\right\}}$.

Thus, $A = -\frac{1}{2}R_0\left[\frac{d\omega}{dR}\right]_{R_0}$ and $B = A - \omega_0$.

Also, $\omega_0 = \frac{\Theta_0}{R_0} = A - B$, and $\left[\frac{d\Theta}{dR}\right]_{R_0} = -(A + B)$.

Recall that, for a given line of sight within the solar circle, a maximum value for ω is reached at the tangent point, where:

$d = R_0 \cos l$, $R_{min} = R_0 \sin l$.

i.e. $v_R(max) = \Theta(R_{min}) - \Theta_0 \sin l$.

For $d << R_0$, we have:

$$(\omega - \omega_0) \approx (R - R_0)\left[\frac{d\omega}{dR}\right]_{R_0} = (R - R_0)\left\{\frac{1}{R_0}\left[\frac{d\Theta}{dR}\right]_{R_0} - \frac{\Theta_0}{R_0^2}\right\} = 2A\frac{(R_0 - R)}{R_0} .$$

$$\therefore \quad v_R(max) = R_0\,(\omega_{max} - \omega_0)\sin l \approx R_0\left(\frac{2A}{R_0}\right)(R_0 - R_{min})\sin l .$$

or $\mathbf{v_R(max) \approx 2A\, R_0\, (1 - \sin l)\sin l}$.

The actual relationship is a series, with the second order term generally being ~10% the magnitude of the first order term:

e.g. $\mathbf{v_R(max) \approx 2A\, R_0 (1 - \sin l)\sin l + \frac{1}{2}\left(\frac{d^2\omega}{dR^2}\right)_{R_0} R_0^3 (1 - \sin l)^2 \sin l}$.

Studies of the radial velocities of stars in the first and fourth quadrants in order to determine $v_R(max)$ generally yield values of AR_0 lying in the range 135–150 km/s.

Optimum Values for the Galactic Rotation Constants

A summary of various studies of the galactic rotation constants (to 1986) is given by Kerr & Lynden-Bell (MNRAS, 221, 1023, 1986). Note that, despite the paper's title ("Review of Galactic Constants"), the various estimates are summarized, not reviewed. Here we try to review the various estimates with a view to obtaining the optimum current values.

Oort's A & B

The predicted effects of galactic rotation on the radial velocities and proper motions of nearby stars appear as a double sine wave dependence of the radial velocities with galactic longitude and a double cosine wave dependence of the proper motions with galactic longitude, the latter offset from zero by the Oort B term. Both effects are clearly seen in the available radial velocity and proper motion data, but different studies have obtained values for A ranging from 11.6 km/s/kpc to 20.0 km/s/kpc, and values for B ranging from –7.0 km/s/kpc to –18 km/s/kpc. A recent proper motion study from the Lick Northern Proper Motion Program (Hanson AJ, 94, 409, 1987) yielded estimates of A = +11.31 ±1.06 km/s/kpc and B = –13.91 ±0.92 km/s/kpc, while a study by Schwan (A&A, 198, 116, 1988) using FK5 system proper motions yielded estimates of A = +12.32 (or 14.22) km/s/kpc and B = –11.85 km/s/kpc (no quoted uncertainties). Radial velocity studies tend to give larger estimates for A, but this is possibly because they sample a larger region of space where the approximations leading to Oort's equations break down. Best estimates for A and B based only upon recent proper motion work are:

$\mathbf{A \approx +12.5 \pm 1.0\ km/s/kpc}$, and

$\mathbf{B \approx -12.5 \pm 1.0\ km/s/kpc}$.

This result has implications for the nature of the local galactic rotation. For the case of solid-body rotation with ω = constant, one predicts that:

$$v_R = R_0 (\omega - \omega_0) \sin l = 0, \text{ and}$$

$$v_T = R_0 (\omega - \omega_0) \cos l - \omega d = -\omega d = 4.74\, \mu_l\, d, \text{ or } \mu_l = -\frac{\omega}{4.74} = \text{constant}.$$

Neither of these predictions satisfy the observations, which means that differential rotation is confirmed. Alternatively, it is possible that Θ is constant, at least locally. In this case,

$$\left[\frac{d\theta}{dR}\right]_{R_0} = 0 , \text{ so that } A = -B.$$

The currently available data do appear to indicate that $A \approx -B$, so a constant circular velocity does appear to exist locally. The case for $\Theta(R)$ = constant = Θ_0 is referred to as a flat rotation curve, and seems to be appropriate for nearly all spiral galaxies, not just the Milky Way. Available data from radio studies indicate that the rotation curve of our Galaxy is fairly simple. It seems to obey solid body rotation close to the galactic centre, and turns into a flat rotation curve in the outermost regions, including the region at the sun's distance from the galactic centre.

Dynamical theory suggests that A and B should also be related through the parameters of the velocity ellipsoid, namely that:

$$\frac{-B}{A} = \frac{\sigma_\Theta^2}{\sigma_\Pi^2 - \sigma_\Theta^2} = \frac{1}{\left(\frac{\sigma_\Pi^2}{\sigma_\Theta^2}\right) - 1},$$

or $$\left(\frac{\sigma_\Theta}{\sigma_\Pi}\right)^2 = \frac{B}{B - A} \equiv \frac{1}{2} \text{ for a flat rotation curve.}$$

In fact, as noted by Kerr & Lynden-Bell, many studies of this ratio do give values for the ratio $\left(\frac{\sigma_\Theta}{\sigma_\Pi}\right)^2$ which are very close to 0.5, with typical values ranging from 0.36 to 0.50, and with late-type giants (which presumably represent a dynamically relaxed system) giving values of 0.49 to 0.50, closest to the result predicted for a flat rotation curve.

Θ_0

In section 15 we showed that the best value of Θ_0 resulting from the study of plunging disk stars and the velocities of nearby members of the Local Group was Θ_0 = **245 ±10 km/s**, and there seems to be no valid reason to modify this. Past studies have suggested values for Θ_0 ranging from 184 km/s to 275 km/s. The value of 250 km/s adopted by the IAU in 1964 was recently adjusted downward to 222.2 km/s by Kerr & Lynden-Bell, but again there appears to be no compelling reason to accept this. A value of Θ_0 this small cannot be reconciled with the velocities of nearby galaxies nor with the data for high-velocity stars.

R_0

Recent estimates for R_0 listed by Kerr & Lynden-Bell range from 6.8 kpc to 10.5 kpc. The direct methods may actually not be capable of yielding a reliable value, given the current uncertainties in the distance scale, so it is important to examine what the indirect methods produce. A value for R_0 can be derived using Oort's constants A and B with Θ_0, since:

$$\mathbf{R_0} = \frac{\Theta_0}{A - B} = \frac{245\ (\pm 10)\ \text{km/s}}{[12.5\ (\pm 1.0) + 12.5\ (\pm 1.0)]\ \text{km/s/kpc}} = \mathbf{9.80\ \pm 0.89\ kpc},$$

using the values quoted earlier. If one is willing to accept values of A = –B = 14.0 ±1.0 km/s/kpc, the resulting value of **R_0 is 8.75 ±0.72 kpc**.

One can also make use of the relationship for the maximum radial velocity along a line of sight in the first and fourth quadrants, namely:

$$v_R(\max) \approx 2A R_0 (1 - \sin l) \sin l + \frac{1}{2}\left(\frac{d^2\omega}{dR^2}\right)_{R_0} R_0^3 (1 - \sin l)^2 \sin l\,,$$

which, as noted, yields estimates of AR_0 = 135 to 150 km/s, although Kerr & Lynden-Bell list values ranging from 103 to 156 km/s. Most of these estimates are susceptible to the adopted values for the sun's LSR velocity, and may contain systematic errors. Recent studies (those since 1974) yield values of AR_0 = 118 ±15 km/s, which corresponds to **R_0 = 9.44 ±1.42 kpc**.

Another method of obtaining R_0 is through the use of zero-velocity stars, as illustrated in the diagram at right. Such objects have no net radial velocity with respect to the LSR, which means that they share the same galactic orbital velocity as the sun, i.e. Θ_0. Their distances are therefore given by:

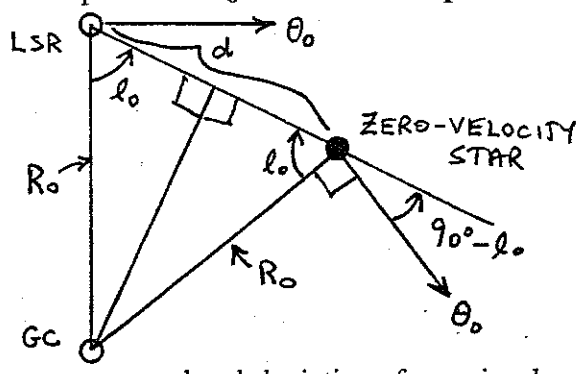

$$d = 2R_0 \cos l_0\,,$$

so $$R_0 = \frac{d}{2\cos l_0} = \frac{d \sec l_0}{2}\,.$$

The method is clearly susceptible to distance scale errors, to any local deviations from circular motion, to any errors in the adopted LSR velocity of the sun, and even to slight errors in l_0. Crampton et al. (MNRAS, 176, 683, 1976) nevertheless obtained a value of **R_0 = 8.4 ±1.0 kpc** using this method for B stars, and this is not a totally unreasonable result.

Some interesting new results have been derived using radio interferometry of the motion of H_2O masers in the region of the galactic centre (Reid et al. ApJ, 330, 809, 1988). A value of **R_0 = 7.1 ±1.5 kpc** was obtained using Sgr B2(N), while a value of R_0 = 10.8 ±4.8 kpc is quoted from the use of W51. Unfortunately, the exact results are susceptible to the adopted LSR velocity of the sun, as well as to the particulars of the model. Perhaps estimates based upon the detection of planetary nebulae or Mira variables in the nuclear bulge should be given more credence. A value of **$R_0 \approx$ 8.1 kpc** was obtained by Pottasch (A&A, 236, 231, 1990) using the planetary nebula luminosity function, although it is not clear how susceptible this value is to reddening corrections. Whitelock et al. (MNRAS, 248, 276, 1991) obtained a value of **R_0 = 8.6 ±0.5 kpc** using Mira variables, noting, however, that the uncertainty in their result might be larger than the quoted value. Racine & Harris (AJ, 98, 1609, 1989) obtained **R_0 = 7.5 ±0.9 kpc** using globular clusters in the nuclear bulge. It would appear that recent estimates of R_0 fall in the range from 7.1

to 8.6 kpc. All estimates appear to be susceptible to various problems. Ideally, however, any adopted value must be consistent with the values obtained for Oort's constants, as emphasized by Kerr & Lynden-Bell.

The best current estimates for the galactic rotation constants according to your instructor are those summarized in the table below:

Parameter	IAU (1964)	IAU (1985)	Turner
R_o	10 kpc	8.54 kpc	9.8 kpc
A	+15 km/s/kpc	+14.45 km/s/kpc	+12.5 km/s/kpc
B	−10 km/s/kpc	−12.0 km/s/kpc	−12.5 km/s/kpc
θ_o	250 km/s	222.2 km/s	245 km/s

19. Galactic Structure Studies

21–cm Radiation of Hydrogen

The 21-cm radiation of neutral hydrogen gas is used to locate hydrogen clouds in the galactic plane using information on their Doppler shifts in conjunction with the relationship for the LSR-corrected radial velocity of an object in an orbit about the galactic centre, i.e.

$$v_R = R_o (\omega - \omega_o) \sin l .$$

It is reasonable to assume that $\omega(R)$ decreases with increasing r, so that the maximum radial motions of hydrogen clouds along the line of sight for $0° < l < 90°$ (the 1st quadrant), and the minimum radial motions of hydrogen clouds along the line of sight for $270° < l < 360°$ (the 4th quadrant) occur at $R_{min} = R_o \sin l$, i.e. the tangent point, where:

$$v_R = R_o\left[\frac{\Theta}{R_o \sin l} - \frac{\Theta_o}{R_o}\right] \sin l = \Theta - \Theta_o \sin l .$$

The maximum and/or minimum observed radial velocities of hydrogen clouds along such lines of sight in the 1st and 4th quadrants, respectively, must originate from gas located at the tangent points, if there is any. In general terms there will always be some hydrogen gas at the tangent points, but their maximum and/or minimum radial motions will be the vector sum of their orbital motion about the galactic centre and their random space motions, which typically average 15–20 km/s. If Θ_o is known, it is possible to construct a relationship for $\Theta(R_o \sin l) = v_R(max) + \Theta_o \sin l$ for $270° < l < 90°$. This relationship can be extrapolated to $R > R_o$ using mainly theoretical expectations (see Blitz, ApJ, 231, L115, 1979), and the resulting $\Theta(R)$ relationship can then be used with 21-cm observations of neutral hydrogen cloud velocity peaks to determine the R-distribution of the higher density regions of hydrogen gas in the galactic plane. The velocities must first be adjusted to the LSR, which is probably the most uncertain step.

The method works reasonably well in the 1st and 4th quadrants, where the $\Theta(R)$ relationship is well established, and also gives fairly consistent results for the 2nd and 3rd quadrants. For any line of sight there are always ambiguities in distance for clouds of any specific radial velocity, since simple mathematical analysis indicates that clouds at two different distances symmetric about R_{min} must have identical radial motions. Such ambiguities can be resolved by mapping the clouds in galactic latiitude b, since nearby clouds should subtend a larger angular extent than distant clouds. The method also breaks down at $l = 0°$ (towards the galactic centre) and $l = 180°$ (towards the anticentre), since there are no predicted radial motions of material arising from galactic rotation in these directions. Within these constraints, however, 21-cm maps exhibit a distinct spiral arm picture which appears to be in fairly good agreement with the maps of other spiral arm indicators, at least in the solar neighbourhood. Evidence for a warp in the distribution of neutral hydrogen is also fairly obvious, with the galactic plane being warped north of $b = 0°$ towards $l \approx 90°$ and south of $b = 0°$ towards $l = 270°$, by perhaps 0.8 kpc at 1.5 R_o. This is usually explained as being due to an interaction of the Galaxy with the Large Magellanic Cloud, the Small Magellanic Cloud, and the other objects in the Magellanic Stream. This feature should not be confused with Gould's Belt, which appears as a local tilting of the nearby spiral arm — below

the galactic plane in the direction of the anticentre and above the plane towards the galactic centre. It is also noteworthy that the hydrogen abundance decreases beyond the solar circle, a feature also detected in the radio continuum data and seen in the decreased numbers of H II regions and massive stars outside of the solar circle.

Molecular Lines

Radiation from the ubiquitous CO molecule can also be used to trace spiral features, although most of the early studies concentrated upon the northern hemisphere. CO originates mainly in large molecular clouds as does most neutral hydrogen, so the different maps from CO and 21-cm radiation should complement each other. Radio molecular radiation is also generated at the frequencies of OH and H_2O in regions of star formation, so studies at these frequencies usually yield different information about galactic structure than do 21-cm or CO maps.

Radio Continuum

Inferences about the spiral structure of the Galaxy also come from detectable "steps" in the continuous radiation from the galactic plane, which mostly originates from non-thermal (synchrotron) radiation from interstellar gas which is spiralling along magnetic field lines. Secondary sources of continuous radiation from the galactic plane include individual thermal sources associated with H II regions. Radio continuum observations exhibit "steps" — discontinuous changes in continuum intensity — as a function of galactic longitude, whenever the line of sight becomes tangent to a spiral arm. Such "steps" have been detected in 21-cm maps, optical light, and CO maps, as well as in radio continuum studies. In both CO and 21-cm maps, the "steps" show up as distinct S-waves in the V_R distributions, and result from opposite streaming motions of material on different sides of spiral arm features. Generally, such streaming motions are in the same sense as galactic rotation on the outer edges of spiral arms, and opposite the sense of galactic rotation on the inner edges of spiral arms. This behaviour is predicted in density wave theory.

The prominent observable "steps" in the continuum radiation occur at the following locations, with origins as indicated:

Step	Associated Spiral Arm
13°	Galactic Nucleus?
31°	?
34°	–II Arm
52°	Sagittarius-Carina Arm
80°	Cygnus Arm
263°	Local (Cygnus) Arm?
286°	Sagittarius-Carina Arm
~310°	Scutum-Norma Arm
332°	?
337°	?

The detection of line radiation (mostly large n series members of neutral hydrogen — radio recombination lines) from H II regions at radio frequencies can be used with the previous kinematic predictions to map the distribution of H II regions in the galactic plane, similar to that done with 21-cm data. The Georgelins, in particular, have published several papers in this area. Several nearby H II regions have been studied using their optical Hα emission, while distant, obscured regions are studied by first detecting them as thermal sources at radio wavelengths, and then searching for either radio continuum radiation from the sources or 21-cm radiation from the neutral hydrogen shells which inevitably surround H II regions. In some cases there has been confusion between whether or not the sources are supernova remnants or H II regions, and this has often led to further observational studies aimed at resolving the uncertainty.

Optical Tracers

Suitable optical tracers can also be used to map the spiral features, at least within about 4 kpc or so of the sun. The best tracers are always extremely young objects, namely H II regions,

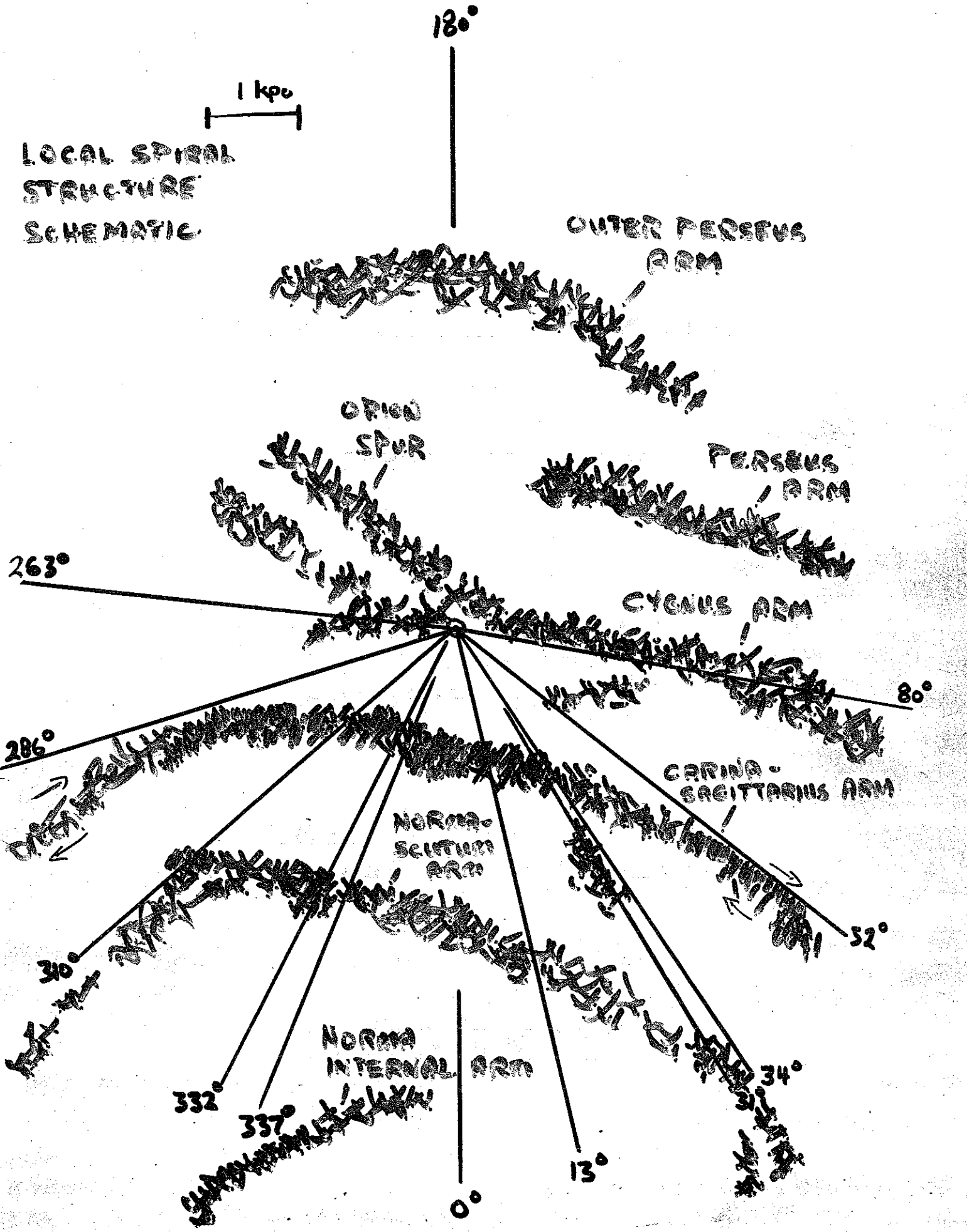
180°
1 kpc
LOCAL SPIRAL STRUCTURE SCHEMATIC
OUTER PERSEUS ARM
ORION SPUR
PERSEUS ARM
263°
CYGNUS ARM
80°
286°
CARINA - SAGITTARIUS ARM
NORMA-SCUTUM ARM
310°
52°
NORMA INTERNAL ARM
332°
337°
34°
13°
0°

young clusters, OB associations, OB stars, R associations, type Ia supergiants (M or B-type), Wolf-Rayet stars, and dust clouds (dark nebulae). Long period Cepheids were once touted as potential spiral arm indicators, but it is not clear if they are truly suitable for this purpose. Most long period Cepheids have ages comparable to those of open clusters with upper main-sequence turnoffs of spectral type B2 or later, which corresponds to an age of several tens of millions of years ($>2 \times 10^7$ yrs) at least. Finally, star counts can often reveal local concentrations of stars which might not be detected in any other way.

Several spiral arm features have been detected optically, although it is not exactly clear how they fit together. Up to six main arms seem to be present in spatial plots of spiral arm indicators. These are:

Outer Perseus Arm (+II) roughly 4 kpc from the sun running from $l \approx 150°$ to the anticentre ($l = 180°$).

Perseus Arm (+I) roughly 2 kpc from the sun in the directions $l \approx 100°$ to 150°.

Cygnus Arm (0) running from Cygnus ($l \approx 80°$) possibly into a spur in Orion ($l \approx 200°$) just outside the sun's location in the Galaxy.

Carina–Sagittarius Arm (–I) roughly 1.5 kpc from the sun running from $l \approx 30°$ to $l \approx 280°$ through the direction of the galactic centre.

Norma-Scutum Arm (–II) roughly 3 kpc from the sun towards Norma ($l = 325°$) and Scutum ($l = 20°$) through the direction of the galactic centre.

Norma Internal Arm (–III) roughly 5–6 kpc from the sun towards Norma ($l \approx 340°$)?

The type of galaxy we inhabit can be determined from various parameters, namely the size of the galactic bulge (visible optically), the local orbital speed of disk stars, the separations of spiral arms seen locally, and the value of R_0. It seems clear that the Milky Way is a supergiant spiral-type galaxy, and its exact classification in the Hubble scheme would be Sb. The mass of the Galaxy can be estimated from the local rotation constants using Kepler's Third Law, i.e.

$$(M_1 + M_2) = a^3/P^2,$$

where M_1 and M_2 are in $M_\odot$, a is in A.U., and P is in years. Adopting values of $\Theta_0 \approx 245$ km/s and $R_0 \approx 9.5$ kpc, and assuming the sun's mass to be negligible in comparison with the mass of the Galaxy, M_G, we find:

$$a = 9.5 \text{ kpc} \times 1000 \text{ pc/kpc} \times 206265 \text{ A.U./pc} = 1.96 \times 10^9 \text{ A.U.}$$

$$P = \frac{\text{circumference}}{\text{orbital velocity}} = \frac{2\pi a}{\Theta_0} = \frac{2\pi \times 1.96 \times 10^9 \text{ A.U.} \times 1.5 \times 10^8 \text{ km/A.U.}}{245 \text{ km/s}}$$

$$= \frac{7.54 \times 10^{15} \text{ s}}{3.16 \times 10^7 \text{ s/yr}} = 2.39 \times 10^8 \text{ years.}$$

$$\therefore \quad M_G = \frac{a^3}{P^2} = \frac{(1.96 \times 10^9 \text{ A.U.})^3}{(2.39 \times 10^8 \text{ yrs})^2} = 1.32 \times 10^{11} M_\odot .$$

Since this must be an underestimate as a consequence of the manner of its derivation (it assumes that all of the mass of the Galaxy is concentrated at its centre), the true mass of the Galaxy must be in excess of $10^{11} M_\odot$, possibly $2–3 \times 10^{11} M_\odot$ to account for the flat rotation curve. M31 has an extimated mass of $\sim 3 \times 10^{11} M_\odot$, presumably slightly greater than that of the Milky Way.

20. Propagation of Spiral Arm Patterns

Spiral Density Wave Theory

The gravitational density wave theory for generating spiral arm patterns in disk galaxies is essentially a theoretical-empirical scheme developed to explain the main features of spiral galaxies like our own. The major developments came in a paper by Lin & Shu (ApJ, 140, 646, 1964), although somewhat more readable summaries can be found in the review by Wielen (PASP, 86, 341, 1974) and in Shu's textbook The Physical Universe.

Many of the concepts of density wave theory are easier to grasp if one considers the simple model for local stellar dynamics as developed in the first half of this century by Lindblad and Oort. The basic characteristics of stellar velocity dispersions suggest that the observed small deviations

from purely circular orbits about the galactic centre can be described to a good approximation using elliptical epicycles whose centres describe circular motion in the direction of galactic rotation. The mathematical implication of using epicycles is that each star makes harmonic oscillations about its mean circular orbit position with a frequency given by $\kappa(R)$, where R is the distance from the galactic centre. This epicyclic frequency κ can be derived from the dynamical angular velocity ω of galactic rotation using the relationship:

$$\kappa^2 = 4\omega^2\left[1 + \frac{R}{2\omega}\frac{d\omega}{dR}\right].$$

The axis ratio of the epicycle is given by the ratio $\kappa/2\omega$, so that, locally, we have:

$$\omega_o = A - B,$$

$$\left[\frac{d\omega}{dR}\right]_{R_o} = -\frac{2A}{R_o},$$

so that $\kappa_o^2 = 4(A-B)^2\left[1 - \frac{A}{A-B}\right] = -4B(A-B),$

and $$\frac{\kappa_o}{2\omega_o} = \left[1 - \frac{A}{A-B}\right]^{1/2} = \left[\frac{-B}{A-B}\right]^{1/2} \approx (0.5)^{1/2}.$$

Thus, the tangential component of stellar orbital motion is greater than the radial component.

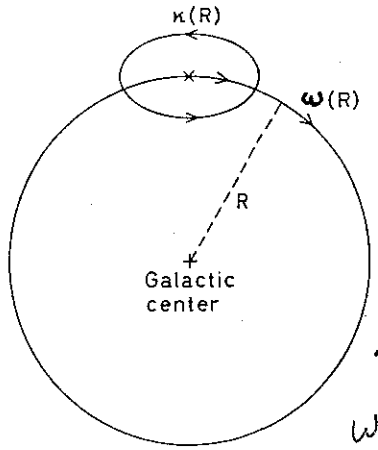

Consider now a density wave of fixed spiral form described by the density law:

$$\sigma(R,\theta,t) = \sigma^* e^{i\chi},$$

where $\chi = m\omega_p t - m\theta + \Phi(R)$,

using a circular coordinate system (R,θ) centred on the galactic centre and a phase function $\Phi(R)$ which is normally described by a logarithmic spiral,

i.e. $$\Phi(R) = \frac{2|k|R}{m}\ln(R/R^*),$$

where m is the number of components of the density wave (normally m = 2), ω_p is the fixed angular velocity of the density wave pattern, t is the time parameter, and k is the wavenumber of the density pattern, normally given by:

$$|k| = \frac{\kappa^2}{\pi G\sigma}\left[1 \pm \frac{m(\omega - \omega_p)}{\kappa}\right].$$

The pitch angle ψ of the spiral density pattern is given by:

$$\tan\psi = \frac{m}{|k|R}.$$

Although any number of arms are permitted in standard density wave theory, since m can be any integer, it turns out that any value of m other than m = 2 is rather impractical. Single-armed spirals (m = 1) do not appear to be very common, and do not appear to be stable configurations, while m > 2 configurations severely limit the region of a galaxy where spiral arms can occur, which also appears to be unrealistic. Thus, one expects that two-armed spirals (m = 2) are the norm. There are certain locations in a spiral galaxy, however, where resonances occur between the circular frequency ω of orbital motion, the epicyclic frequency κ describing deviations from smooth circular flow, and the pattern rotational frequency ω_p. These resonances occur when the ratio $(\omega - \omega_p)/\kappa$ takes on specific rational values. The most important resonances are the following:

i. **Corotation.** $\omega_p = \omega.$

ii. **Inner Lindblad Resonance.** $\omega_p = \omega - \frac{\kappa}{2}.$

iii. **Outer Lindblad Resonance.** $\omega_p = \omega + \frac{\kappa}{2}.$

The resonance points correspond to locations in the galaxy where wave structures cannot exist, so spiral wave patterns can only be produced between the regions of the inner and outer Lindblad resonances. For galaxies with flat rotation curves,

$$\kappa = \sqrt{2}\ \omega ,$$

and the inner and outer Lindblad resonances occur at:

$$R = (1 \pm \sqrt{2}/m)R_0,$$

namely 0.293 R_0 and 1.707 R_0 for m = 2. Note that the inner and outer Lindblad resonances for m = 4 occur at 0.646 R_0 and 1.354 R_0, respectively. Since the detected spiral arms in the Milky Way are observed over a region of perhaps 8 kpc or more, it seems clear that $m \neq 4$ for our own Galaxy, although m = 2 is permitted.

The response of various components of a typical galaxy to a passing density wave depends directly upon the dispersion in their epicyclic frequences, i.e. upon σ_Π^2. Interstellar gas and dust has a fairly small dispersion in epicyclic frequencies, and responds much more nonlinearly to a spiral density wave than do typical disk stars of larger dispersion. Halo objects have a very large dispersion in their epicyclic frequencies, and do not respond at all to spiral density waves. Thus, one predicts that interstellar gas and dust should exhibit a very pronounced spiral structure due to a density wave disturbance, that disk stars should exhibit only a weak spiral structure, and that halo stars should be unperturbed from their smooth spherical density distribution. The nonlinear shock effects of gas and dust perturbed by a spiral density wave should trigger star formation as local gas densities are pushed over the limit for Jeans' instability. The theory therefore predicts many of the observable features of well-studied spiral galaxies like our own, namely:

i. dust clouds and gas clouds should lie along the inside edges of spiral arms defined optically, since newly-formed stars will appear after the crest of the density wave has passed.
ii. the spiral pattern should disappear for the innermost and outermost regions of galaxies at the location of the Lindblad resonances.
iii. there should be velocity discontinuities at the wave edges due to the response of the gas and dust to the passing density wave.
iv. most spiral galaxies should be two-armed spirals.

Some of these features are indeed observed. The radial velocity discontinuities observed on alternate sides of radio spiral arms and the streaming motions of stars on alternate sides of spiral arms (Humphreys, A&A, 20, 29, 1972 — for Carina Arm) bear out the predictions from density wave theory. However, the origin of density waves is another matter. Wielen lists several potential generating mechanisms, including the gravitational influence of neighbouring galaxies, a central asymmetry in the galactic nucleus, local gravitational instabilities in the disk, angular momentum transfer from the inner to the outer parts of spiral galaxies, two-stream instabilities between the different components of disk galaxies, and eruptive activity of galactic nuclei (as originally suggested by Ambartsumian in 1958). All may play some role in driving the observed spiral density waves of grand-design spirals.

Stochastic Self-Propagating Star Formation

Gerola & Seiden (ApJ, 223, 129, 1978) and Seiden & Gerola (ApJ, 233, 56, 1979) have used models to explore the possibility that star formation may be a continuous sequence which evolves through the mechanics of H II region development and/or supernova remnant expansion into nearby molecular clouds. In this way, the differential nature of galactic rotation assures that newly-created clumps of stars generated by such a mechanism will be rapidly sheared into a spiral form much like that observed in disk galaxies. The resulting models of spiral galaxies which are produced through the continuous process of star formation and stellar evolution influencing nearby regions have a rather feathery structure in comparison with the prominent structure of density wave models. Such a mechanism is therefore unlikely to be the dominant mechanism for generating spiral galaxies. It does, however, provide a means for producing offshoots from major spiral arms like the Orion spur and Vulpecula features seen locally. Presumably such features are not part of the main spiral density pattern in our Galaxy, and should not be used to trace the main spiral pattern.

21. Galactic Dynamics

Force Law Perpendicular to the Galactic Plane (Mihalas 12–3)

Define the force exerted by the Galaxy in the z-direction to be K_z, which is measured in a positive sense for positive values of z. The potential energy of an object a distance z from the galactic plane is therefore given by:

$$\Phi(z) = -\int_0^z K_{z'}\,dz' ,$$

where $\Phi(z)$ and $K_{z'}$ are defined per unit stellar mass. If an object leaves the vicinity of the galactic plane perpendicularly with a velocity Z_0 and reaches a height z above the plane with a velocity Z, then:

$$\tfrac{1}{2}Z^2 + \Phi(z) = \tfrac{1}{2}Z_0^2 \quad \text{from the relation for conservation of energy.}$$

$$\therefore \quad \tfrac{1}{2}Z^2 - \int_0^z K_{z'}\,dz' = \tfrac{1}{2}Z_0^2 .$$

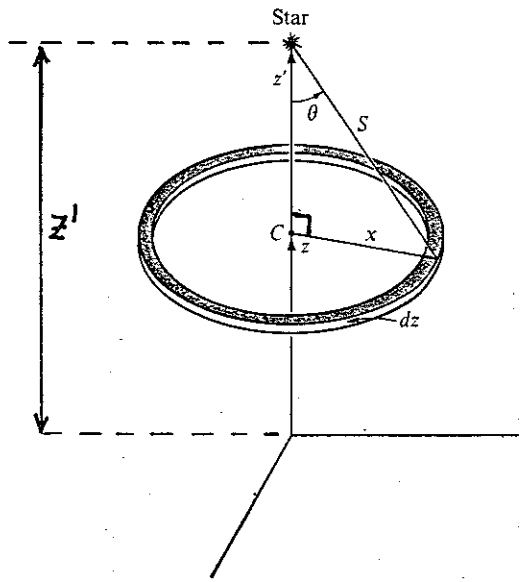

In order to evaluate K_z, it is useful to consider a ring of material of radius x located a distance z from the galactic plane. The force exerted by this ring on a star located a distance z' above the galactic plane contributes the amount $\delta(\delta K_{z'}) = \delta^2 K_{z'}$ to K_z, and can be evaluated as follows. To the star it appears that all of the mass of the shell is concentrated at the centre of the shell, so the direction of the force is towards this point. With the density of the matter in the shell given by $\rho(z)$, the gravitational force exerted by the shell per unit stellar mass is given by :

$$\delta^2 K_{z'} = \frac{G\,2\pi x\,\rho(z)\,dx\cos\theta}{s^2}\,dz$$

$$= 2\pi G\rho(z)\,dz\,\frac{x\,dx}{s^2}\cos\theta .$$

But $\cos\theta = \dfrac{(z' - z)}{s}$, and $s^2 = x^2 + (z' - z)^2$.

$$\therefore \quad \delta^2 K_{z'} = 2\pi G\rho(z)\,dz\,\frac{(z' - z)\,x\,dx}{[x^2 + (z' - z)^2]^{3/2}} .$$

The contribution to K_z of all such shells is found by integrating over all possible x-values, i.e.

$$\delta K_{z'} = 2\pi G\rho(z)\,dz\,(z' - z)\int_0^\infty \frac{x\,dx}{[x^2 + (z' - z)^2]^{3/2}}$$

$$= 2\pi G\rho(z)\,dz\,(z' - z)\left[\frac{-1}{[x^2 + (z' - z)^2]^{1/2}}\right]_0^\infty$$

$$= \frac{2\pi G\rho(z)\,dz\,(z' - z)}{[(z' - z)^2]^{1/2}} = 2\pi G\rho(z)\,dz .$$

$K_{z'}$ can now be found by integration over all shells dz:

$$K_{z'} = 2\pi G\left[\int_{z'}^{\infty}\rho(z)\,dz - \int_{-z'}^{z'}\rho(z)\,dz - \int_{-\infty}^{-z'}\rho(z)\,dz\right].$$

By symmetry, $\rho(-z) = \rho(z)$.

$$\therefore \quad \int_{z'}^{\infty} \rho(z)\,dz = \int_{-\infty}^{-z'} \rho(z)\,dz, \text{ and } \int_{-z'}^{0} \rho(z)\,dz = \int_{0}^{z'} \rho(z)\,dz.$$

$$\therefore \quad K_{z'} = -4\pi G \int_{0}^{z'} \rho(z)\,dz.$$

For small values of z, $\rho(z) \approx \rho_0$ (constant).

$$\therefore \quad K_{z'} = -4\pi G \rho_0 z', \text{ and } \frac{dK_z}{dz} = -4\pi G \rho_0.$$

At large values of z one expects K_z to have more of a $1/z^2$ dependence, since the Galaxy begins to look more like a massive slab at large distances from the plane. The complete equation for K_z is described by **Poisson's equation**, namely:

$$\frac{\partial K_z}{\partial z} = -4\pi G\rho - \left(\frac{\partial K_r}{\partial r} - \frac{K_r}{r}\right),$$ where K_r is the radial dependence of the galactic force law.

For small z, the terms in K_r are small and unimportant. The general relationship is therefore usually written as:

$$\nabla^2 \Phi(z) = 4\pi G\rho.$$

Finding K_z From Observations

The standard method used to derive K_z is to make use of stars as tracers of the z-potential because their numbers and velocities can be derived. The standard techniques were developed by Hill (BAN, 15, 1, 1960) and Oort (BAN, 15, 45, 1960) using K giants, as described by Mihalas. The resulting force law is approximated by:

$$K_z = \langle Z_o^2 \rangle \frac{d \ln [\nu(z)/\nu_o]}{dz},$$

where $\nu(z)$ is the relative number density of stars at z. The results by Hill and Oort indicate that stars with the following Z-velocities will reach distances above the plane of:

Z_o (km/s)	z_{max} (pc)
9	100
37	500
60	1000

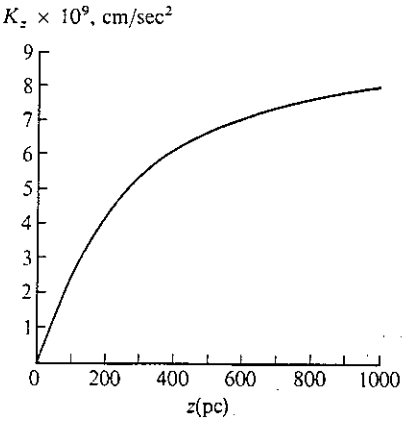

These results are obtained from the relationship given earlier:

$$\frac{1}{2} Z^2 - \int_{o}^{z} K_{z'}\,dz' = \frac{1}{2} Z_o^2,$$

which, with Z = 0 km/s at $z = z_{max}$, becomes:

$$Z_o^2 = 2 \int_{o}^{z_{max}} -K_{z'}\,dz'.$$

According to the results of Hill and Oort, $K_z = -1.4 \times 10^{-14}$ km/s² at z = 50 pc. Thus, with the stellar units summarized by Mihalas (Chapter 9):

$$\rho_o = -\frac{1}{4\pi G}\frac{dK_z}{dz} = \frac{232\,M_\odot}{4\pi\,(pc \times (km/s)^2)} \frac{1.4 \times 10^{-14}\,km/s^2}{50\,pc} \frac{206265 \times 1.496 \times 10^8\,km}{pc}$$

$$= 0.16\,M_\odot/pc^3.$$

Correction of this estimate for the terms in K_r still leaves a local mass density for the galactic plane of $\rho_o \approx 0.15\,M_\odot/pc^3$. Best estimates for the local space densities of stars and gas are $\sim 0.05\,M_\odot/pc^3$ and $\sim 0.03\,M_\odot/pc^3$, respectively. This means that roughly half of the local density of matter must be in some unobserved form, perhaps molecular clouds, black dwarfs, etc. This minor discrepancy is an ongoing problem to be resolved, and is often investigated along with flat galactic rotation curves. An interesting new insight into this problem has recently been provided by Soares

(Rev.Mex.Astron.Astrofis., 24, 3, 1992), who demonstrates how a buoyancy force in the galactic disk produces flat rotation curves without the need for introducing any missing matter.

Runaway Stars

Blaauw (ARA&A, 2, 213, 1964) describes runaway stars from OB associations as stars characterized by similar ages and distances to the stars in particular OB associations, but with space velocities of up to ~200 km/s relative to their parent associations. They appear to be reasonably isotropically distributed about OB associations, and are mainly massive stars with masses in excess of ~10 $M_\odot$. They also appear to be mostly single systems, a fact which some researchers have used to argue for their origin via slingshot ejections from massive binary systems during supernovae explosions. The circular velocity in a typical massive binary system with $M_1 + M_2 \approx 20\,M_\odot$ and $a \approx 0.5$ A.U., for example, is $v_{cir} \approx 189$ km/s [Recall that $v_{cir}^2 = G(M_1 + M_2)/a = 29.8$ km/s for objects in the solar system.]. In other words, the orbital velocities of stars in massive binary systems are typically close to ~200 km/s, which must therefore be close to the ejection velocities of stars from systems undergoing rapid mass loss via a supernova explosion. An attractive alternate possibility is that OB runaways originate from interactions between stars in their original OB clusters. Note that stars need only ~60 km/s of ejection velocity perpendicular to the galactic plane to reach distances of 1 kpc above the plane. This may be important for explaining the large numbers of early-type stars which have been found well away from the galactic plane (Tobin & Kilkenny, MNRAS, 194, 937, 1981; Keenan & Dufton, MNRAS, 205, 435, 1983).